STRESS-FUNCTION VARIATIONAL METHODS FOR STRESS ANALYSIS OF COMPOSITE LAMINATES AND ADHESIVELY BONDED COMPOSITE JOINTS

A Thesis
Submitted to the Graduate Faculty
of the
North Dakota State University
of Agriculture and Applied Science

By

Xiao Wang

In Partial Fulfillment of the Requirements
for the Degree of
MASTER OF SCIENCE

Major Department:
Mechanical Engineering

October 2015

Fargo, North Dakota

North Dakota State University
Graduate School

Title

Stress-Function Variational Methods for Stress Analysis of Composite Laminates and Adhesively Bonded Composite Joints

By

Xiao Wang

The Supervisory Committee certifies that this ***disquisition*** complies with North Dakota State University's regulations and meets the accepted standards for the degree of

MASTER OF SCIENCE

SUPERVISORY COMMITTEE:

Dr. Xiangfa Wu
Chair

Dr. Long Jiang

Dr. Majura Selekwa

Dr. Zhibin Lin

Approved:

11/5/2015
Date

Dr. Alan Kallmeyer
Department Chair

ABSTRACT

Adhesively bonded composite joints (ABCJs) have been broadly used to connect multi-materials and show their structural and economic advantages compared to traditional bonding methods. However, robust methods are still desired for efficient and accurate lay-wise stress analysis of ABCJs involving multiple boundaries and layers.

The purpose of this work was to extend the stress-function variational method for free-edge stress analysis of composite laminates with a finite length. At each interface of the laminate, two unknown Lehknitskii's stress potential functions were introduced to interpolate the stresses across the layer. A set of 4^{th}-order governing ODEs of the functions was obtained via evoking the complementary virtual work, solved by eigenvalue-function method under proper traction conditions. Corresponding MATLAB™ program was developed and validated by the FEM (ANSYS®). This method can also examine the stress-suppression effect after composite laminates interleafing. Consequently, the above method was furthered for determining the lay-wise stress distribution in ABCJs.

ACKNOWLEDGMENTS

I would like to acknowledge my advisor, Dr. Xiangfa Wu, in the first place, whose expertise, patient guidance and support throughout my graduate study significantly increased my academic experiences at NDSU. Dr. Wu's research supervision enlightened me in the scientific seriousness in research, professional thesis writing, and in-depth understanding in this field. I also need to extend my appreciations to the other professors on my graduate supervisor committee: Dr. Jiang Long, Dr. Majura Selekwa, and Dr. Zhibin Lin.

In the last, I also express my thanks to my wife and my parents, whose supports are so necessary for me to pursue my master's degree at NDSU.

TABLE OF CONTENTS

LIST OF FIGURES

1. INTRODUCTION

In the past five decades, advanced composite materials have been widely used in aircraft industry and aerospace applications due to their high specific modulus and strength, excellent corrosion resistance, and superior manufacturability, among others. Meanwhile, with the development of joints technology, bolted joints have been gradually replaced by adhesively-bonded joints due to the unavoidable weight penalty and stress concentration of bolted joints. As a result, adhesively-bonded multilayer composite joints (ABCJs) have been developed and utilized in broad modern industrial structures. This demands the intensive research in the field of designing and analyzing adhesively-bonded multi-layered composite joints.

Owing to the unique features of adhesively bonded and multi-layered composite joints, it is necessary to understand the mechanical properties of these composite joints, such as hygrothermal effects, mechanical strength, failure mechanisms (debonding, delamination, fiber pull-out, etc.), etc., when integrating these materials into structures. Since the mismatch of mechanical properties of adjacent layers, stress concentration is common at the regions close to the edges of overlap bonding lines and the free edges of adherends of multi-layered composite laminates. In the early design and stress analysis of composite laminates, it has been found that the stress concentration exists near the free edges of composite laminate, which is called free-edge effects. In adhesively boned joints, shear stress also exhibits near the edges of the overlap boding lines; however, regardless of composite laminates or adhesively bonded joints, the regions far from the free edges only carry a small portion of the loads, similar to the in-plane and out-of-plane shear stresses and normal stresses. In reality, such high interfacial stress concentrations near the free edge may result in debonding or delamination failure. On the other

hand, the hash loading environment, in realistic cases, can raise much complicated stress state in ABCJs, such as those induced by combined mechanical and hygrothermal loads. Hence, it is crucial to conduct accurate stress analysis for optimizing structural design and prediction of the mechanical strength of ABCJs. And then, to engineers, a desire has been raised to develop robust models for predicting the interfacial stress variation of ABCJs. Such joint models are expected to be efficient, high accurate and also capable of taking into account the effects of different material properties, (such as Young's modulus, coefficients of hygro or thermal expansion, Poisson's ratio, etc), design parameters and external loadings (e.g., mechanical, hygrothermal, etc,), etc.

In the past five decades, substantial investigation has been made on the stress analysis of adhesively-boned joints laminated composites. Yet several technical deficiencies exist in most of the pioneering studies on the stress analysis of ABCJs. Firstly, nearly all the analytic and semi-analytic methods available in the literature are oversimplified and therefore led to noticeable errors in the stress analysis of these structures. Among those, the most significant issue is that the stresses predicted from these analytical methods do not satisfy the traction free boundary conditions at the free-edges. When a composite laminate is subjected to a tensile deformation, nontrivial shear stresses are predicted by almost all the literature models at the free edges of the laminate. Secondly, existing analytical models are unable to predict the stresses in the multi-layered joint structures. Thirdly, though quite a few purely numerical approaches have been formulated in the literature for the stress analysis of these adhesively bonded joints and composite laminates, the computational efficiency rapidly decays with increading structural complexity such as the number of layers. Fourthly, current interfacial stress analysis only considers composite laminates with semi-infinite length. In reality, composite laminates are typically designed with finite length such that the ratio of length over thickness of the laminate

will influence the variations of the interfacial stresses in the composite laminates, especially when the width of the laminates is small.

The purpose of this thesis work was to extend the stress-function variational method for free-edge stress analysis of composite laminates developed by Yin (1994a, 1994b) and modified by Wu (2003). This method introduces two unknown Lehknitskii's stress potential functions $F(y,z)$ and $\Psi(y,z)$ at each laminate interface to interpolate the stresses in each layer of the laminate. Theorem of complementary virtual work was employed to gain a set of coupled 4^{th}-order ODEs, which is used to determine two sets of unknown coefficients via solving the corresponding eigenvalue problem. Correspondingly, an efficient MATLAB™ code was developed for predicting the variations of interfacial stresses of the composite laminates under consideration. The semi-analytic method developed in this study can be applicable for the stress analysis of composite laminates with finite length and examination of the interleafing effect in interfacial stress suppression of the advanced composite laminates toughenend with plastic interlayers. Furthermore, similar to the recent theoretical work on the interfacial stress analysis of bonded and adhesively bonded joints by Wu & Jenson (2011) and Wu & Zhao (2012), the above stress-function variational method was further extended for interfacial stress analysis of ABCJs, in which the traction boundary conditions were gained by using classical laminate plate theory. The numerical results of the interfacial stresses in ABCJs predicted by the present model have been compared with previous cases, and show the obvious advantages of efficient and accurate stress analysis and structural optimization of composite laminates and ABJCs.

2. LITERATURE REVIEW

2.1. Development of Joints Technology

Adhesively bonded joints (ABJs) are the types of most structurally efficient methods of connecting structure members through adhesive bonding. They have become an important alternative to mechanical joints in recent decades due to their quite a few advantages over conventional bolted/riveted or welded joints structured in numerous modern industrial applications. Adhesive bonding could be considered as a process by using an adhesive to bond surfaces together by solidifying, therefore it brings ABJs with the advantages such as the low weight, low cost, concise design and high tolerance to damage, among others. These significant factors have resulted in the rapid development of ABJs in recent decades. On the other hand, due to the booming of fiber-reinforced polymer matrix composites (PMCs) technology since 1970s, many industrial applications attempted to use PMC laminates as an alternative adherend materials of ABJs. These had attracted more researchers to study the mechanical performance of adhesively bonded composite joints (ABCJs). During 1970s to early 1980s, pioneering studies on ABCJs were initiated, in order to fit the rapidly growing applications of PMC laminates in aerospace industries. Over the past three decades, numerous approaches to approximate the stresses in composite laminates have been developed. These approaches are based mostly on analytical solutions, finite element methods (FEMs) and experimental studies. A comprehensive review given by Matthews et al. (1982) was focused on the strength of fiber-reinforced adhesively bonded joints. Later, there have been a large number of the numerical approaches developed based on FEM, whereas the ones based on the analytical solutions were relatively less

popular than the former. Some studies on the stress analysis of ABCJs have been performed, which were focused on the structural design of bonded joints. In principle, the discontinuities in both the geometry of composite laminates and the material properties across the ply interfaces will lead to high stress concentration near the free edges. In order to minimize the free edge effects, Adams and Wake (1984) had considered the stress and strength analysis of a variety of joint structures. In their studies, the classical joint structures can be classified into single-lap joints, double-lap joints, single-sided bonded joints, double-sided bonded joints, single-sided strapped joints and double-sided strapped bonded joint, as illustrated in Figure 1. Furthermore, there are also other types of joint configurations considered in their studies, such as strap joints, butt joints, butt strap joints, corner joints, stepped-scarf joints, T-shaped joints, L-shaped joints, double-double joints, tubular lap joints, etc. Another study by Chamis and Murthy (1991) listed several steps of designing procedure for ABCJs subjected to static and cyclic loadings as well as various environmental conditions such as high temperature and moisture.

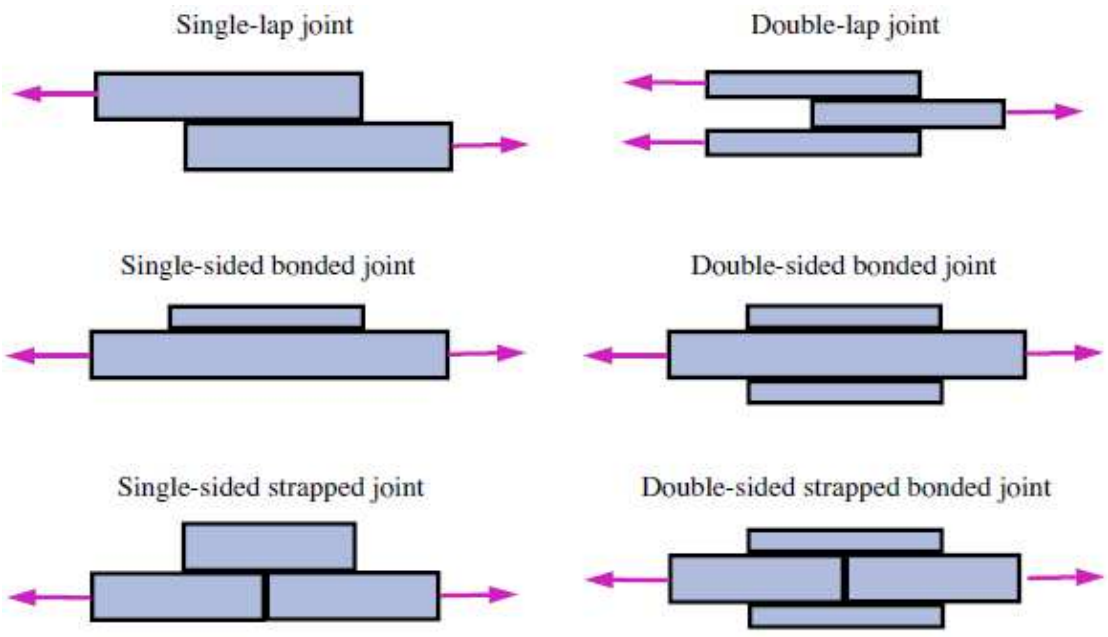

Figure 2.1. Types of typical adhesive bonded joints.

Among broad strength/failure studies, researchers had concluded that the strength of ABCJs depends largely on the stress variation across the interface between adherends and adhesive. On the other hand, the interfacial stress variation in joints was determined by the geometry of the joints and the mechanical properties of the adhesive and adherends. However, when using PMC laminates as adherends, due to the low through-thickness strength, the relatively high through-thickness stresses in the overlap ends of ABCJs would cause the failure in the composite laminate other than the adhesive failure as shown in Figure 2. Thus, in the course of designing ABCJs, it is desired to suppress the stress concentrations near the free edges of the ABCJs. In typical ABCJ studies, it is more reasonable to analyze the strength and failure of PMC laminates and the adherend/adhesive together.

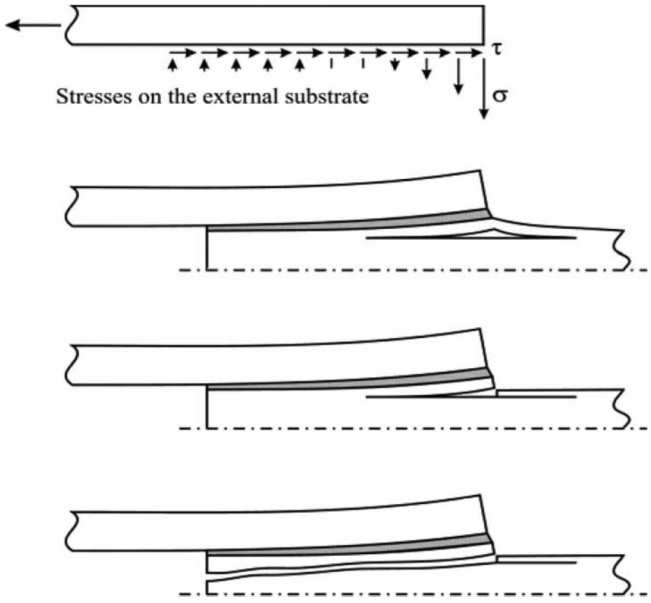

Figure 2.2. Failure in adhesively bonded double-lap joints due to the large transvers stresses of the adherend.

2.2. Analytic approaches to free-edge stresses in composite laminates and adhesively bonded joints

With the rapidly growing applications of PMCs in aerospace, aeronautical and ground vehicles, sports utilities, offshore structures, etc., it is critically important to understand the stress state in PMC structures, especially adhesively bonded joints with multiple materials joined to form complicated geometries, in order to avoid catastrophic failure. Among various failure modes in PMC laminates and joints, edge delamination has been received a significant attention since 1970s. Pipes and Pagano (1971) were the pioneers to first analyze the free-edge stresses in angle-ply laminates by using finite difference method, which was validated by FEM and experimental observations made by other researchers. Pipes and Pagano's studies indicated that high interlaminar stresses exist and concentrate near the free edges of PMC laminates.

Essentially inspired by Pipes and Pagano's pioneering studies, a number of similar investigations on the free-edge stress analysis of PMC laminates have been made in the past four decades, which were conducted mainly by means of FEM. Meanwhile, researchers also proposed various purely numerical and semi-analytic approaches to model the free-edge stresses in PMC laminates. So far, for the purpose of designing PMC laminates and evaluating the free-edge stresses in PMC laminates, quite a few efficient numerical methods have been formulated for efficient and accurate prediction of the interlaminar stresses at the free-edges of PMCs laminates. These theoretical contributions have been used for the stress and strength analysis of adhesively boned joints. Below gives a brief historical review on free-edge stress and strength analysis of PMC laminates.

Wang and Choi (1984) introduced the boundary-layer stress function for free-edge stress analysis of composite laminates. Wang and Choi's method combined Lekhniskii's potential functions and eigenfunction method. Kaaapoglou and Lagace (2001) formulated an efficient semi-analytic method to determine the free-edge stresses of composite laminates based on minimization of the total potential energy, in which the force and moment equilibrium equations were satisfied at a few specified points. This method provided a simple approximation for free-edge stress analysis of composite laminates. Yet, the methods aforementioned cannot well balance the computational accuracy and efficiency. In addition, Yin (1994) provided an important alternative in this field. Yin formulated an innovative semi-analytic method based on the classical laminate plate theory, which is capable of providing a semi-analytical solution. The numerical procedure of this semi-analytic method is straightforward, and no obvious numerical errors are induced during the numerical process. Besides these semi-analytical methods, most of numerical methods reported in the literature were based mainly on FEM. In addition, finite

difference methods (FDM) and boundary element methods (BEM) have been also considered for free-edge stress analysis of composite laminates. In addition, quite a few studies have also been conducted on the stress and strength analysis of bonded and adhesively bonded joints. The pioneering stress analysis of ABJs was conducted by Volkersen (1938). He formulated a simple ABJ model with the assumption that the axial tension in adherends and the shear stress in adhesive layer are constant across the layer thickness. However, since the shear and transverse moduli of composite materials are much lower than the axial ones, Volkersen's solution was unable to explain the effert induced by the adherend bending or the shear deformation in the adherends. This study was further extended by Goland and Reissner (1944), who studied the shear and peel stress variations between the adhesive and aluminum alloy adherends. However, their stress solution does not satisfy the shear-free conditions at the ends of the adherends.

Furthermore, Hart-Smith (1996) proposed an ABJ model with a simple analytical solution based on the assumption that the adhesive layer behaves as an ideal elastoplastic solid. This model improved the prediction of the mechanical behavior of the ductile adhesive layer, in which the failure of the adhesive layer was based on its strain energy. Furthermore, Hart-Smith's ABJ model can also be utilized for examining the thermal effect on the mechanical behavior of ABJs. For instance, thermal mismatch would reduce joint strength. However, most of the earlier analytical theories of ABJs did not take into account the shear deformation in the transverse direction. In reality, shear deformation has been considered as an important influential factor of the structural strength of adherends made of composite laminates, because of their relatively low shear modulus in the transverse direction. Renton and Vinson (1975) considered the stress analysis of ABJs made of composite laminates in their study, which included first and higher-order shear deformation theories. They formulated an analytical approach by taking into account

the deformations induced by the transverse shear and normal strains. Such method can be exploited for analyzing the shear deformation in the composite adherends consisting of high modulus fibers and low modulus resin. Based on their formulation, they predicted the linear elastic behavior of adherends and adhesive in a single-lap joint and discovered that Young's modulus of adherends, length and material properties of adhesive layer are the most influential parameters in design of single lap joints.

Srinivas (1975) used a similar approach to formulate the analytic solution for the analysis of the shear deformation in ABJs of composite laminates. In addition, the nonlinear geometric effects in single-lap and double-lap joint structures can be interpreted with this theory. Furthermore, to analyze the structural strength of ABCJs, Dattguru et al. (1984) and Rickett and Hollaway (1985) respectively developed two nonlinear joint models for determining the stress distribution in single-lap and double-lap joints in closed-form analytic expressions by assuming that the mechanical behavior of the adhesive follows that of elastic-perfectly plastic solids. In addition, Allman (1977) developed alternative approach, by using both the minimum complimentary strain energy method and Hart-Smith's elastic-plastic approach. In such approaches, the gained solutions were able to satisfy not only the free-edge traction conditions of the adhesive but also the equilibrium equations in the adherends. It was discovered from the results of nonlinear analysis that the adhesive properties played a dominant factor in the mechanical performance of the joints.

Based on Allman's works (1977), Adams and Mallick (1992) further investigated the nonlinear behavior of adhesive by means of a one-dimensional (1D) finite-element method (FEM). They modeled the stress variation across the layer thickness of the adhesive layer and the composite adherends made of different materials of varying thickness. Their predictions were

found to be very close to those predicted by FEM, though being a little bit underestimated. By using the first-order laminate plate theory, Yang and Pang (1993, 1996) formulated an analytical approach, which considered the adherends as orthotropic materials, such as unidirectional or cross-ply composite laminates. This analytic approach was utilized for determination of the stress distribution in single-lap joints, with symmetric or asymmetric structures, subjected to extension and bending loadings. This approach is capable of analyzing the effects of transverse shear deformation and asymmetry of the adherends layers on the stress variation. Their results were validated by means of FEM. In addition, Wu et al. (1997) studied the stress distribution in ABCJs consisting of dissimilar adherends of varying thickness and lengths. A set of governing ordinary differential equations (ODEs) was formulated for investigation of ABCJs made of fiber-reinforced composite laminates. In his study of stress analysis of double-lap ABCJs, Tong (1997) discovered that nonlinear models were more accurate for predicting the loading capacity of these joints than linear models available in the literature. In this study, a simplified 1D joint model and a finite-element model were utilized for estimating the mechanical strength of the ABCJs. Correspondingly, well-controlled joint tests were formulated for the purpose of validating the numerical results predicted by the models utilized in the study. It was found that the theoretical results based on these nonlinear methods were in a good agreement with those measured in the experiments. In contrast, the results predicted by the linear models can only reach half of the values measured in the experiments. Frostig et al. (1999) further formulated a closed-form high-order theory based on their former works on modeling the free-edge shear stress at the ends of the overlap in sandwich panels. However, if the adherends are made of composite materials, the shear deformation cannot be neglected because most of composite laminates carry relatively high axial modulus and low transverse shear modulus. By employing the classic laminate plate theory,

Zuo et al. (2004) analyzed the stress distribution in single-lap and single strapped joints subject to combination of tensile and bending loadings. The theoretical results based on this model were validated by means of FEM. In addition, Zhang et al. (2006) formulated a theoretical approach for analyzing the multi-axial stress state in composite joints by modeling the adherends of orthotropic laminates as wide plates subjected to cylindrical bending and the adhesive layer as a linearly elastic material. This approach is capable of determining the in-plane and interlaminar stresses in adherends, which accommodates the in-plane strain in the transverse direction and the hygrothermal effect in the joint. The advantage of this approach over other analytical ones is that it can be applied to more general joint conditions, such as joints of various geometries, both linearly and nonlinearly elastic adhesive, unbalanced laminates, and broader loading situations.

Most analytical methods available in the literature assume that the adherends are in linearly elastic condition, and some others assume that only the adhesive layer behaves as that of elastoplastic solids. In addition, a few other joint models are capable of determining the stress variation across the adhesive layer. Nevertheless, when taking into account the nonlinear response of the joint due to the plastic behavior of the adhesive, it is challenging to formulate feasible analytical methods due to the complexity of mathematical formulation.

2.3. Stress analysis of adhesively bonded joints based on finite elements approaches

As aforementioned, a significant number of investigations have been performed to predict the joint strength using continuum mechanics approach, in which the adhesive and adherends were commonly treated as continuum solids In addition, the adhesive was considered to be perfectly bonded to the adherends. Based on such an assumption, finite-element approaches

without involving the interface properties of the adhesive layer have been extensively used. There is no general criterion for determining the failure of the joint since either the maximum stress and strain or strain energy density of plasticity has been considered. In addition, due to existence of stress singularities near the free-edge of two bonded dissimilar materials, failure criteria based on the maximum stress or strain lose their physical meaning. In this case, at the ends of bonded joints, stress and strain singularities always exist. Therefore, the maximum stress and strain obtained using FEM highly depend upon the magnitude of the singularity and the mesh size used in the FEA. Adams and Harris (1987) pointed out that the singularity can be removed by introducing rounding. However, the value of peak stress or plastic strain energy density would be affected by the rounding degree. Currently, researchers are investigating on use of rounding without loss of the strength of joint. Thus, in order to predict the strength accurately, the exact degree and shape of the rounding are the key influencing factors. Failure criterion plays as the key parameter in the fracture mechanics approach. Within the framework of fracture mechanics, it is possible to analyze the normal and shear deformations at the crack tip. The concepts of mixed-mode facture would enable researchers to calculate the joint strength, through predicting the crack path when different loading situations are applied.

Groth (1988) proposed a failure criterion at the corners of bonded joints such that if the generalized stress-intensity factor is beyond a critical value, it would lead to the initiation of fracture. Using a similar approach, Gleich at al. (2001) studied the magnitude of stress singularity and strength of bonded joints of varying adhesive thickness. They concluded and verified by experiments that the increase of adhesive thickness would increase the stress-intensity factor, which, in contrast, would decrease the strength of joints. In the present study, a new numerical method was formulated for the stress analysis of adhesively bonded composite joints, in which

the joints (either single-sided bonded joints, single-side strap joints, or single-lap joints herein) are considered to be made of adherends as slender anisotropic fiber-reinforced composite laminates. Such joints are also subjected to torsion, bending, and extension which put forward new challenges of interfacial stress analysis.

2.4. Interleafing

Delamination is the common failure mode of laminated composites. Historically, a number of techniques have been developed to suppress delamination failure such as laminate stitching, matrix-toughening, edge cap, etc. Among these techniques, interleafing can be described as using plastic interleaved layers as the toughening materials inserted between layers of composite laminates. So far, researches have performed significant experimental research on interleafing technique, such as testing the performance of fiber-reinforced composite laminates interleaved by electrospun polymeric nanofiber layers (1991**)**. In this Ph.D. research, Wu (2003) first performed the systematic experimental studies on the toughening effect of electrospun nanofiber-based interlayers on the interlaminar fracture toughness of advanced polymer composites under varying loading cases of static and quasistatic to dynamic and impact loadings. In the investigation, continuous polymer fibers with the diameter around 300 nm were produced by the low-cost, top-down electrospinning technique and utilized to reinforce the interlaminar fracture toughness of reinforce graphite/epoxy composite. . Magniez et al. (2010) performed the experimental study on the toughening effect of polyvinylidene fluoride (PVDF) nanofibers on the mode Ⅰ and mode Ⅱ fracture toughness of carbon/epoxy composite laminates, in which the PVDF nanofiber layers behaved as the interleafing materials. In this study, the original research

goal was to investigate the effect of PVDF's molecular weight on the mechanical performance of the composite laminates. However, the experimental results showed only a little improvement on the fracture toughness of the composite laminates. Li et al. (2008) examined the toughening effect of two interleafing materials: the polysufone (PSF) film and electrospun PSF nanofiber films, which were embedded between the plies of carbon/epoxy laminates, respectively. By comparing the experimental results, it was concluded that nanofibrous films are capable of significantly enhancing the mode Ⅰ interlaminar fracture toughness, which was better than the PSF films. Zhang et al. (2012) also tested the interfacial toughening effect of three interleafing materials, i.e., polycaprolacton (PCL), PVDF and polyacrylonitrile (PAN) on the modeⅠ interlaminar fracture toughness, respectively. Comparison of the experimental results demonstrated that only when the polymerization-induced phase separation occurred between interleaved and composite layers, the modeⅠ interlaminar fracture toughness can be enhanced. In addition, Liu et al. (2006) investigated the mode Iinterlaminar fracture in a composite laminate by interleafing layers of epoxy 609. It is believed that within a certain thickness, the nanofibers had negligible effect on the performance of modeⅠ delamination failure. Despite numerous experimental studies on the effect of interleaves on delamination resistance of composite laminates, no systematical studies have been conducted on the stress variation of the interleaved composite laminates due to introducing the plastic interleafing interlayers.

2.5. Outstanding problems in ABCJs

Based on the recent theoretical studies on stress analysis of bonded and adhesively bonded joints in the current research group (Wu & Jenson, 2011; Wu & Zhao, 2012; Wu et al., 2003), this thesis work was targeted to study the free-edge stress variation, as well as the effect of interleafing on free-edge stresses, in composite laminates with finite width and general layup. Furthermore, a systematic stress-function variational method was formulated for the stress analysis of ABCJs.

In Chapter 3, a revised stress-function variation method was made to determine the free-edge stresses in composite laminates with arbitrary ply layup and finite width. This study was formulated on the basis of the robust, high-efficiency stress-function variational method (Yin 1994a, 1994b; Wu 2003, 2009) for free-edge stress analysis of composite laminates with infinite width, in which two Lehknitskii's stress functions were introduced at each ply surface and the free-edge stresses of composite laminates were determined via solving the resulting eigenvalue problem to satisfy the traction boundary conditions. A compact Matlab^{TM} computational code was designed for demonstration of the efficiency and effectiveness of the present method for free-edge stress analysis of composite laminates with finite width. In addition, scaling analysis was performed to examine the dependency of free-edge stresses upon the ply layup and thickness.

In Chapter 4, by varying the mechanical properties of the layers and the ply configuration, the present model was further utilized for free-edge stress analysis of composite laminates structured with interleafing layers. Critical interfacial stresses of the composite laminates were predicted, which were responsible to the mode Ⅰ and II delamination of the composite laminates.

In Chapter 5, variation of interfacial stresses in ABCJs was studied. The method was formulated based on the concepts introduced in Chapter 3 with relocating the traction boundary conditions.

In Chapter 6, summary on the present study and expectation on the future research of the topic were made.

3. STRESS-FUNCTION VARIATIONAL MEHTHOD FOR FREE-EDGE STRESS ANALYSIS OF COMPOSITE LAMINATE WITH FINITE LENGTH

3.1. Free-edge stress analysis of composite laminates using stress-function varational method

3.1.1. Introduction

Chapter 2 provides a brief review of the analytic and numerical methods for free-edge stress analysis of composite laminates. Two aspects of the methods, i.e., the computational efficiency and accuracy, are considered to be crucial. A number of numerical methods, e.g., FEA methods, can achieve excellent numerical accuracy in the cost of decreasing computational efficiency. Since the semi-analytical solutions are approaches that could well-balance the efficiency and accuracy, Yin (1994a, 1994b) proposed a method by introducing two Lehknitskii's stress potential functions and then determined the free-edge stresses in composite laminates via solving eigenvalue problems. By comparison with many other existing methods available in the literature, Yin's method was considered as one of the most efficient and accurate for free-edge stress analysis of composite laminates. Yin's method has two noticeable advantages superior to others, one is that all the traction boundary conditions (BCs) of the composite laminates are completely satisfied, and the other is that Yin's method is capable of evaluating out-of-plane shear stresses in high accuracy. However, when calculating interfacial stresses in composite laminates with the ply number more than 5 , the accuracy of Yin's method may drop and the related numerical process becomes unstable, due to the nearly ill-conditioned matrices used for evaluating the generalized eigenvalue problems.

In this chapter, a modified Yin's method is introduced for free-edge stress analysis of multilayered angle-ply composite laminate. Wu (2003) has revised the stress potential functions originally introduced by Yin (2014a & 2014b), and therefore the computational stability and efficiency of the resulting generalized eigenvalue problems have been improved significantly. Wu's computational studies on free-edge stress analysis were mainly focused on composite laminates with semi-infinite length (Wu, 2003 & 2009), which was based on the assumption that the laminate length was typically much larger than the laminate thickness. However, in many cases that the composite laminates carry the width is compatible with the laminate thickness, the effects of both free-edges of the composite laminates should be taken into account. Also, composite laminates were typically designed with finite width in industrial applications; however, many semi-analytic approaches available in the literature can only predict the interfacial and free-edge stresses in a composite laminate with semi-finite or infinite width. Therefore, substantial improvement of the currently available models for free-stress analysis of composite laminates is still desired in order to model the interlaminar stresses in composite laminates with arbitrary layup and width. In this chapter, firstly, Wu's theoretical studies on free-edge stress analysis (Wu, 2003 & 2009) was further extended to integrate all the traction boundary conditions for predicting free-edge stresses at any interfaces of composite laminates with arbitrary layup and finite width. Secondly, the improved Yin's and Wu's methods were further used for scaling analysis of stress variation along the free-edge and interface of composite laminates with varying laminate width.

3.1.2. Model formation

Consider a composite laminate under axial tensile load and two laminate ends in traction-free condition, as shown in Fig. 3.1. All plies of the laminate are treated as unidirectional lamina with a uniform thickness. Each lamina of the laminate is considered to be oriented in the (x,y)-plane. In contracted notations, at an arbitrary orientation angle of the ply, the constitutive law of each lamina can be expressed as

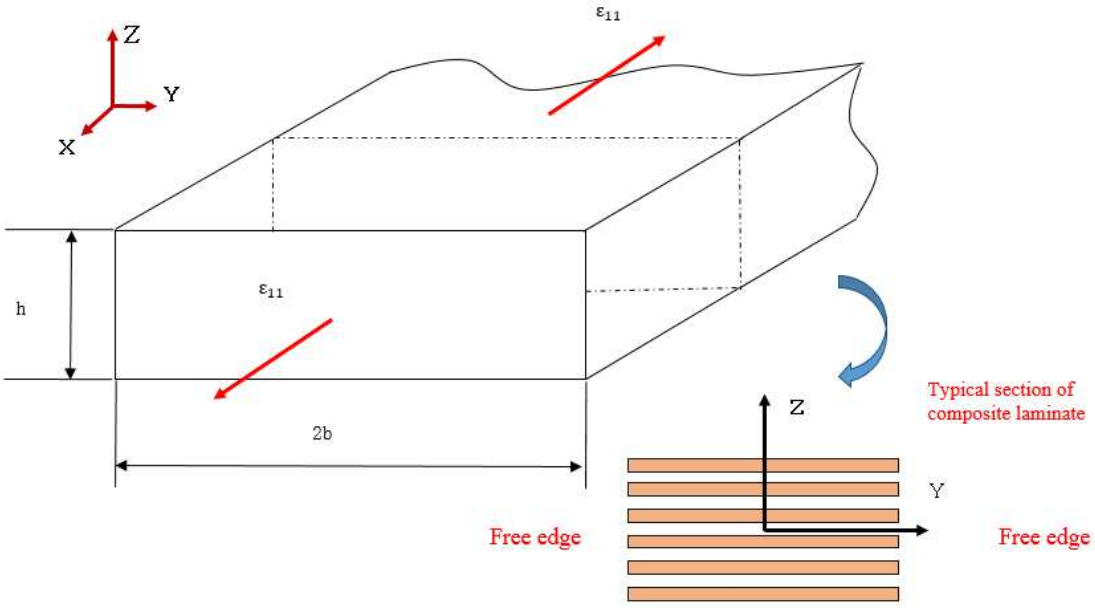

Figure 3.1. Geometry and coordinate system of free-edge laminate problem.

$$\begin{Bmatrix}\varepsilon_1\\ \varepsilon_2\\ \varepsilon_3\\ \varepsilon_4\\ \varepsilon_5\\ \varepsilon_6\end{Bmatrix}=\begin{bmatrix}S_{11} & S_{12} & S_{13} & 0 & 0 & S_{16}\\ S_{12} & S_{22} & S_{23} & 0 & 0 & S_{26}\\ S_{13} & S_{23} & S_{33} & 0 & 0 & S_{36}\\ 0 & 0 & 0 & S_{44} & S_{45} & 0\\ 0 & 0 & 0 & S_{45} & S_{55} & 0\\ S_{16} & S_{26} & 0 & 0 & 0 & S_{66}\end{bmatrix}\begin{Bmatrix}\sigma_1\\ \sigma_2\\ \sigma_3\\ \sigma_4\\ \sigma_5\\ \sigma_6\end{Bmatrix}+\begin{Bmatrix}\alpha_1\\ \alpha_2\\ \alpha_3\\ 0\\ 0\\ 0\end{Bmatrix}\Delta T \tag{3.1}$$

In the above, $[S_{ij}]$ is the transformed compliance matrix; $[\alpha_i]$ is the transformed thermal expansion coefficients; ΔT is term of the value of temperature change; the subscript indices (1, 2, 3) express (x, y, z), respectively.

In Eq. (3.1), the adopted contracted notations are

$$\sigma_1=\sigma_{11},\sigma_2=\sigma_{22},\sigma_3=\sigma_{33},\sigma_4=\sigma_{23},\sigma_5=\sigma_{13},\sigma_6=\sigma_{12}$$

$$\varepsilon_1=\varepsilon_{11},\varepsilon_2=\varepsilon_{22},\varepsilon_3=\varepsilon_{33},\varepsilon_4=2\varepsilon_{23},\varepsilon_5=2\varepsilon_{13},\varepsilon_6=2\varepsilon_{12} \tag{3.2}$$

In the case of a plane-strain composite lamina under uniaxial tension ε_1 along x-direction, solving Eq. (3.1) leads to the axial stress σ_1 as

$$\sigma_1=\frac{\varepsilon_1-\alpha_1\Delta\mathrm{T}-S_{ij}\sigma_j}{S_{11}}\ ,(\mathrm{j}=2,3,6) \tag{3.3}$$

Then, by applying the generalized Hooke's law, the ε_i can be evaluated as

$$\varepsilon_i=S'_{ij}\sigma_j+\frac{S_{i1}S_{1j}}{S_{11}}\varepsilon_1+\alpha'_i\Delta T,(i,j=2,3\ldots,6) \tag{3.4}$$

where S'_{ij} and α'_i are expressed as following

$$S'_{ij}=S_{ij}-\frac{S_{i1}S_{1j}}{S_{11}},\quad \alpha'_i=\alpha_i-\frac{S_{1i}}{S_{11}}\alpha_1 \tag{3.5}$$

In Yin's formulation (1994a & 1994b), two Leknitiskii's stress potentials $F(y,z)$ and $\psi(y,z)$ (Lekhnitskii, 1968) are introduced for the problem due to the laminate is in a state of plane strain. Thus, stress components in the i-th ply can be expressed in terms of $F(y,z)$ and $\psi(y,z)$ such that

$$\sigma_2^i = F_{,zz}^i, \sigma_3^i = F_{yy}^i, \sigma_4^i = -F_{,yz}^i \tag{3.6a}$$

$$\sigma_6^i = \psi_{,y}^i,\ \sigma_5^k = -\psi_{,z}^i \tag{3.6b}$$

Besides, since the composite laminate is in the state of traction-free at two edges and the top and bottom surfaces, the corresponding boundary conditions of the problem, as shown in Fig. 3.1, can be listed in Eq. (3.7a, b) as following

$$\sigma_4 = \sigma_5 = \sigma_6 = 0, (y = -b, y = b) \tag{3.7a}$$

$$\sigma_3 = \sigma_4 = \sigma_5 = 0.\ \left(z = \pm\frac{h}{2}\right) \tag{3.7b}$$

Within the framework of classical plate theory, each in-plane stress varies linearly across the plate thickness, and this feature is still valid approximately in each ply of a composite laminate. Hence, in the *i*-th ply, the stress function *F* can be approached by a polynomial function of degree three in η-direction, and ψ can be approached by another polynomial function of degree two in η-direction. By modifying Yin's work (Yin, 1994a & 1994b; Wu, 2003 & 2009), Wu assumed that $t^2F_i(y)$ and $t\psi_i(y)$ are the stress functions at the interface $z = z_i$, meanwhile $t^2F_{i-1}(y)$ and $t\psi_{i-1}(y)$ are the ones at the interface $z = z_{i-1}$, where *t* is the thickness of the ply. Hence, expressions of the compatible in-plane stress functions can be approached using a cubic-polynomial approximation in the *i*-th ply as

$$F^{(i)}(y,\eta) = (1 - 3\eta^2 + 2\eta^3)t^2F_{i-1}(y) + (\eta - 2\eta^2 + \eta^3)t^2G_{i-1}(y) + (3\eta^2 - 2\eta^3)t^2F_i(y) + (\eta^3 - \eta^2)t^2G_i(y). \quad (i = 1,2 \ldots\ldots, n+1) \tag{3.8}$$

Where a nondimensional thickness coordinate η in each (*i*-th) laminae is to be introduced and defined by

$$\eta = \frac{z - z_{i-1}}{z_i - z_{i-1}} \tag{3.9}$$

In Eq. (3.8), the $G_i(y)$ and $G_{i-1}(y)$ are the first derivatives of $F_i(y)$ and $F_{i-1}(y)$ with respect to *y*. Furthermore, based on the traction-free boundary conditions at the top and bottom surfaces of the laminate, $F_0(y) = G_0(y) = F_{n+1}(y) = G_{n+1}(y) = 0$.

In addition, the out-of-plane stress function in the *i*-th ply can be expressed by a quadric polynomial approximation as

$$\psi^{(i)}(y,\eta) = (1-\eta^2)t\psi_{i-1}(y) + \eta^2 t\psi_i(y) + (\eta - \eta^2)tH_{i-1}(y) \quad (i = 1,2,\dots,n+1) \tag{3.10}$$

In Eq. (3.10), across the interface, $H_{i-1}(y)$ is generally discontinuous, since it is the first derivative of $G_i(y)$ at the upper side of the same interface. In addition, $\psi_0(y) = \psi_{n+1}(y) = 0$ based on the traction-free conditions at the top and bottome surfaces of the laminate.

These stress potential functions $F(y,z)$ and $\psi(y,z)$ are obtained and modified from Yin's approach (1994a, 1994b) by Wu (2003 & 2009). The modifications of both of the functions improved stability of evaluation and efficiency of solving the generalized eigenvalue problems even for a large matrix rank.

By using theorem of maximum complementary strain energy, the governing equation of the composite laminate can be obtained as the mathematical variation of the elastic strain energy of the system as

$$\delta U = \iint_{\Omega} \varepsilon \delta\sigma dy d\,\eta = \iint_{\Omega} \left[\sigma_i S'_{ij}\delta\sigma_j + \left(\frac{\varepsilon_1 S_{j1}}{S_{11}} + \alpha'_i\right)\delta\sigma_j\right] dy d\,\eta = 0. (i,j = 2,3,\dots,6) \tag{3.11}$$

By substituting (3.9) and (3.10) into (3.11) and then integrating by parts and by ply, a system of ordinary differential equations (ODEs) is obtained (Wu, 2003 & 2009):

$$\{\delta Y\}^T \left\{ \left[W t^4 \frac{d^4}{dy^4} + V t^2 \frac{d^2}{dy^2} + U \right] \{Y\} - \{b\} \right\} = \{0\} \tag{3.12}$$

where {Y} is consisted of

$$Y_i = F_i(y),\ Y_{n+i} = G_i(y) \tag{3.13a}$$

$$Y_{i+2n} = \psi_i(y), (i = 1,2, \dots, n) \tag{3.13b}$$

$$Y_{i+3n+1} = H_i(y), (i = 0,1,2, \dots, n) \tag{3.13c}$$

where {b} is the column related to the external mechanical and thermal loads, which is assembled from $\{b^e\}$ of each ply. ***W***, ***V***, **and *U*** as the global coefficient matrices are assembled from the element matrices W^e U^e and V^e in each ply, which are constant real symmetric square matrices as shown below.

$$b^e = \left\{0, \quad 0, \quad -\frac{S'_{12}\varepsilon_1}{S'_{11}}, \quad \frac{S'_{12}\varepsilon_1}{S'_{11}}, \quad -\frac{S'_{12}\varepsilon_1}{S'_{11}}, \quad \frac{S'_{12}\varepsilon_1}{S'_{11}}, \quad 0\right\}^T \tag{3.14}$$

$$W^e = S'_{33}\begin{bmatrix} \frac{13}{35} & & & Symmetric \\ \frac{9}{70} & \frac{13}{35} & & \\ \frac{11}{210} & \frac{13}{420} & \frac{1}{105} & \\ -\frac{13}{420} & -\frac{11}{210} & -\frac{1}{140} & \frac{1}{105} \end{bmatrix} \tag{3.15}$$

$$U^e = \begin{bmatrix} 12S'_{22} & & & & & & \\ -12S'_{22} & 12S'_{22} & & Symmetric & & & \\ 6S'_{22} & -6S'_{22} & 4S'_{22} & & & & \\ 6S'_{22} & -6S'_{22} & 2S'_{22} & 4S'_{22} & & & \\ -2S'_{26} & 2S'_{26} & 0 & -2S'_{26} & \frac{4S'_{66}}{3} & & \\ 2S'_{26} & -2S'_{26} & 0 & 2S'_{26} & -\frac{4S'_{66}}{3} & \frac{4S'_{66}}{3} & \\ -2S'_{26} & 2S'_{26} & -S'_{26} & -S'_{26} & \frac{S'_{66}}{3} & -\frac{S'_{66}}{3} & \frac{S'_{66}}{3} \end{bmatrix} \tag{3.16}$$

$$V^e = \begin{bmatrix} -\frac{6}{5}(S'_{23}+S'_{44}) & & & & & & \text{Symmetric} \\ \frac{6}{5}(S'_{23}+S'_{44}) & -\frac{6}{5}(S'_{23}+S'_{44}) & & & & & \\ -\frac{1}{10}(11S'_{23}+S'_{44}) & \frac{1}{10}(S'_{23}+S'_{44}) & -\frac{2}{15}(S'_{23}+S'_{44}) & & & & \\ -\frac{1}{10}(S'_{23}+S'_{44}) & \frac{1}{10}(11S'_{23}+S'_{44}) & \frac{1}{30}(11S'_{23}+S'_{44}) & -\frac{2}{15}(S'_{23}+S'_{44}) & & & \\ -\frac{1}{10}(S'_{36}+S'_{45}) & -\frac{7}{10}(S'_{36}+S'_{45}) & -\frac{1}{15}(S'_{36}+S'_{45}) & \frac{1}{10}(S'_{36}+S'_{45}) & \frac{-8S'_{55}}{15} & & \\ \frac{3}{10}(S'_{36}+S'_{45}) & \frac{1}{10}(7S'_{36}-3S'_{45}) & \frac{1}{15}(S'_{36}+S'_{45}) & -\frac{1}{10}(S'_{36}+S'_{45}) & \frac{-2S'_{55}}{15} & \frac{-S'_{55}}{5} & \\ \frac{1}{5}(S'_{36}+S'_{45}) & -\frac{1}{5}(S'_{36}+S'_{45}) & \frac{1}{60}(S'_{36}+S'_{45}) & \frac{1}{60}(S'_{36}+S'_{45}) & \frac{-7S'_{55}}{60} & \frac{-S'_{55}}{20} & \frac{-S'_{55}}{35} \end{bmatrix} \quad (3.17)$$

where each matrix is related to a variable column:

W^e is related to $\left[F_i^{(4)},\ F_{i-1}^{(4)},\ G_i^{(4)},\ G_{i-1}^{(4)}\right]^T$;

U^e is related to $\left[F_i^{(0)},\ F_{i-1}^{(0)},\ G_i^{(0)},\ G_{i-1}^{(0)},\ \Psi_i^{(0)},\ \Psi_{i-1}^{(0)},\ H_i^{(0)}\right]^T$;

V^e is related to $\left[F_i^{(2)},\ F_{i-1}^{(2)},\ G_i^{(2)},\ G_{i-1}^{(2)},\ \Psi_i^{(2)},\ \Psi_{i-1}^{(2)},\ H_i^{(2)}\right]^T$;

b^e is related to $[F_i,\ F_{i-1},\ G_i,\ G_{i-1},\ \Psi_i,\ \Psi_{i-1},\ H_i]^T$.

The coefficient matrix $\boldsymbol{W}$ of the operator $\frac{d^4}{dx^4}$ has the nontrivial elements only in a $2n \times 2n$ square submatrix in the upper left corner. If $\{Y\}$ is satisfied the Euler-Lagrange equation as shown below, Eq. (3.12) will be satisfied for arbitrary variations $\delta F_i, \delta G_i, \delta\psi_i$ and δH_i.

$$\left[Wt^4\frac{d^4}{dy^4} + Vt^2\frac{d^2}{dy^2} + U\right]\{Y\} = \{b\} \tag{3.18}$$

Based on the traction free boundary conditions:

$$H_0 = 0, F_i = F'_i = G_i = G'_i = 0 \tag{3.19a}$$

$$\psi_i = H_i = 0, (\mathrm{i} = 1,2,3,\ldots,\mathrm{n}) \text{ at } y = -b \text{ and } y = b \tag{3.19b}$$

Eq. (3.18) is a set of nonhomogeneous ODEs which can be solved by using the method of eigenfunction method. Hence, firstly, assume $\{Y\} = \{X_0\}e^{\frac{\lambda y}{t}}$ be the solution to the set of homogenous ODEs corresponding to Eq. (3.18) (by setting $\{b\}$=0), which leads to a generalized eigenvalue problem:

$$[W\lambda^4 + V\lambda^2 + U]\{X_0\} = \{b\} \tag{3.20}$$

Secondly, the particular solution to Eq. (3.18) can be expressed as

$$\{Y_0\} = U^{-1}\{b\} \tag{3.21}$$

The particular solution (3.21) can be understood as the stress potential functions of an finite laminate (without edges) subjected to exactly the same uniaxial tensile strain along *x*-direction. To further solve the eigenvalue problem, $\boldsymbol{V}$ and $\boldsymbol{U}$ are divided into 4 sub-matrices, respectively, as shown

$$V = \begin{bmatrix} V_{11(2n\times 2n)} & V_{12[(2n+1)\times 2n]} \\ V_{12}^T & V_{22[(2n+1)\times(2n+1)]} \end{bmatrix}, \quad U = \begin{bmatrix} U_{11(2n\times 2n)} & U_{12[(2n+1)\times 2n]} \\ U_{12}^T & U_{22[(2n+1)\times(2n+1)]} \end{bmatrix}.$$

Let $\{X_0\} = \begin{Bmatrix} X_{10} \\ X_{20} \end{Bmatrix}$, where $\{X_{10}\} = \{F_1, F_2, \dots, F_n, G_1, G_2, \dots, G_n\}^T$ and

$\{X_{20}\} = \{\Psi_1, \Psi_2, \dots, \Psi_n, H_1, H_2, \dots, H_n\}^T$.

In order to convert the resulting eigenvalue problem to a generalized eigenvalue problem, an auxiliary vector $\{X_1\} = \lambda^2\{X_{10}\}^T$ is introduced, and then the Eq. (3.21) can be expressed as shown below

$$A\begin{Bmatrix} X_{10} \\ X_{20} \\ X_1 \end{Bmatrix} = \lambda^2 B\begin{Bmatrix} X_{10} \\ X_{20} \\ X_1 \end{Bmatrix} \tag{3.22}$$

where

$$A_{(6n\times 2)\times(6n\times 2)} = \begin{bmatrix} U_{11} & U_{12} & V_{11} \\ U_{12}^T & U_{22} & V_{12}^T \\ 0_{2n\times 2n} & 0_{2n\times(2n+1)} & I_{2n\times 2n} \end{bmatrix},$$

$$B_{(6n\times 2)\times(6n\times 2)} = \begin{bmatrix} 0_{2n\times 2n} & -V_{12} & W \\ 0_{(2n+1)\times 2n} & V_{22} & 0_{(2n+1)\times 2n} \\ -I_{2n\times 2n} & 0_{2n\times(2n+1)} & 0_{2n\times 2n} \end{bmatrix}.$$

In the matrices, **I** and **0** are the diagonal unite matrix and zero matrix, respectively. Therefore, the general solution of Eq. (3.18) can be expressed as

$$\{Y\} = \sum_{i=1}^{6n+1}\left(\alpha_i^{(1)} e^{\frac{\lambda_i y}{t}} + \alpha_i^{(2)} e^{\frac{-\lambda_i y}{t}}\right)\Phi_i + Y_0, (-b \le y \ge b) \qquad (3.23)$$

where λ_i $(i = 1, 2, \dots, 6n+1)$ are the eigenvalues; $\Phi_i (i = 1, 2, \dots, 6n+1)$ are the corresponding eigenvectors; $\alpha_i^{(1)}$ and $\alpha_i^{(2)}$ $(i = 1, 2, \dots, 6n+1)$ are 12*n*+2 unknowns, which may be determined by the traction-free conditions aforementioned. At the end, the $\{Y\}$ will provide all of the stress components via combining with Eqs. (3.13) and (3.6).

3.1.3. Validation of the polynomial stress functions

Below gives the brief derivation of the polynomials specified above. First introduce the general cubic expression of the $F^{(i)}$ function as

$$F^{(i)}(y,\eta) = (A_0 + A_1\eta + A_2\eta^2 + A_3\eta^3)t^2 F_{i-1}(y) + (B_0 + B_1\eta + B_2\eta^2 + B_3\eta^3)t^2 G_{i-1}(y) + (C_0 + C_1\eta + C_2\eta^2 + C_3\eta^3)t^2 F_i(y) + (D_0 + D_1\eta + D_2\eta^2 + D_3\eta^3)t^2 G_i(y),\ (i = 1,2, \dots . n+1) \qquad (3.24)$$

Due to the stress continuity across the interfaces as aforementioned, it reads$F^{(i)}(y,\eta) = F_{i-1}(y)$ at $\eta = 0$ and $F^{(i)}(y,\eta) = F_i(y)$ at $\eta = 1$, which leads tothe following relations:

$$A_0 = 1, B_0 = C_0 = D_0 = 0 \tag{3.25a}$$

$$A_0 + A_1 + A_2 + A_3 = 1 \tag{3.25b}$$

$$B_1 + B_2 + B_3 = 0 \tag{3.25c}$$

$$C_1 + C_2 + C_3 = 0 \tag{3.25d}$$

$$D_1 + D_2 + D_3 = 0 \tag{3.25e}$$

What we should be noticed that $G(y)$ is the derivative of $F(y,\eta)$ in η-direction. So in the *i*-th layer, $F^{(i)}(y,\eta)$ can be expressed as

$$\frac{d\eta}{dy}\frac{dF^{(i)}(y,\eta)}{d\eta} = G^i(y,\eta) \tag{3.26}$$

Then

$$\frac{d\mathrm{F}^{(i)}(\mathrm{x},\eta)}{d\eta} = G^i(y,\eta) \tag{3.27}$$

On the other hand, $\psi^{(i)}(y,\eta)$ and $H^i(y,\eta)$ can be expressed as

$$\frac{d\psi^{(i)}(y,\eta)}{d\eta} = H^i(y,\eta) \tag{3.28}$$

By considering at $z = z_i$ and $z = z_{i-1}$ interfaces, the shear stresses can be determined as $\tau_{yz}^{i} = -G_i(y)'$ and $\tau_{yz}^{i-1} = -G_{i-1}(y)'$. And the stress field in the *i*-th layer satisfies the equilibrium equation such that $\tau_{yz}^{i} = -F_{,yz}$.

The equation can be formulated as

$$F^{(i)}(y,\eta)_{,xy} = \left(A_1 + 2A_2\eta + 3A_3\eta^2\right)tF_{i-1}(y)' + \left(B_1 + 2B_2\eta + 3B_3\eta^2\right)tG_{i-1}(y)' +$$

$$\left(C_1 + 2C_2\eta + 3C_3\eta^2\right)tF_i(y)' + \left(D_1 + 2D_2\eta + 3D_3\eta^2\right)tG_i(y)', \ (i = 1,2 \ldots\ldots n+1) \tag{3.29}$$

Based on the stress continuity conditions aforementioned, we can find that at $\eta = 0$, $F^{(i)}(y,0)_{,yz} = G_{i-1}(y)'$; at $\eta = 1, F^{(i)}(y,1)_{,yz} = G_i(y)'$. Some of the coefficients can be determined as

$$B_1 = 1, A_1 = C_1 = D_1 = 0 \tag{3.30a}$$

$$2A_2 + 3A_3 = 0 \tag{3.30b}$$

$$B_1 + 2B_2 + 3B_3 = 0 \tag{3.30c}$$

$$2C_2 + 3C_3 = 0 \tag{3.30d}$$

$$2D_2 + 3D_3 = 1 \tag{3.30e}$$

Then, we can determine the rest of coefficients as

A_2=-3, A_3=2, B_2=-2, B_3=1, C_2=3, C_3=-2, D_2=-1, D_3=1

Similarly, we can also prove the other polynomial functions by an additional condition mentioned above as

$$H_{i-1}(x) = \psi^{(i)}(x,0)_{,y} \tag{3.31}$$

The validation of the stress potential functions was straighforward, due to the stress continuity conditions and the relationships between stresses and the stress potential functions.

3.1.4. Examples for free-edge stress analysis of composite laminates with finite length

Due to the importance of estimating the free-edge stresses of composite laminates for layup design and strength/failure analysis, the numerical scheme introduced above can be applied for the free-edge stress evaluation and comparison for any multilayered anisotropic laminates. Hereafter, several examples are demonstrated to show the free-edge stress variations in

composite laminates by using the present method. The material properties of a graphite/epoxy composite lamina are given as

E_1=20MPa

E_2= E_3=2.1MPa

G_1=$G2$= G_3=0.85MPa

$\nu_1 = \nu_2 = \nu_3 = 0.21$

$\alpha_1 = 0.22 \times 10^{-6}$ m/m /℃,

$\alpha_2 = 15.2 \times 10^{-6}$ m/m /℃,

where 1, 2 and 3 relate to the directions of the reinforcing fibers, the transverse and thickness directions in each ply, respectively. The thickness of each ply is assumed as 1 mm; the width of the laminate is assumed as16 mm; the value of the specified constant strain along *x*-direction is 0.02.

1) $[0/90]_s$

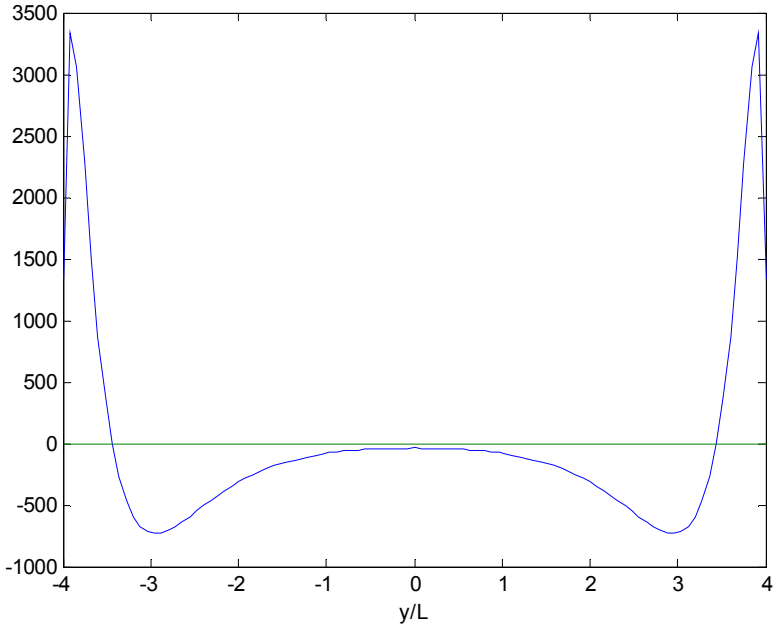

Figure 3.2. Variation of σ_{zz} along the $0^o/90^o$ interface in $[0^o/90^o]$s laminate.

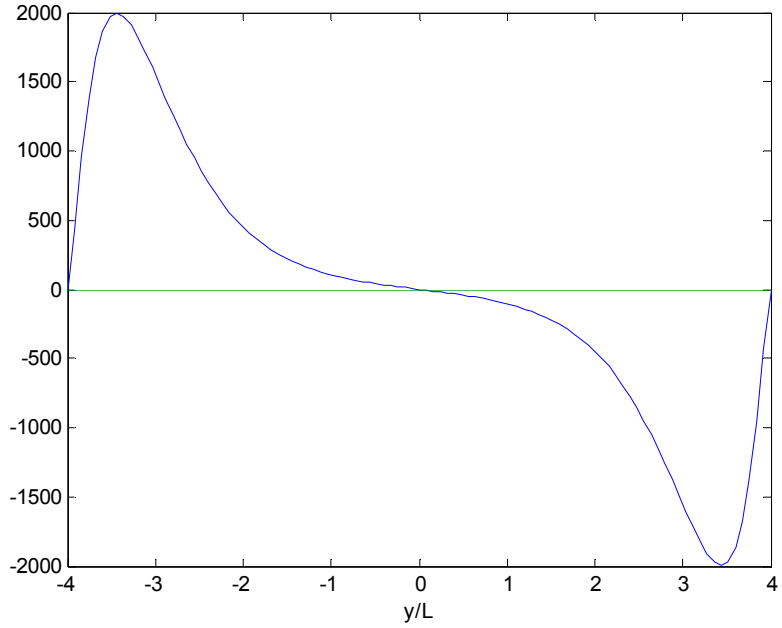

Figure 3.3. Variation of τ_{yz} along the $0^o/90^o$ interface in $[0^o/90^o]_s$ laminate.

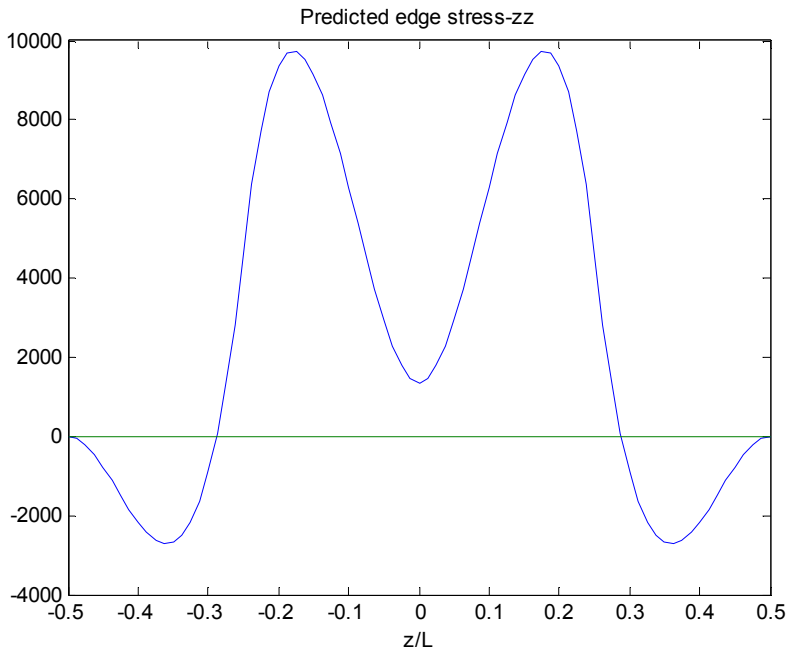

Figure 3.4. Variation of σ_{zz} at free edge along the thickness of $[0^o/90^o]_s$ laminate.

2) $[45^o/-45^o]_s$

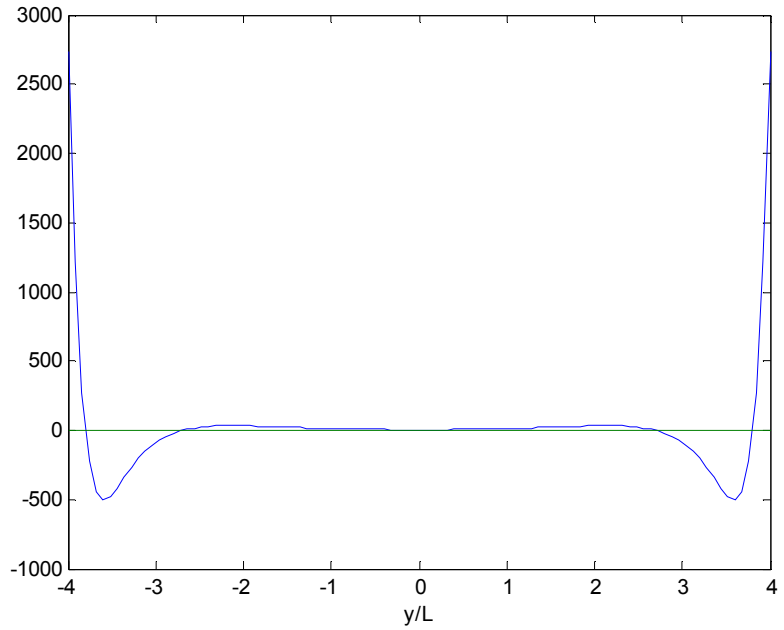

Figure 3.5. Variation of σ_{zz} along the $45^o/-45^o$ interface in $[45^o/-45^o]_s$ laminate.

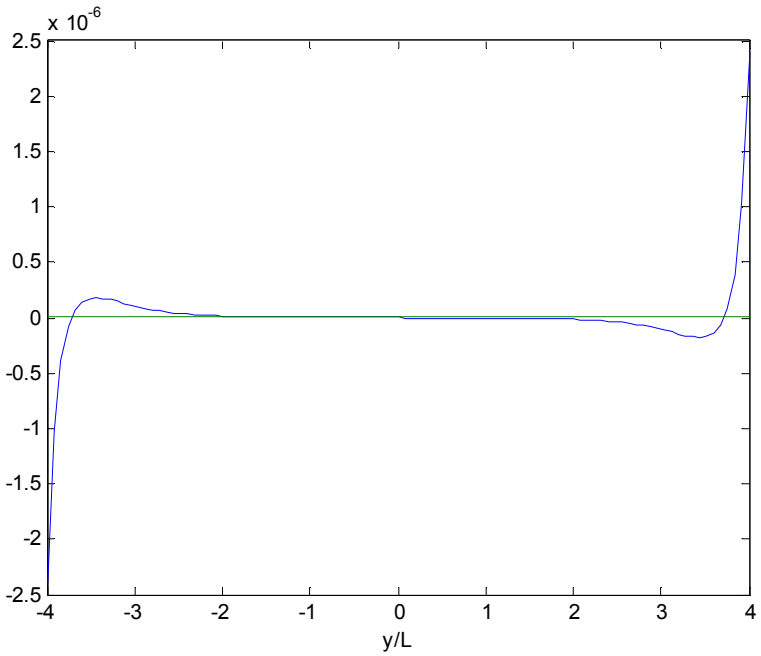

Figure 3.6. Variation of τ_{xz} along 45º/-45º interface in [45º/-45º]s laminate.

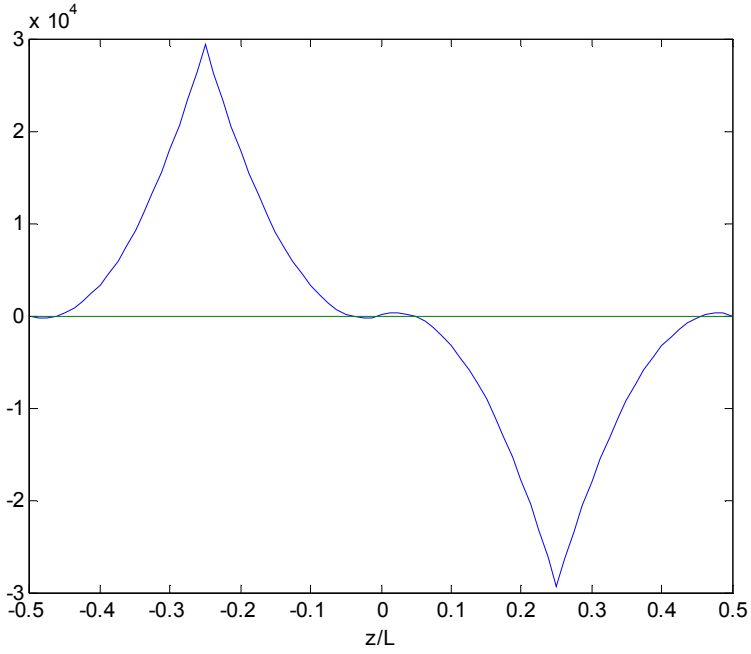

Figure 3.7. Variation of τ_{xz} at free edge along the thickness of $[45º/-45º]_s$ laminate.

3) $[45^o/-45^o/0^o/90^o]_s$

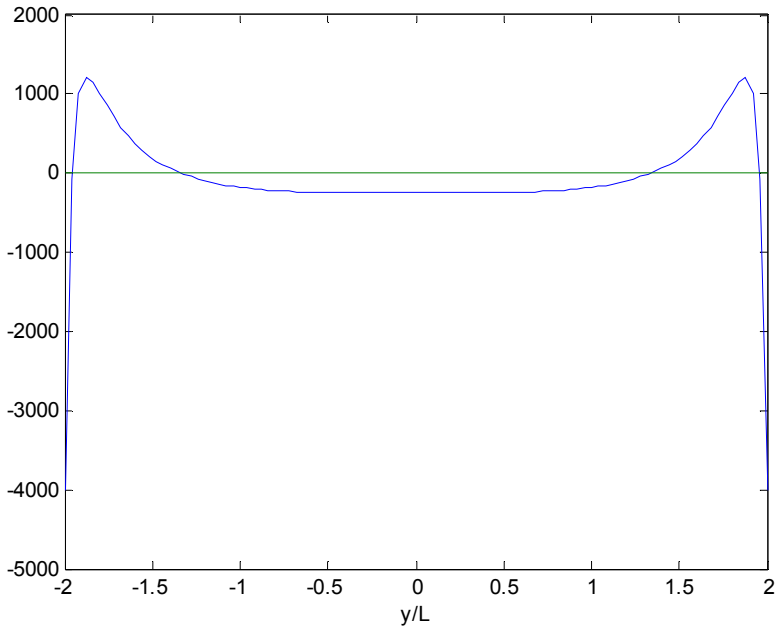

Figure 3.8. Variation of σ_{zz} along the $90^o/90^o$ interface of $[45^o/-45^o/0^o/90^o]_s$ laminate.

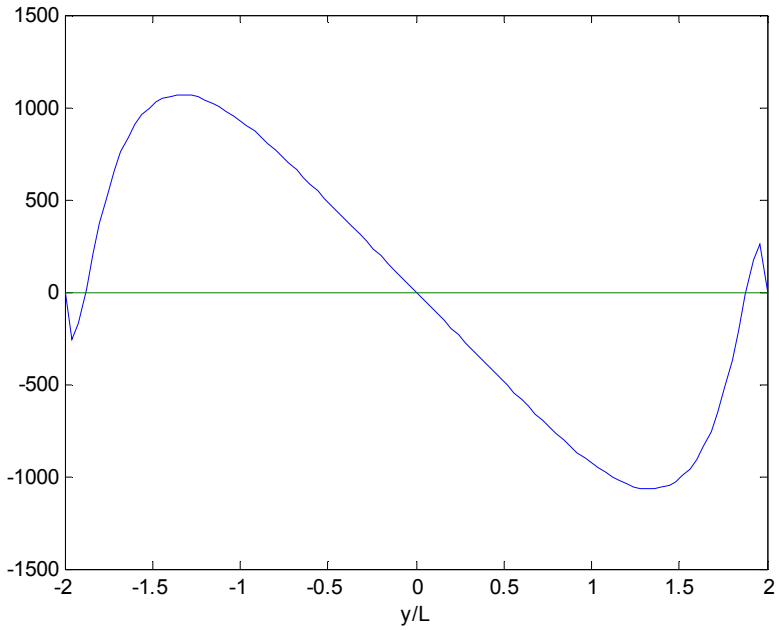

Figure 3.9. Variation of τ_{yz} along the $90^o/90^o$ interface of $[45^o/-45^o/0^o/90^o]_s$ laminate.

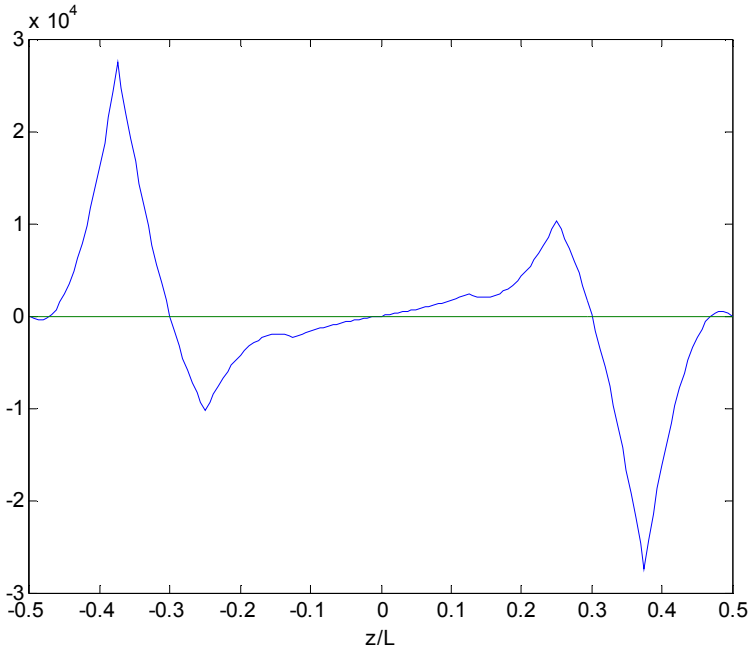

Figure 3.10. Variation of τ_{xz} at free edge along the thickness of $[45^o/-45^o/0^o/90^o]_s$ laminate.

4) $[45^o/-45^o/0^o/90^o]_{2s}$

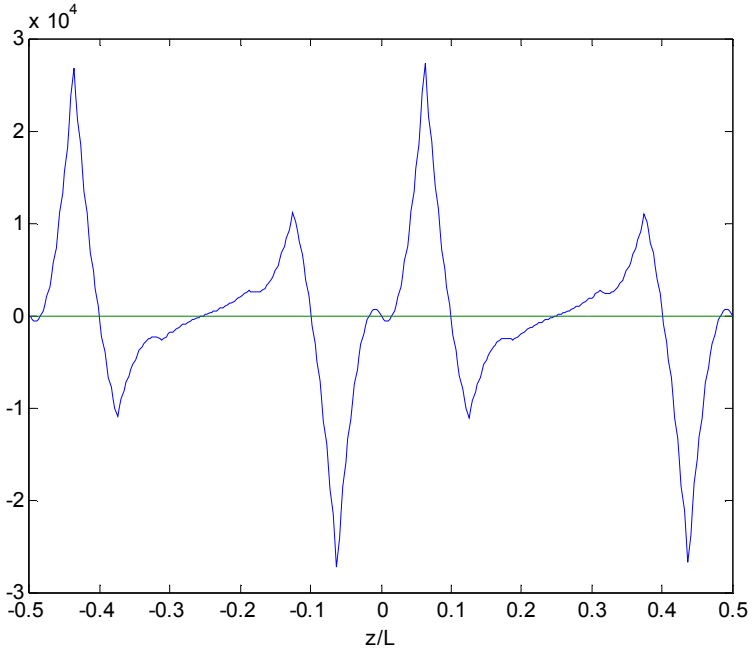

Figure 3.11. Variation of τ_{xz} at free edge along thickness of $[45^o/-45^o/0^o/90^o]_{2s}$ laminate.

5) $[0^o/45^o/\text{-}45^o/0^o]_{2s}$

Free-edge stress prediction as shown in Fig. 3.12 provides the approximate in-plane and out-of-plane stress variations at the $45^\circ/-45^\circ$ interface of the laminate, and the distributions of σ_{zz} and σ_{xz} along one of the free edges across the thickness of the laminate.

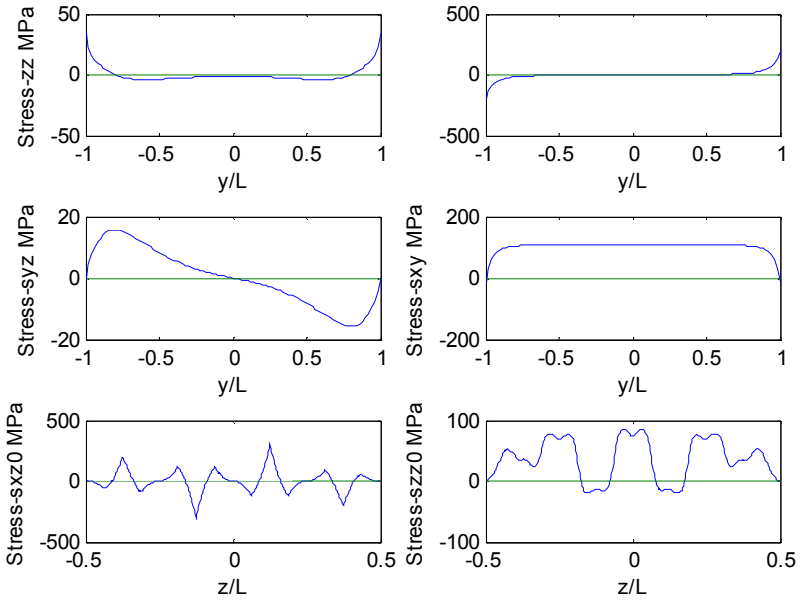

Figure 3.12. Stresses variation long $45^\circ/-45^\circ$ interface and at free edge of the laminate.

Above results are very close to the previous researches given by Pipes and Pagano (1970), Yin (1994a& 1994b), and Wu (2003 & 2009).

3.2. Validation by FEA

In the literature, almost all the analytic and semi-analytical methods can only predict interfacial stresses in semi-finite laminates. Thus, in the present case of free-edge stress analysis

of finite-wide composite laminates, it is feasible to validate the present model by means of FEM. In this section, (ANSYS™ version 14.5) was applied for the validation. For the convenience of the numerical validation of the present stress-function variational method for free-edge stress analysis of finite-width laminates, a cross-ply composite laminate was considered. The material properties of the uniaxial composite ply are given below.layup: $[90^o/0^o]_s$;

Width = 16 mm, ply thickness = 1 mm

E_1 = 32 GPa,

$E_2 = E_3$= 10.4GPa,

$\upsilon_{12} = \upsilon_{13}$= 0.34,

υ_{23} = 0.5,

$G_{12} = G_{13}$ =3.5,

G_{23} = 4.7 GPa;

By evoking the symmetric structure of the cross-ply laminate under consideration, quarter-symmetric part of this laminate was modeled in the FEM simulation (ANAYS™). Eight-node element, PLANE183, and uniform quadrilateral meshes were adopted in the simulation. Besides, assume that the laminate was subjected to a uniaxial tensile strain, i.e., ε11= 0.02, along x-direction. In order to simulate the loading condition of this cross-ply composite laminate, an equivalent thermal-loading was generated to substitute the uniaxial tensile strain (Wu, 2003). The coefficients of orthotropic thermal expansion of the laminate are set as (1, 0, 0) referred to in x, y, and z direction, respectively. The thermal loading, as temperature change, is +0.02℃. The FEM results were compared with the interfacial stresses at the first interface predicted by current stress-function variational model. Due to the unique nature of the cross-ply composite laminate,

only the nontrivial peeling stress σ_{zz} and in-plane shear stress τ_{yz} were considered and plotted. The numerical results of the stress components, σzz and τyz of the cross-ply composite laminate predicted by FEM are as shown in Figs. 3.13-3.17. It can be clearly observed that variations of the interfacial stresses τ_{yz} and σ_{zz} from the present semi-analytic stress-function variational model are very close to those predicted by means of FEM. ANSYSTM-based FEM method shows that the maximum shear stress exists close to the free edges. However, the numerical results based on FEM do not satisfy the shear-free condition at the free edges due to mismatch of the material properties across the interface and existence of stress singularity at the free-edges. As a result, the stress-function variational method for laminate with finite width is capable of satisfying the multiple free-shear boundary conditions in composite laminates. Obvious shear stress concentration can be detected near both the free edges of the laminate as shown in Fig. 3.14. Furthermore, the present numerical simulations indicate that the shear and peeling stresses carry the similar varying tendency at the interface far from the edges. However, the some deviation t of the peeling stress is noticed at the free edge. Such a high peeling stress concentration at the free edges dominate the debonding failure of the composite laminate.

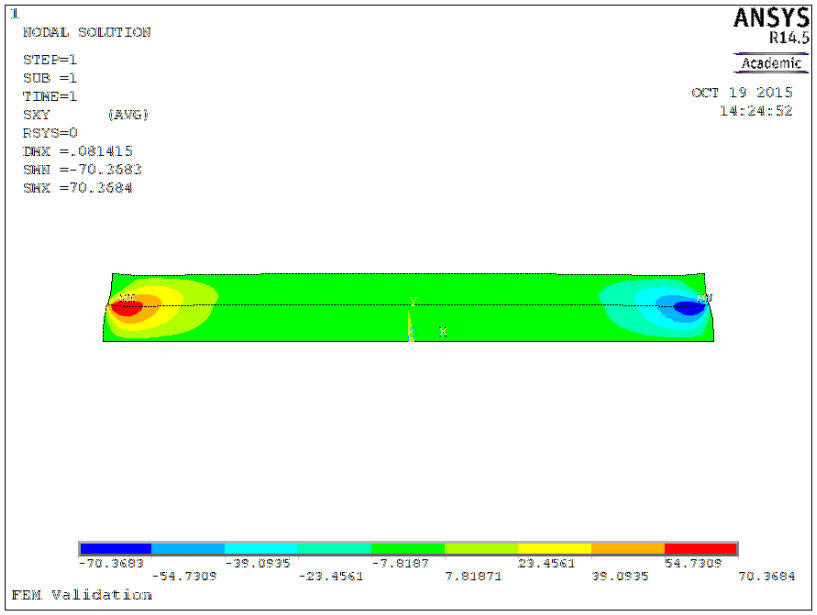

Figure 3.13. Variation of τ_{yz} in the upper half cross-section of the $[0^o/90^o]_s$ laminate.

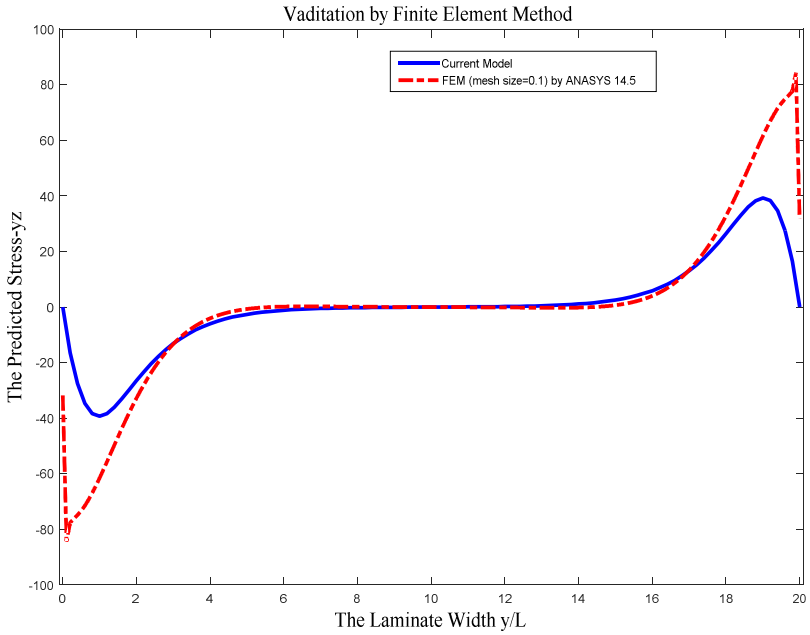

Figure 3.14. Variation of the interfacial stress τ_{yz} at $0^o/90^o$ interface based on FEA (ANSYS®) and the present semi-analytic stress-function variational model.

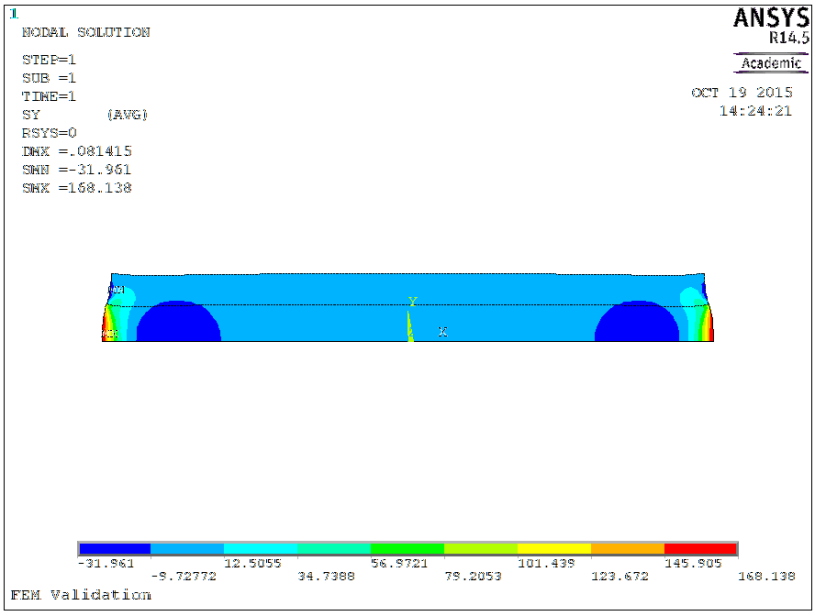

Figure 3.15. Variation of σ_{zz} in the upper half cross-section of the $[0^o/90^o]_s$ laminate.

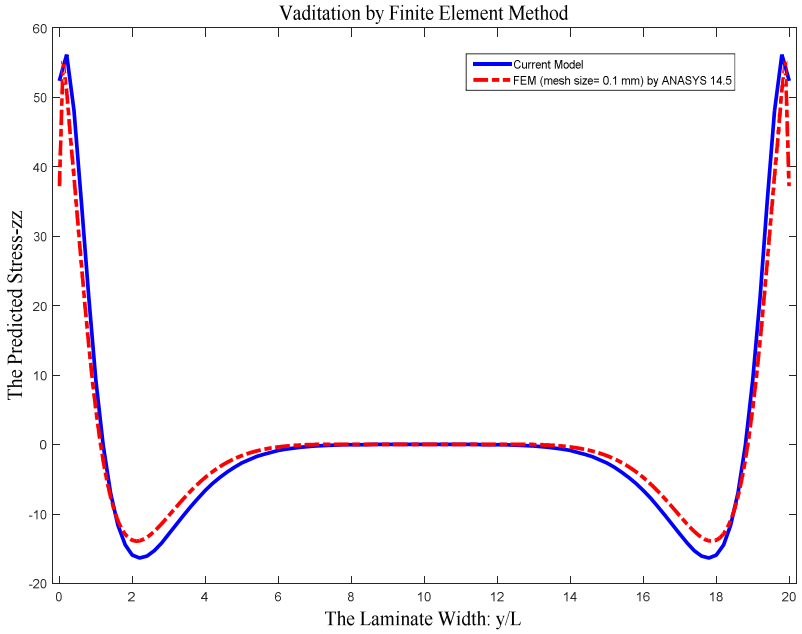

Figure 3.16. Variation of the interfacial stress σ_{zz} at $0^o/90^o$ interface based on FEA (ANSYS®) and the present semi-analytic stress-function variational model.

3.3. Scaling analysis of free-edge stresses in multilayered anisotropic laminates

Subjected to external loads, composite laminates exhibit much more complicated stress and strain fields due to their layered anisotropic structures. Given a composite laminate under in-plane stressing, the ratio of the laminate width over thickness may also affect the mechanical performance of the laminate. In this section, the stress-function variational method formulated in this chapter is further used to investigate the variation of the free-edge stresses in composite laminates with the varying ratio of laminate width over thickness. Herein, the out-of-plane shear stress τ_{xz} and in-plane stress σ_{zz} along the free-edge and their distribution along a given interface of the laminate are considered. For composite laminates, the interlaminar strength and fracture toughness are much lower than those of in-plane ones. Therefore, delamination and composite failure mostly first occur along laminate interfaces. Thus, the stress distribution of σ_{zz} and τ_{xz} is dominating factor for laminate design. The composite laminate considered in this study is assumed as glass-fiber/epoxy composite laminates made of unidirectional plies of the mechanical properties given as

$E_1 = 40$ GPa,

$E_2 = E_3 = 8$ GPa,

$\upsilon_{12} = \upsilon_{13} = \upsilon_{23} = 0.3$,

$G_{12} = G_{13} = G_{23} = 4$ GPa;

where 1, 2, and 3 refer to the fiber, transverse and thickness directions, respectively. The layup of the laminate is $[45/-45]_s$, and the geometry of plies is shown in Fig. 13:

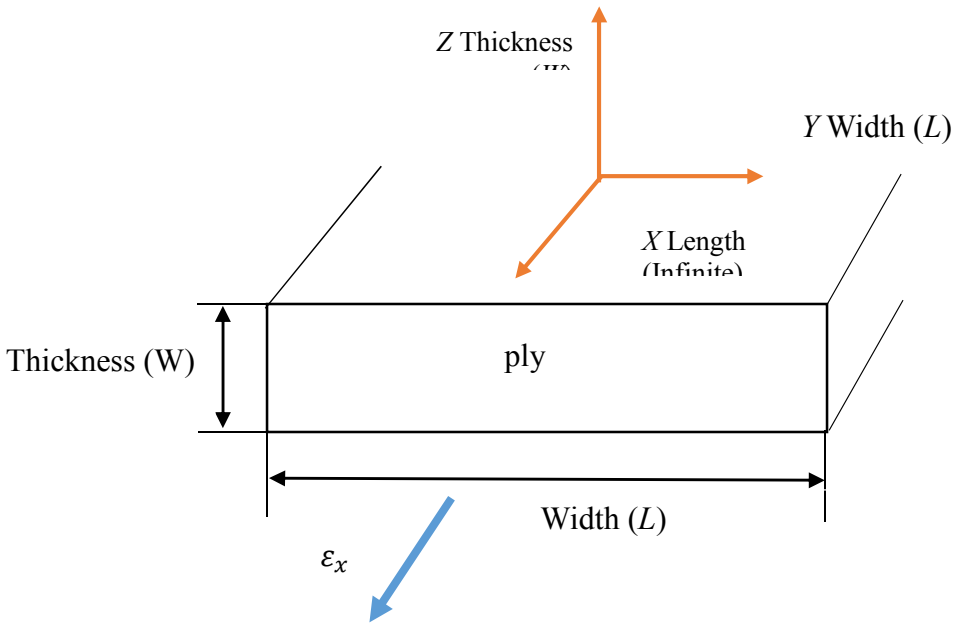

Figure 3.17. The geometry of the ply of the glass-fiber/epoxy composite laminate.

It can be found from Fig. 3.18 and 3.19 that as the ratio of *W/t* varying from 0.2 to 1, the peak value of stresses σ_{zz} and τ_{xz} at the interface increases correspondingly. In addition, Figures 20 and 21 shows the variation of free-edge stresses σ_{zz} and τ_{xz} across the laminate thickness, and it is noticed that the peak values of σ_{zz} and τ_{xz} appear at the 45°/-45° interfaces.

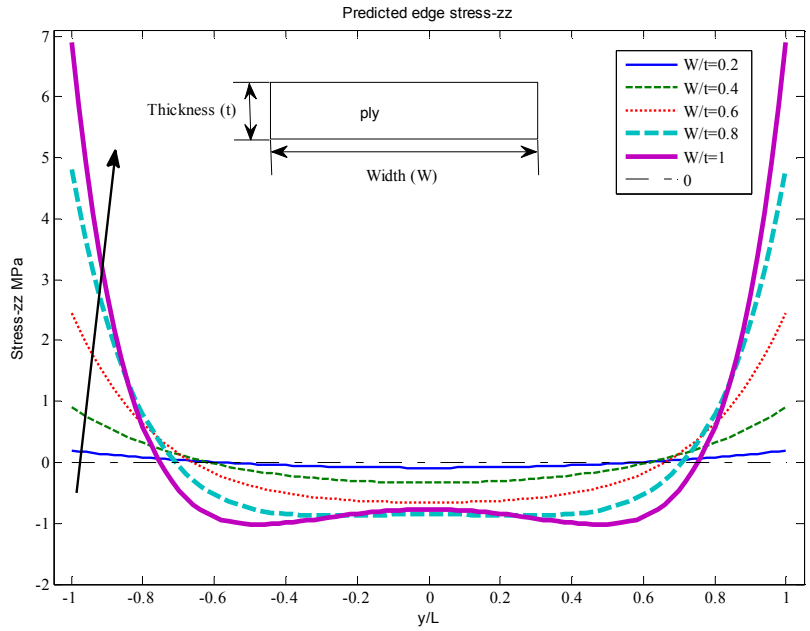

Figure 3.18. σ_{zz} variation long the 45º/-45º interface in the composite laminate with W/t=0.2,0.4,0.6,0.8,1.0, respectively.

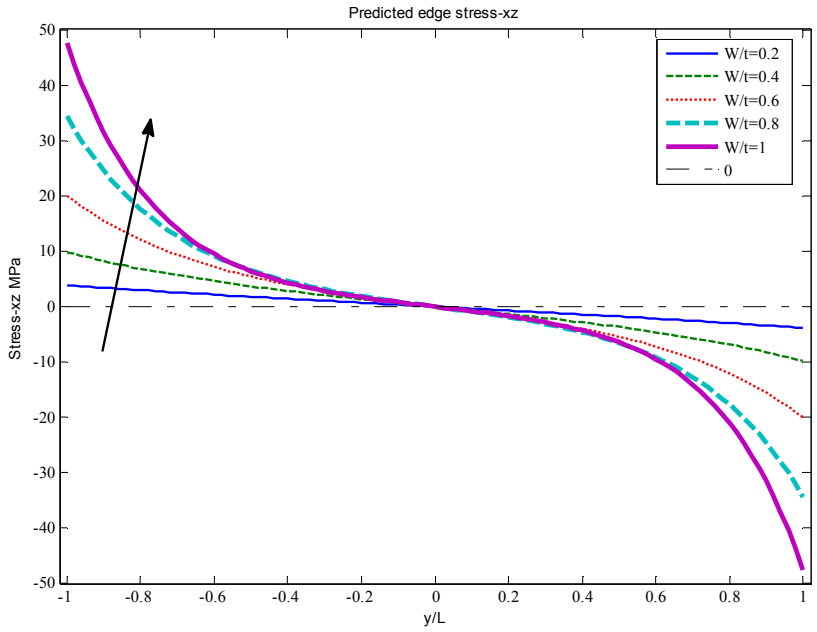

Figure 3.19. τ_{xz} variation long the 45º/45º interface in the composite laminate with W/t=0.2,0.4,0.6,0.8,1.0 respecively.

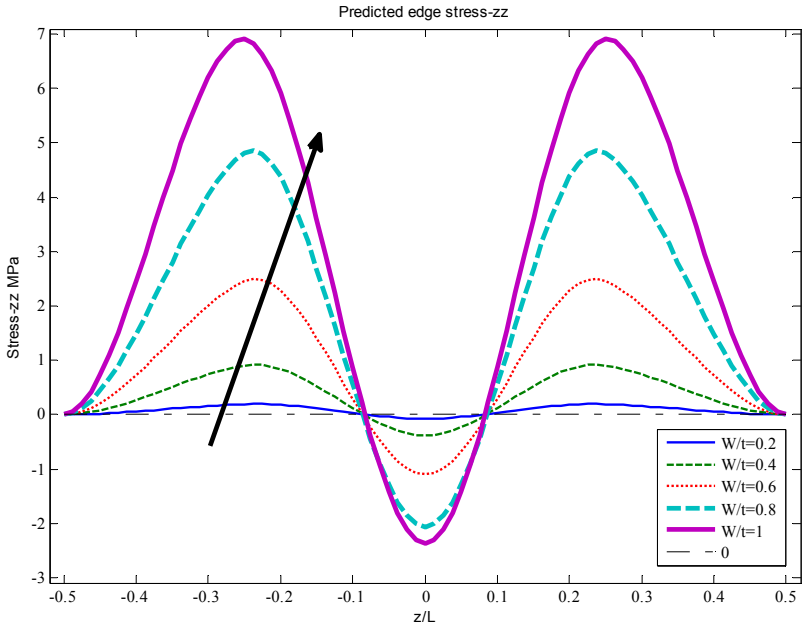

Figure 3.20. σ_{zz} variation at free edgeacross the thickness of the composite laminate with W/t=0.2,0.4,0.6,0.8,1.0, respectively.

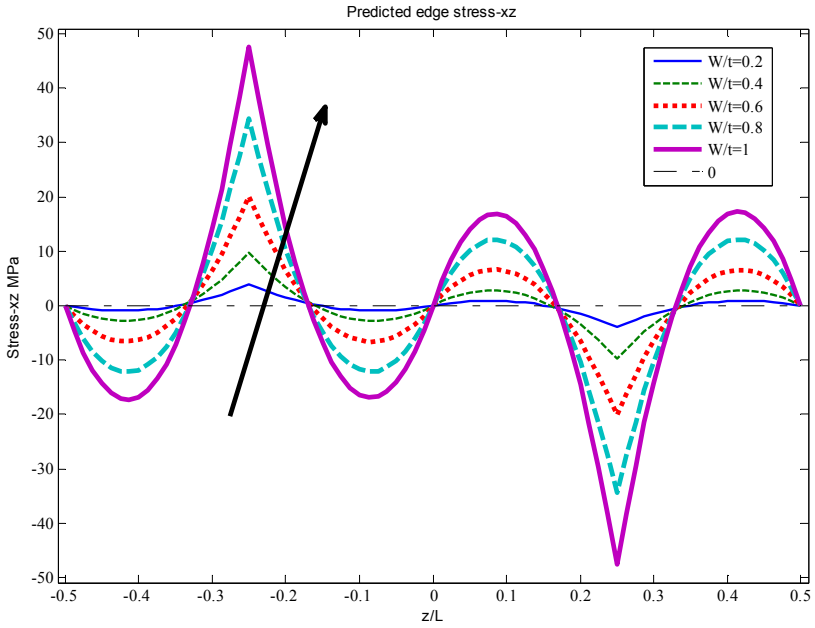

Figure 3.21. τ_{xz} variation at free edge across thickness of the composite laminate with W/t=0.2,0.4,0.6,0.8,1.0, respectively.

When the aspect ratio is greater than 1.0, the varying tendency of peeling stress σ_{zz} along the interface decreases with increasing length of the laminate, as shown in Fig. 3.18. However, along the free-edge, the peak value of stress σ_{zz} in each aspect ratio of the composite laminate appears at the 45°/45° interfaces when the length-thickness ratio is greater than 1.0. Such peak value of stress σ_{zz} at the 45°/-45° interface reaches the maxima at the width-thickness ratio 4.0. On the other hand, the varying tendencies of stress σ_{xz} at both free-edges across the laminate thickness and at the 45°/45° interface are much simpler.

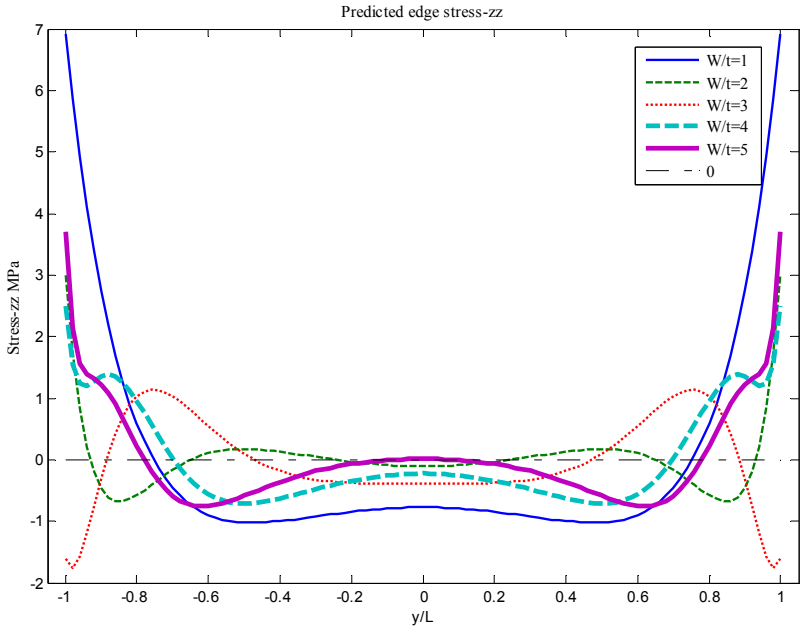

Figure 3.22. σ_{zz} variation long the 45°/-45° interface in the composite laminate *W/t*=1, 2, 3, 4, 5, respectively.

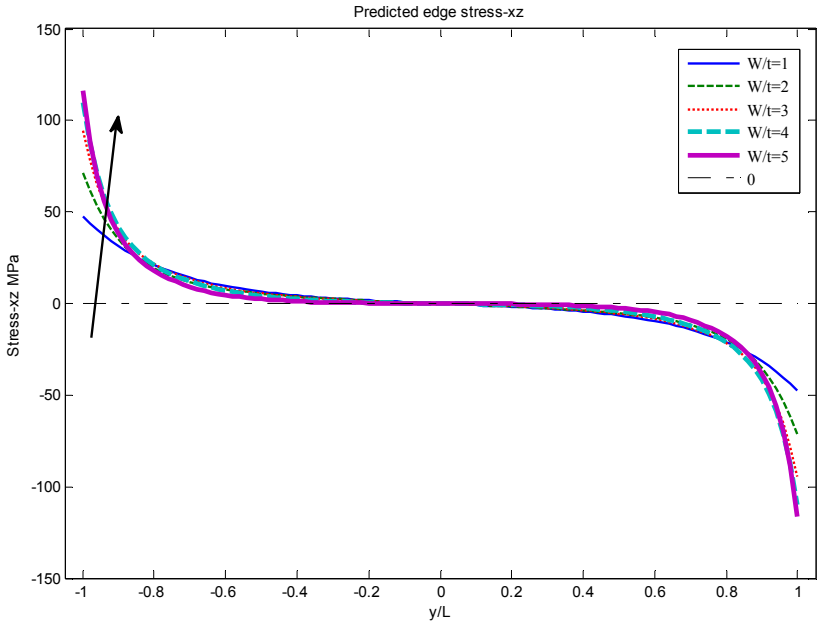

Figure 3.23. τ_{xz} variation long the 45°/-45° interface in the composite laminate with W/t=1, 2, 3, 4, 5, respectively.

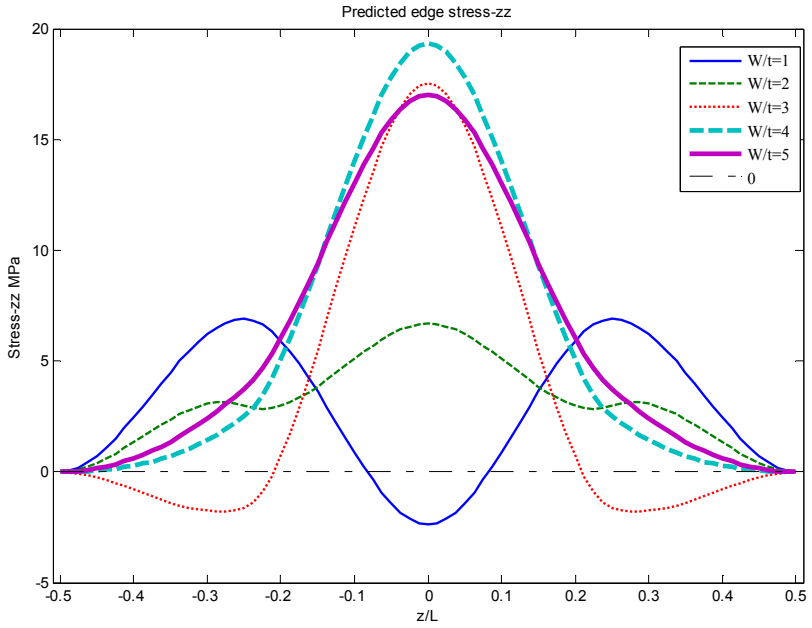

Figure 3.24. σ_{zz} variation at free edge across thickness of the composite laminate with W/t=1, 2, 3, 4, 5, respectively.

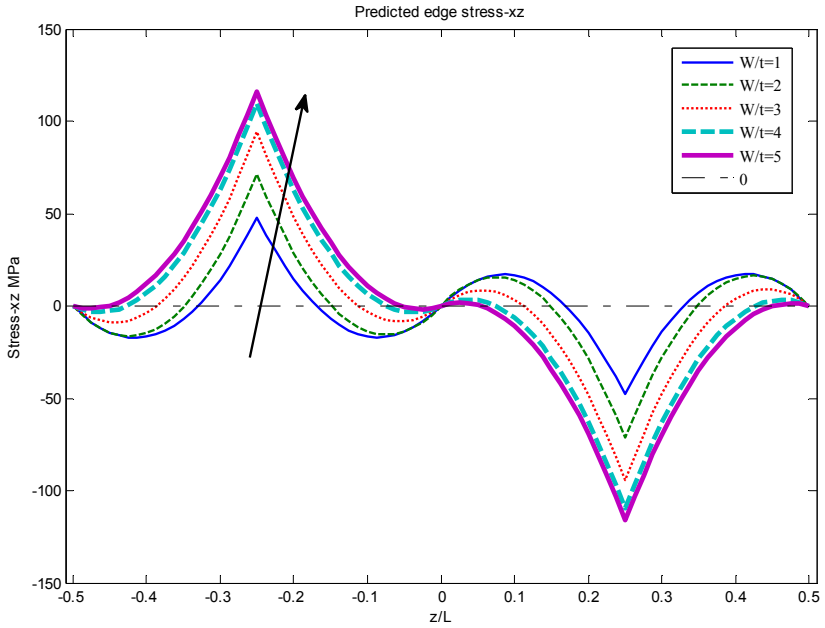

Figure 3.25. τ_{xz} variation at free edge across thickness of the composite laminate with W/t=1, 2, 3, 4, 5, respectively.

With the increase of laminate width, the peak value of each stresses tends to stable around a fixed value as shown in Figs. 22-25.

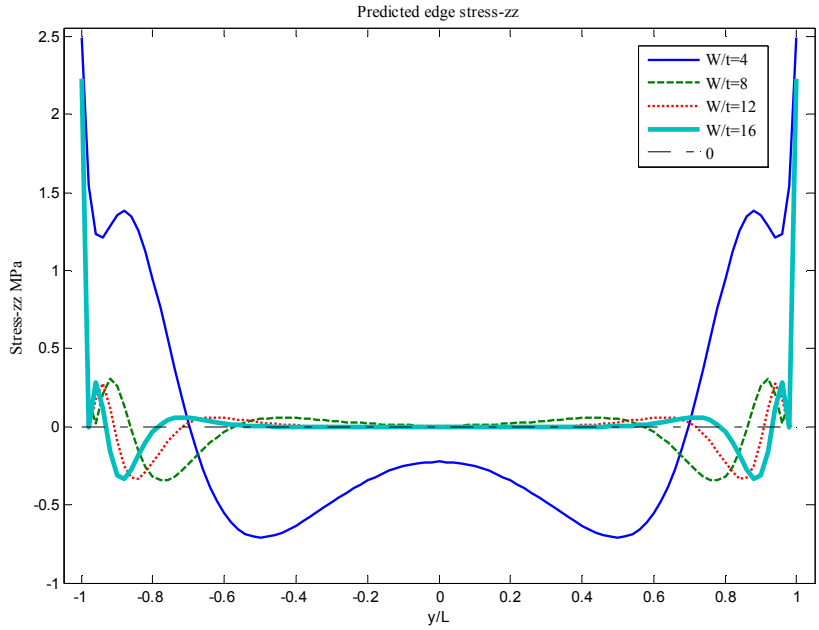

Figure 3.26. σ_{zz} variation long the 45º/-45º interface in the composite laminate with W/t=4,8,12,16,respectively.

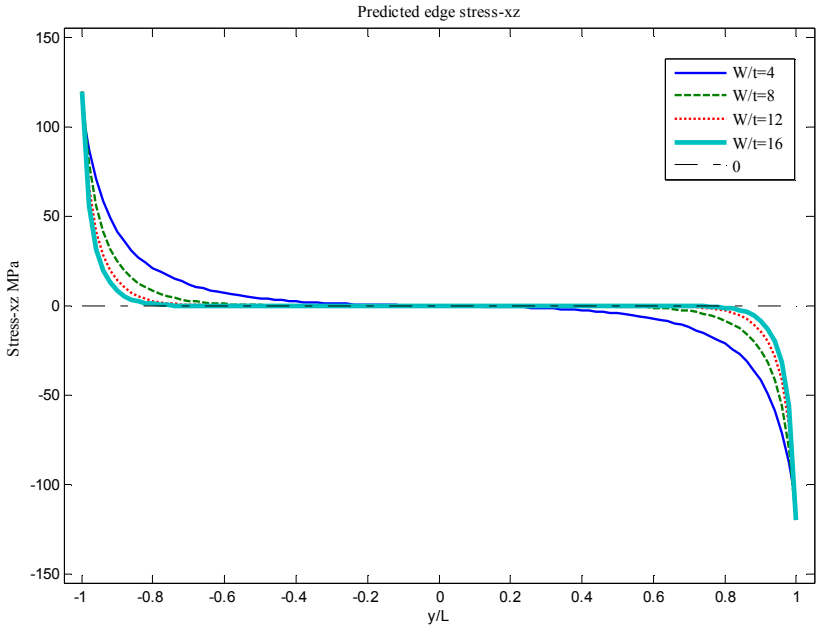

Figure 3.27. τ_{xz} variation long the 45º/-45º interface in the composite laminate with W/t=4, 8, 12, 16, respectively.

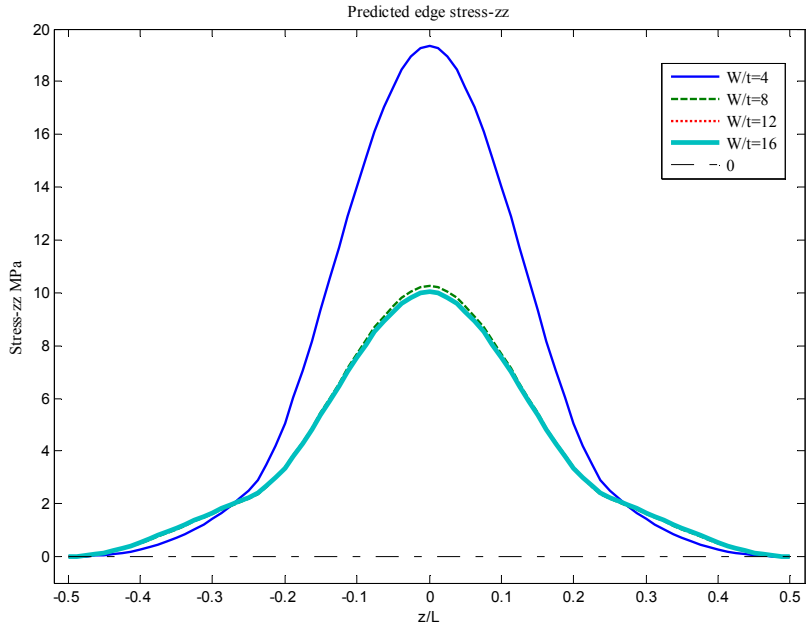

Figure 3.28. σ_{zz} variation at free edge across thickness of the composite laminate with W/t=4, 8, 12, 16, respectively.

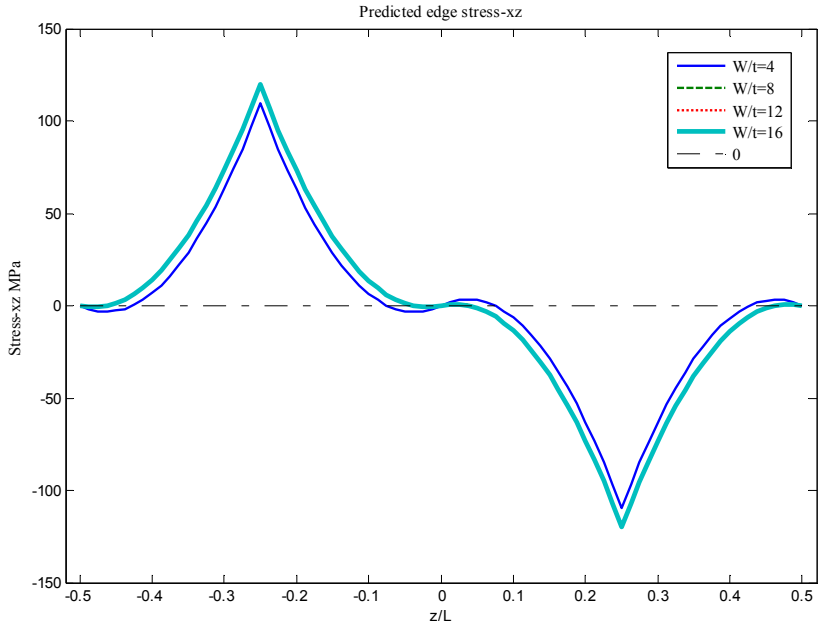

Figure 3.29. τ_{xz} variation at free edge across thickness of the composite laminate with W/t=4, 8, 12, 16, respectively.

In the above, scaling analysis of the interfacial stresses in an angle-ply composite laminate with varying laminate width has demonstrated the effect of the laminate width on the variation of the stresses σ_{zz} and σ_{xz} along the interface and at free edge across the laminate thickness. This effect can be useful to the design and strength/ failure analysis of composite laminates.

3.4. Conclusion

In this chapter, the efficient robust semi-analytical efficient stress-function variational method has been revised and furthered for the free-edge stress analysis of multilayered anisotropic laminates with finite laminate width due to in-plane mechanical loading. During the model formulation, two Lehknitskii's stress potential functions, approached by polynomial functions, were introduced to approximate the interfacial stress variation in an arbitrary composite laminate. By evoking the principle of minimum complementary strain energy, a set of governing ODEs was obtained. The set of governing ODEs was solved by means of eigenvalue method, of which the particular solution was obtained by evoking the traction-free BCs. The general solution has been obtained and applied to free-edge stress analysis in all composite laminates (multilayered anisotropic laminates with the number of layer up to 70). The interfacial stresses predicted by the present model not only satisfy the traction-free BCs, but also are close to those predicted by other methods available in the literature and present FEA results.

4. LAYERS STRESS-FUNCTION VARIATIONAL METHOD FOR ANALYSIS OF INTERFCAIAL STRESS SUPRESSION IN COMPOISTE LAMINATE WITH INTERLEAFING

4.1. Introduction

Advanced polymer matrix composites (PMCs) made of compliant polymeric resins (e.g., epoxy, etc.) reinforced with high-performance microfibers (e.g., carbon fibers) have found extensive applications in aerospace, aeronautical, and ground vehicles, offshore structures and sports utilities due to their unique superior specific strength and toughness, excellent manufacturability, and superior corrosion resistance, among others. Yet, due to their typically layered structures, PMCs usually behave with low interlaminar strength and toughness, which are responsible for the common interlaminar failure in advanced PMCs such as delamination and related ultimate failure of composite laminates. Within the framework of fracture mechanics, the fracture modes can be classified as modes I, II and III, as shown in Fig. 4.1.

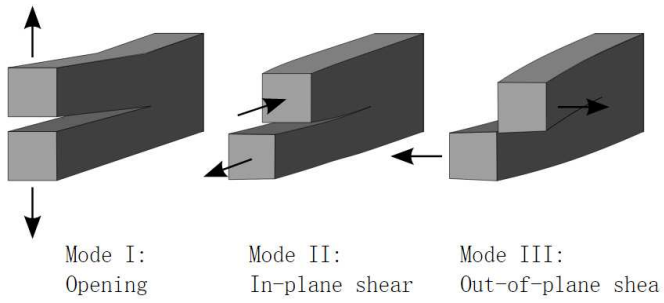

Figure 4.1. The schematic of fracture modes (www.wikie.org).

For fiber-reinforced composite laminates, the mode I and mode III cracking are the dominated failure modes during the common delamination process, as shown in Fig. 4.2.

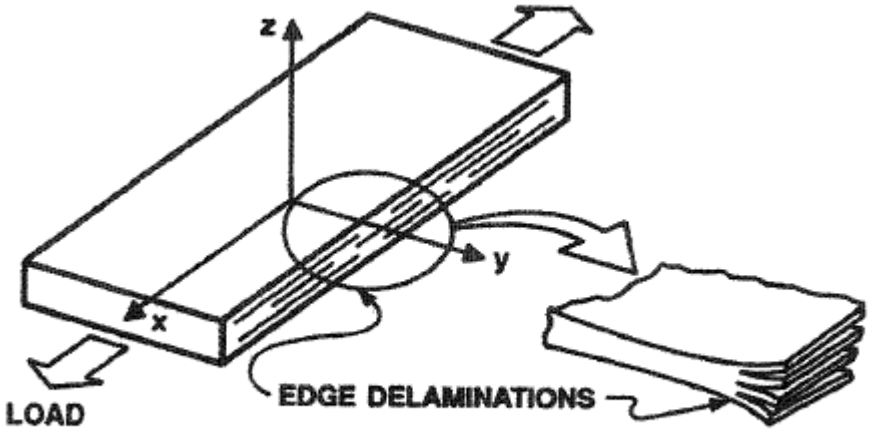

Figure 4.2. Schematic of edge delamination of composite laminate (Wu, 2003).

Figure 4.3 shows the microstructure of the cross-section of a cross-ply carbon-fiber reinforced composite laminate, from which it can be observed that a matrix (resin) layer exists between the neighboring 0^o and 90^o plies. In advanced PMCs, the thin interface matrix layer as a discrete phase exist between neighboring plies, of which the microstructure and properties can be designed to enhance the interlaminar fracture toughness and damage tolerance. As a matter of fact, delamination is considered as a life-limiting factor and one of the most prevalent failure modes in PMCs. Delamination may severely reduce the in-plane strength and stiffness, and then cause catastrophic failure of PMCs. Nowadays, materials engineers and scientists have developed several technologies to successfully increase the delamination resistance, such as 3D

fabric, transverse stitching, toughening matrix resin, etc. (Singh & Partridge, 1995). These techniques can improve the interlaminar strength and fracture toughness of PMCs.

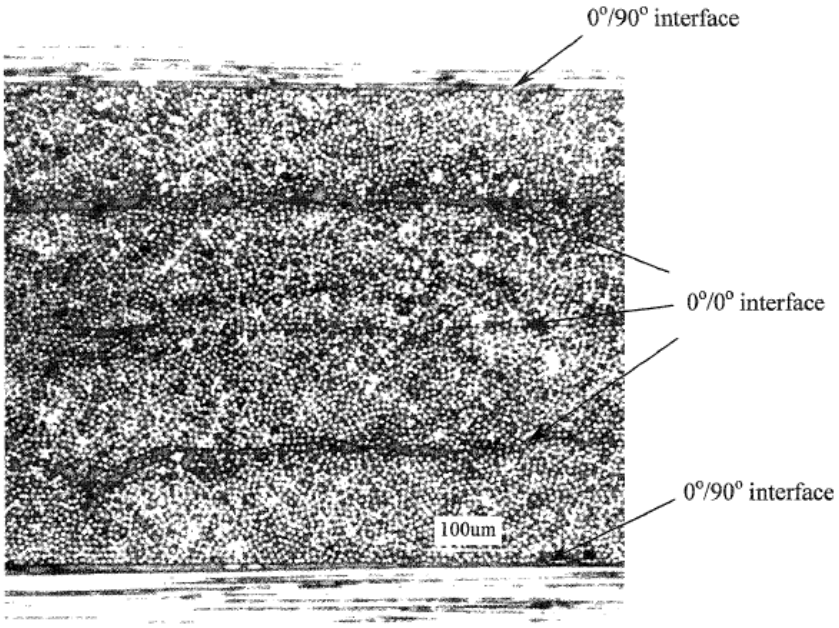

Figure 4.3. Microstructure of a cross-ply carbon-fiber/epoxy composite laminate (Reifsnider, 1991).

So far, a promising interface toughening technique termed as interleafing has been incorporated into the PMC manufacturing process to enhance the interlaminar toughness and impact resistance. In the early 1970s, American Cyanamid, Inc. achieved the improvement of the damage tolerance of PMC laminates via integrating toughening plastic layers, as illustrated in Figure 4.4. This approach can efficiently improve the interlaminar fracture toughness and damage tolerance of the composite laminates. Furthermore, with the high shear failure strain, the interleafing resin can also increase the interface toughness between neighboring plies to suppress delamination.

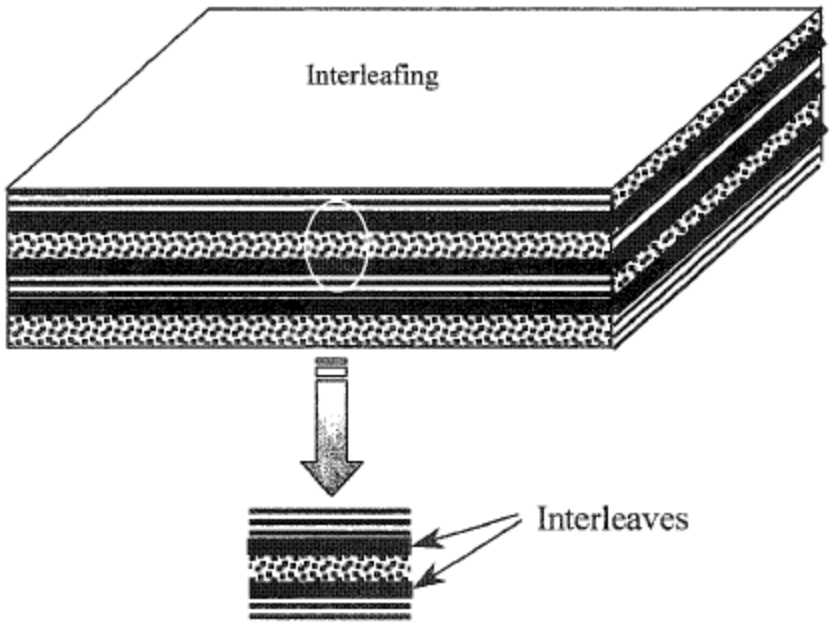

Figure 4.4. Schematic of interleafing (Wu, 2003).

On the other hand, both impact tolerance and dynamic delamination toughness of composite laminates are improved, since the redundant shear strains can be introduced by interleafing. The key parameter of the impact damage tolerance is also be characterized with the high shear failure strain, which can be enhanced by introducing the interleaved discrete thermoplastic layers (Wu, 2003). Most experiments have indicated that interleafing can greatly increase the mode II delamination toughness while slightly increasing in mode I delamination toughness. Hence, interleafing cannot be applied for suppressing opening fracture failure. In addition, one of the negative effect of interleafing is that interleafing noticeably increases the total thickness and weight of the composite laminate, which reduces the specific stiffness and strength of PMC laminates. Despite a number of other interface toughening approaches have been developed to toughen specific composite systems, to date interleafing is still used as the most popular method

to toughen the interfaces of composite laminates. In addition, researchers are working on use of nanotechnology to overcome the disadvantages of interleafing such as increase of the overall weight and decrease of the specific in-plane strength and stiffness (Wu, 2003).

4.2. Scalar analysis of interleafing

4.2.1. Material properties and geometries

To date, research on interleafing has been based mainly on experiments, whereas modeling work on interleafing is really rare. In this chapter, the stress-function variational method for free-edge stress analysis is further utilized for investigating the stress variation in composite laminates with interleafing. The mechanical properties of the interleaved layer: (Epoxy 977-3):

E_m=3.7 GPa; v_m=0.35; G_m=1.37 GPa

And the mechanical properties of the unidirectional composite plies of the composite laminate: (Carbon/Epoxy):

E_1=147 GPa;

E_2=E_3=10.3 GPa;

v_{23}=0.54;

v_{12}= v_{13}=0.27;;

G_{23}=3.7 GPa

G_{12}= G_{13}=7.0 GPa

In this numerical investigating, the composite laminate is assumed to be subjected to a constant uniaxial tensile strain along x-direction, i.e., $\varepsilon_{xx} = 0.02$. The geometries and coordinate

system of the composite laminate are shown in Fig. 5. Furthermore, all the interleaved layers are assumed to carry 1/2 thickness of the plies of the composite laminate. In addition, three typical laminate layups are employed in this section to examine the suppression of the interfacial stresses by merging interleaved layers.

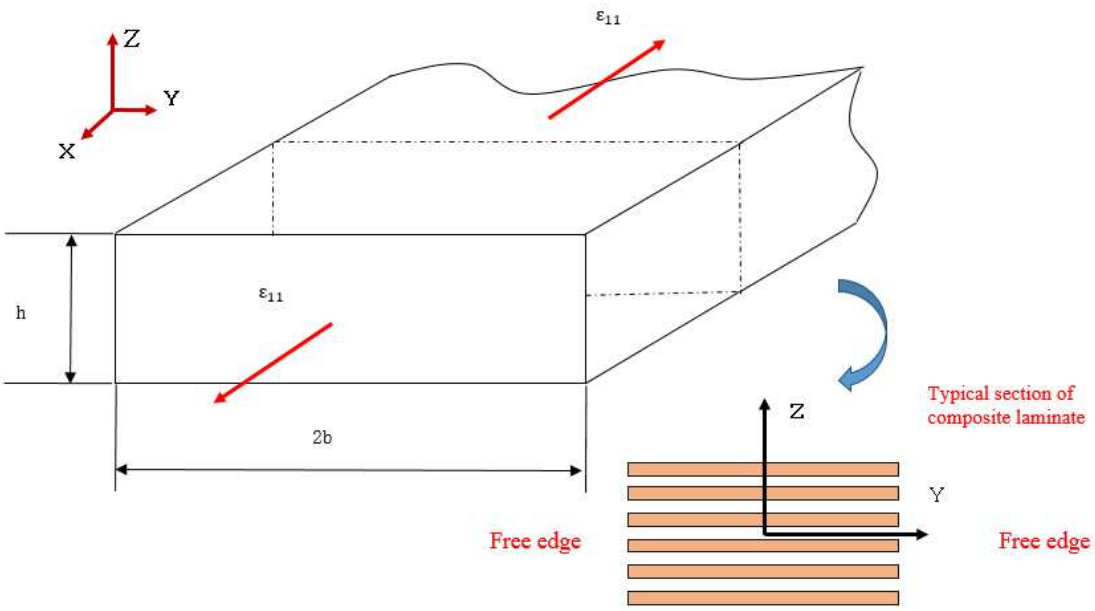

Figure 4.5. Geometry and coordinate system of the laminate.

4.2.2. Scalar analysis of interleafing

1. $[45^o/-45^o]_s$

As shown in Figs. 4. 6 (*a*) and 4. 7 (*a*), variation of the peeling stress σ_{zz} and out-of-plane shear stress τ_{xz} at the free edge along the thickness. Due to the discontinuity of the material properties across the interface, the peak values of σ_{zz} and τ_{xz} are both located at the $45^o/-45^o$ interface. By merging an epoxy layer at the $45^o/-45^o$ interface, though the values of the stresses

σ_{zz} and τ_{xz} at the interfaces become larger, the peak values of both stresses decrease significantly, as shown in Figs. 4.6 (*b*) and 4.7 (*b*), which are proximately only 1/5 of the laminates without interleafing.

Furthermore, Figs. 4.8 and 4.9 show the variation of the interfacial stresses at the 45°/-45° interface. As shown in Figs. 8 (*a*) and 8(*b*), the peeling stress σ_{zz} is suppressed substantially after inserting the interleaved layer, and the peak value of the peeling stress has been reduced to only one-tenth. The same situation also happens to the out-of-plane shear stress τ_{xz}. By comparing Figs. 4.6 (*b*) and 4.8 (*b*), it is found that the peak value of the peeling stress is no longer located at the interface after interleaving,

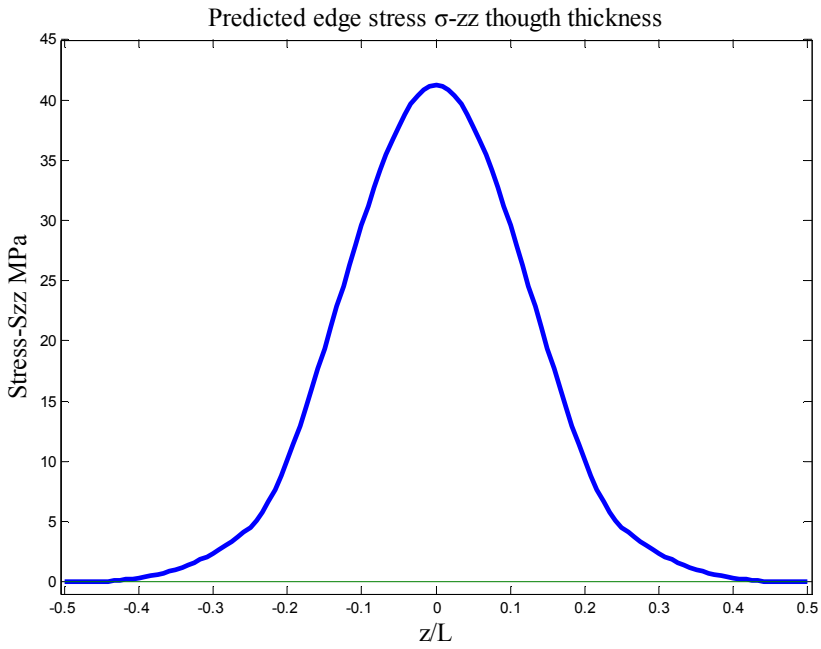

(*a*)

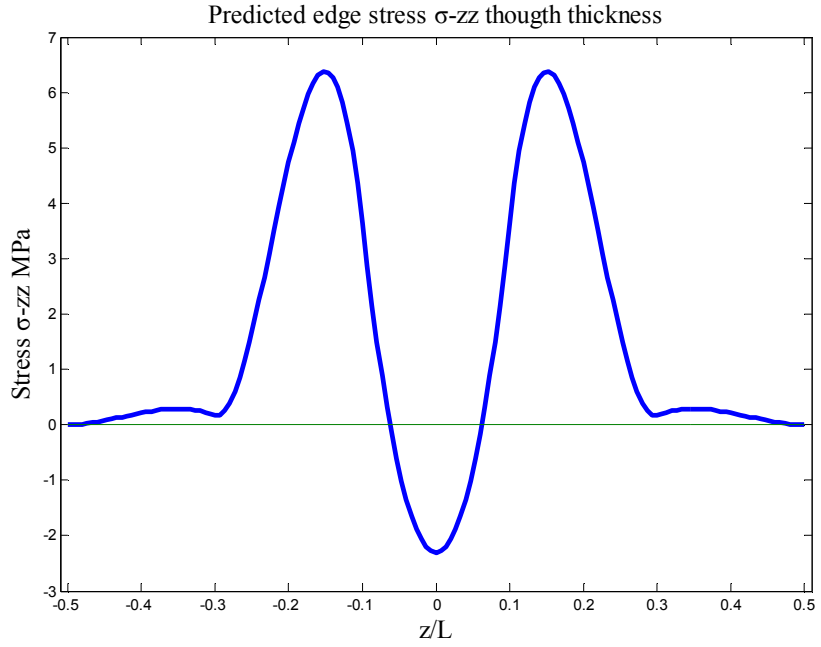

(*b*)

Figure 4.6. (a)Variation of the peeling stress σ_{zz} along the thickness at a free edge without interleaved layers; (b)Variation of peeling stress σ_{zz} along the thickness at a free edge without interleaved layers.

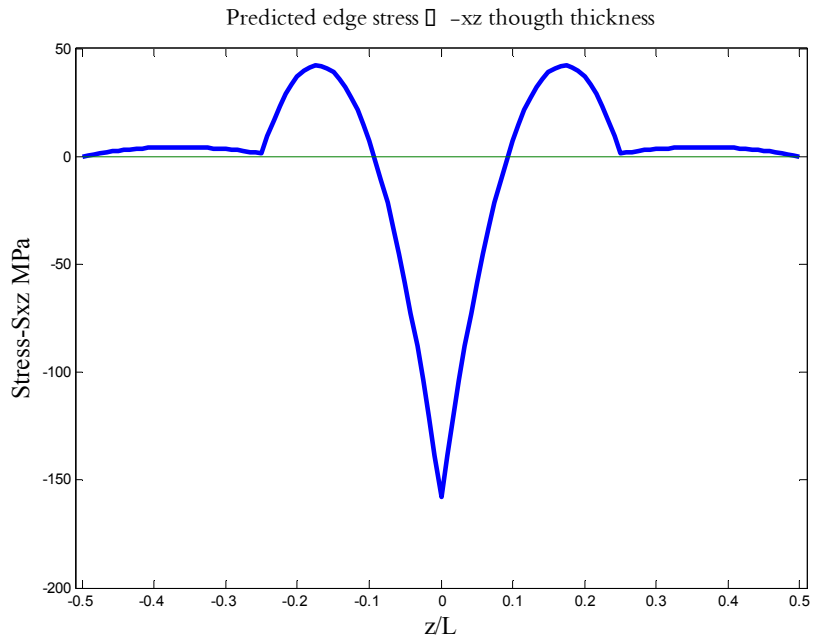

(a)

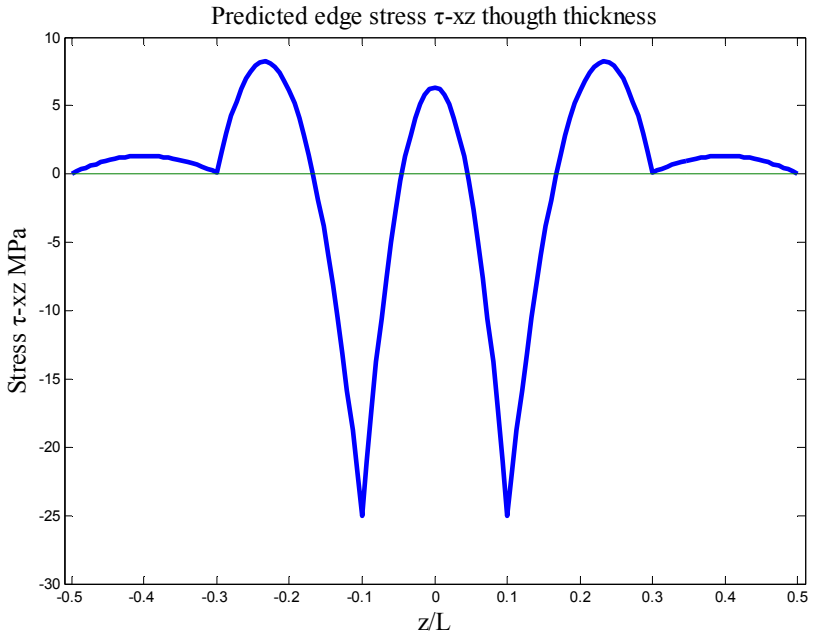

(b)

Figure 4.7. (a)Variation of the shear stress τ_{xz} along the thickness at a free edge without interleaved layers; (b)Variation of the shear stress τ_{xz} along the thickness at a free edge with interleaved layers.

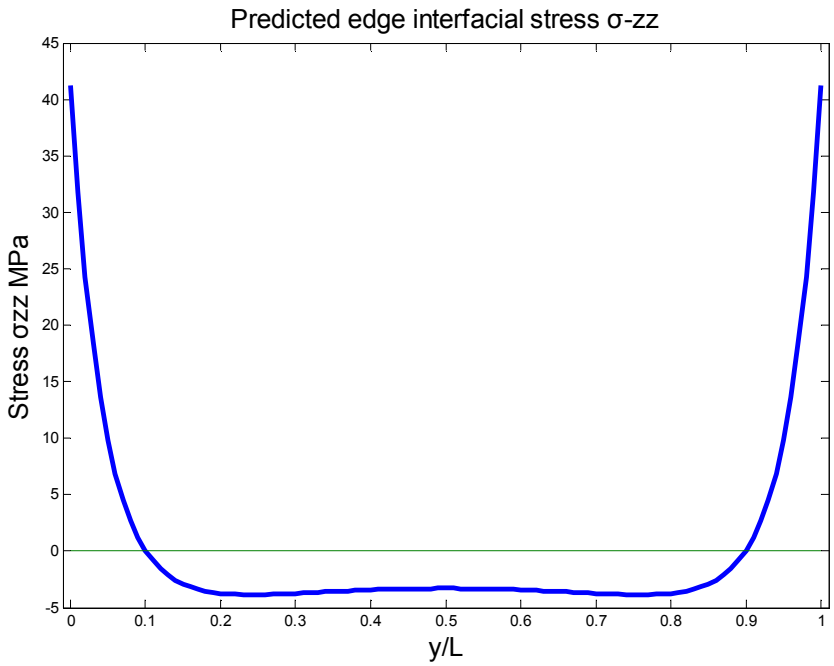

(a)

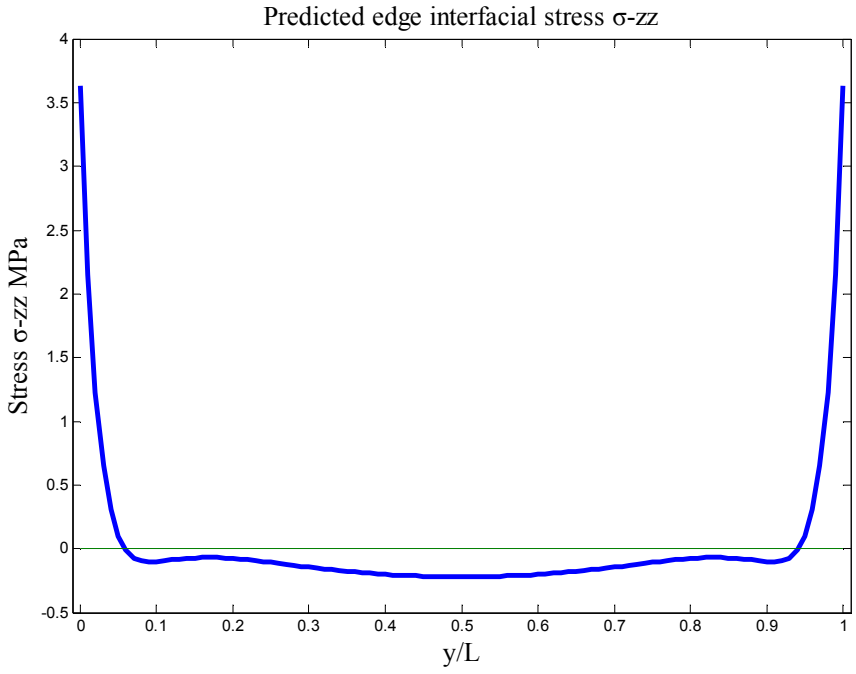

(*b*)

Figure 4.8. (a)Variation of the interfacial stress σ_{zz} at the 45°/-45° interface without interleaved layers; (b)Variation of the interfacial stress σ_{zz} at ply and interleaved layers.

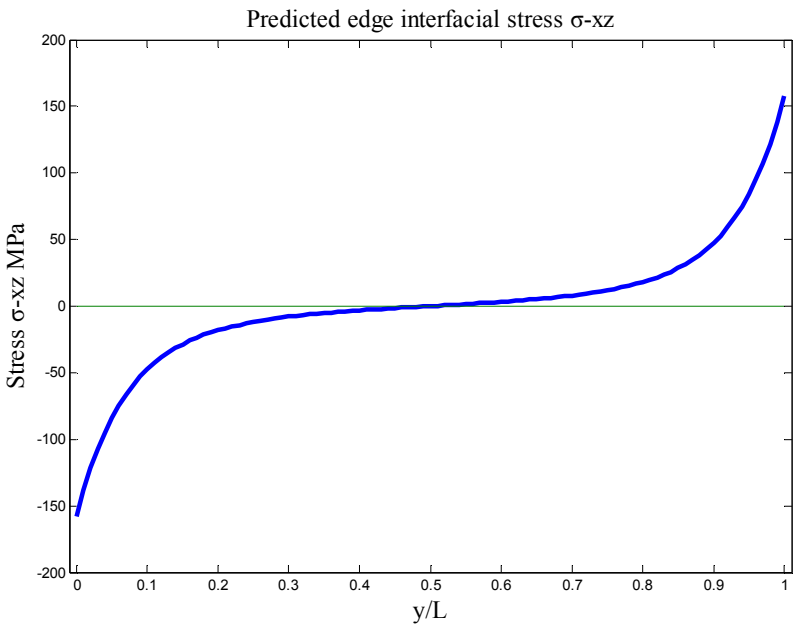

(a)

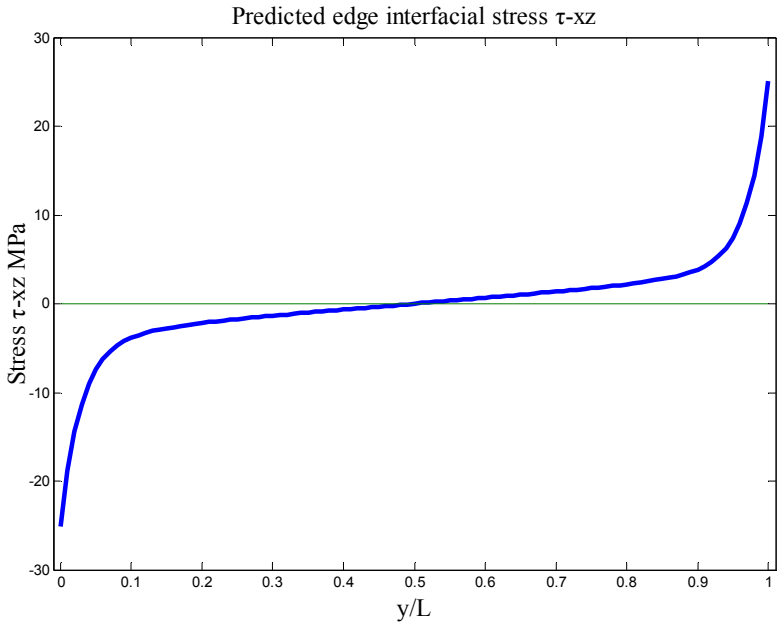

(b)

Figure 4.9. (a)Variation of the interfacial stress τ_{xz} at the 45°/-45° interface without interleaved layers; (b)Variation of interfacial stress τ_{xz} at the 45°/-45° interface with interleaved layers.

2. $[45^o/-45^o]_s$

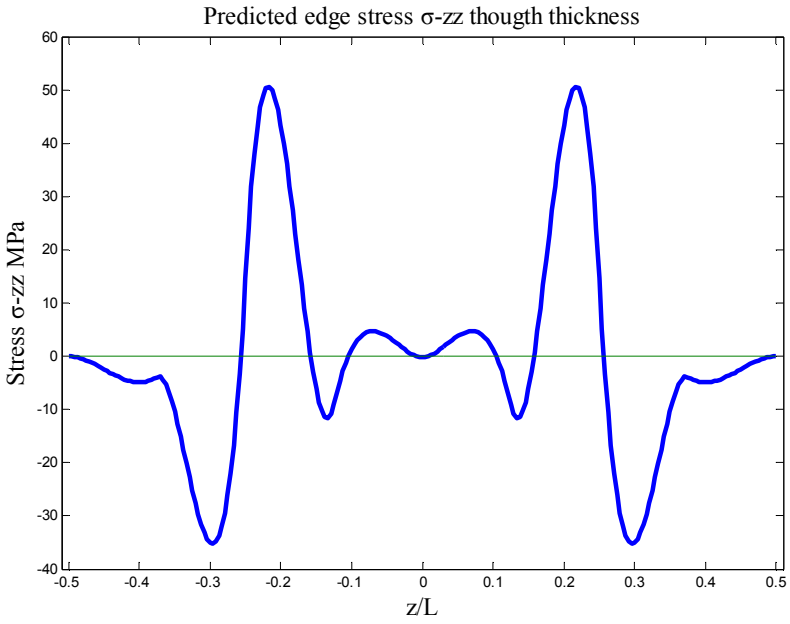

(a)

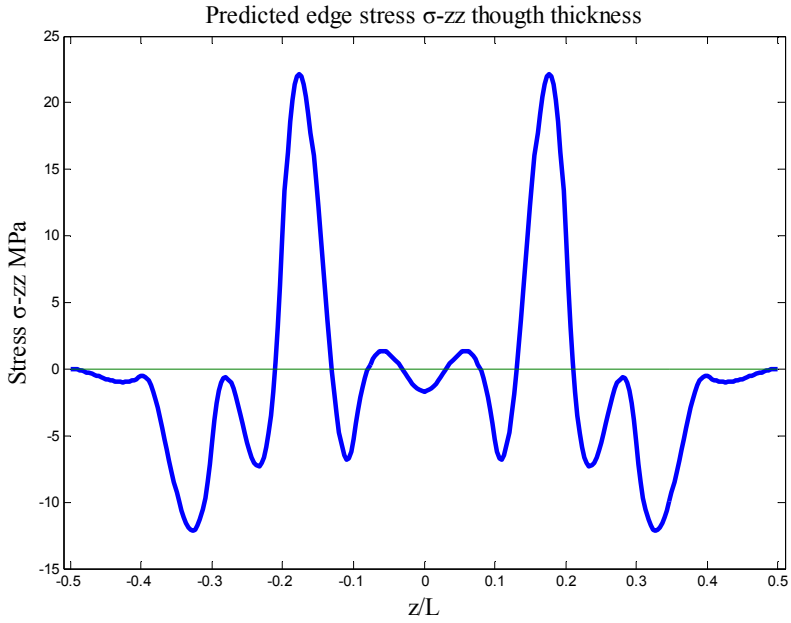

(*b*)

Figure 4.10. (a)Variation of peeling stress σ_{zz} along the thickness at a free edge without interleaved layer; (b)Variation of the peeling stress σ_{zz} along the thickness at a free edge without interleaved layer.

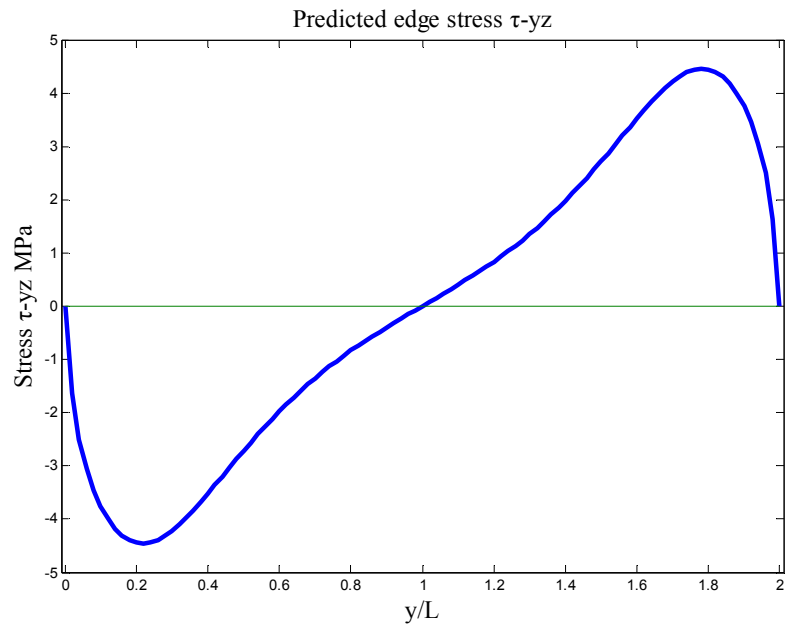

(a)

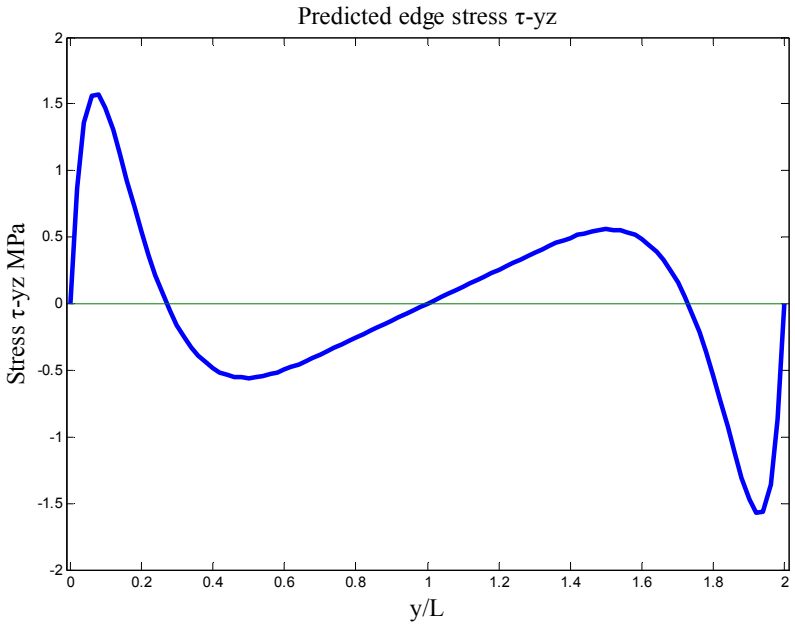

(*b*)

Figure 4.11. (a)Variation of the interfacial stress τ_{yz} at the 45°/-45° interface before interleafing; (b)Variation of the interfacial stress τ_{yz} at the 45°/-45° interface with interleaved layers.

As shown in Figs. 4.10- 4.11, $[0^o/90^o]_s$ layup has been commonly used in composite laminates. One of the advantages of such layup is that under a pure extension loading, no shear-tension coupling exists and the out-of-plane shear stress τ_{xz} is close to zero, i.e., no out-of-plane shear stresses are evoked. Also, as shown in Figs. 4.10(a) and 4.10(b), the peak value of the peeling stress at the free edge along the thickness does not appear at the interfaces but at the edge of the 90^o plies. When interleaved, the level of the peeling stress at the free edge suppressed significantly, which is only half that of the virgin laminate. Also, as shown in Figs. 4.11(a) and 4.11(b), the in-plane interfacial shear stress τ_{yz} between the interleaved interlayer and the composite ply is also half the one of the virgin laminate.

The coupling effect in the composite laminate with the $[-45^o/45^o]_s$ layup is much more significant than that in the composite laminate with the $[0^o/90^o]_s$ layup. From Figs. 4.11(a) and 4.11(b), it can be concluded that the interleaved layers can efficiently suppress the out-of-plane shear stresses.

3 $[-45^o/45^o/0^o/90^o]_s$

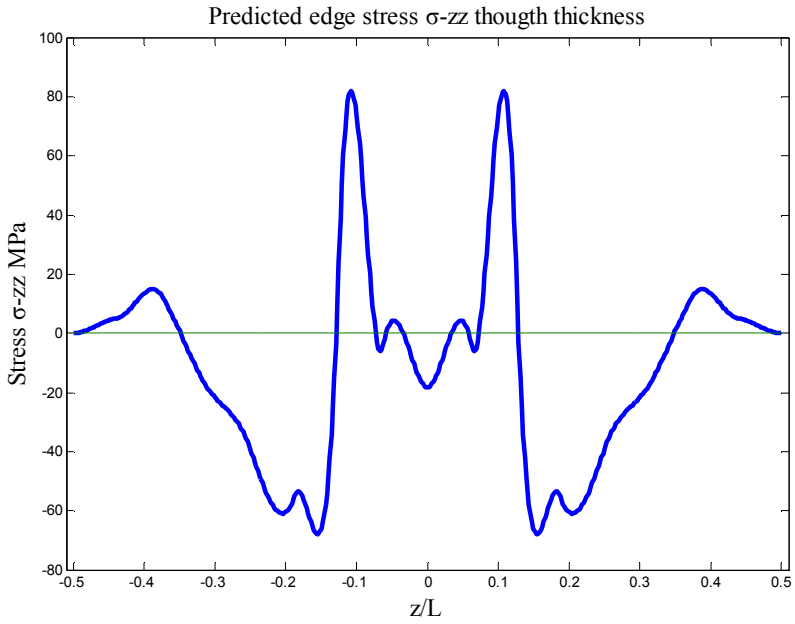

(a)

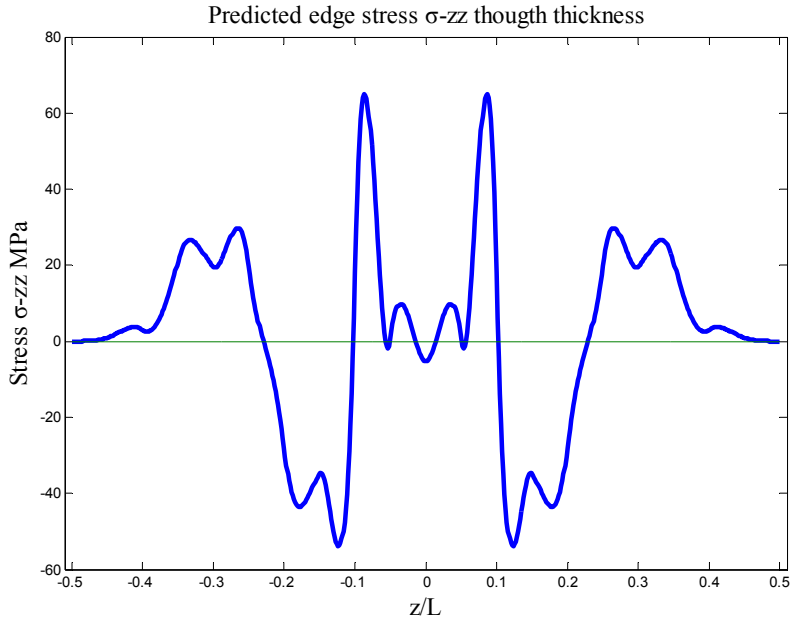

(b)

Figure 4.12. (*a*)Variation of the peeling stress σ_{zz} across the laminate thickness at free edge without interleaved layers; (*b*)Variation of the peeling stress σ_{zz} across the laminate thickness at free edge with interleaved layers. Layup of the composite laminate: $[-45^o/45^o/0^o/90^o]_s$.

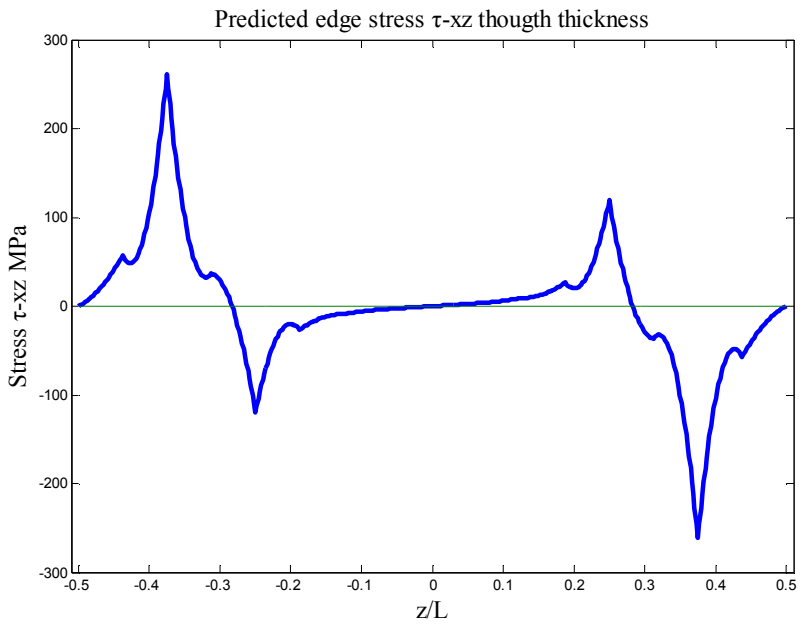

(a)

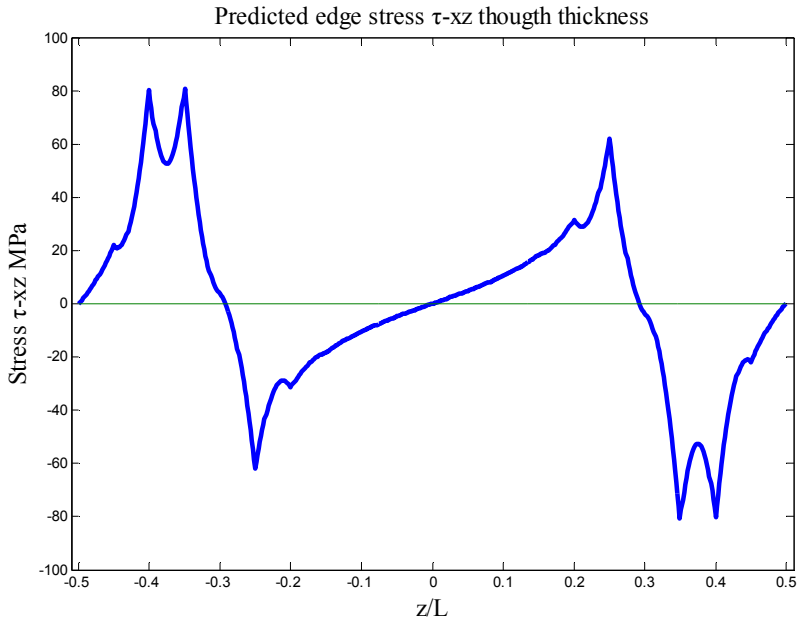

(b)

Figure 4.13. (a) Variation of the shear stress τ_{xz} across the laminate thickness at free edge without interleaved layers; (b) Variation of the shear stress τ_{xz} across the laminate thickness at free edge with interleaved layers. Layup of the composite laminate: $[-45^o/45^o/0^o/90^o]_s$.

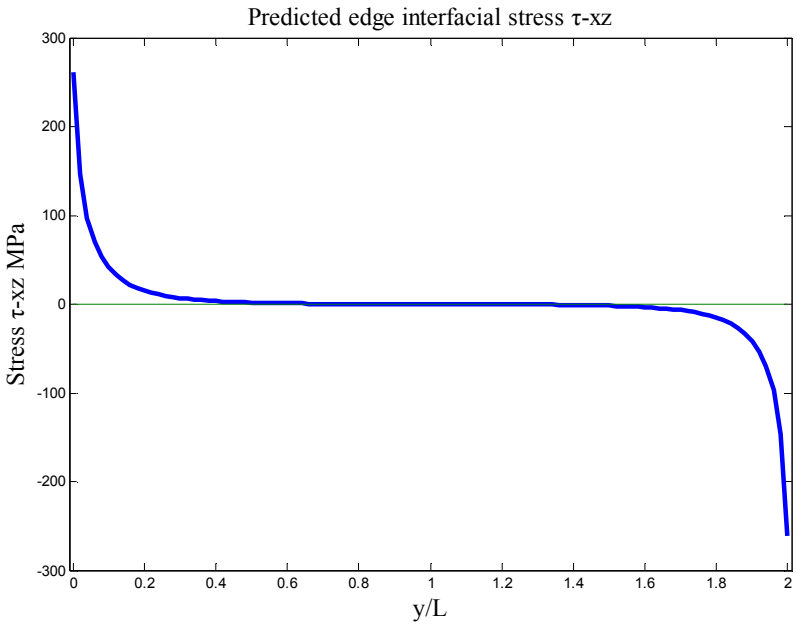

(a)

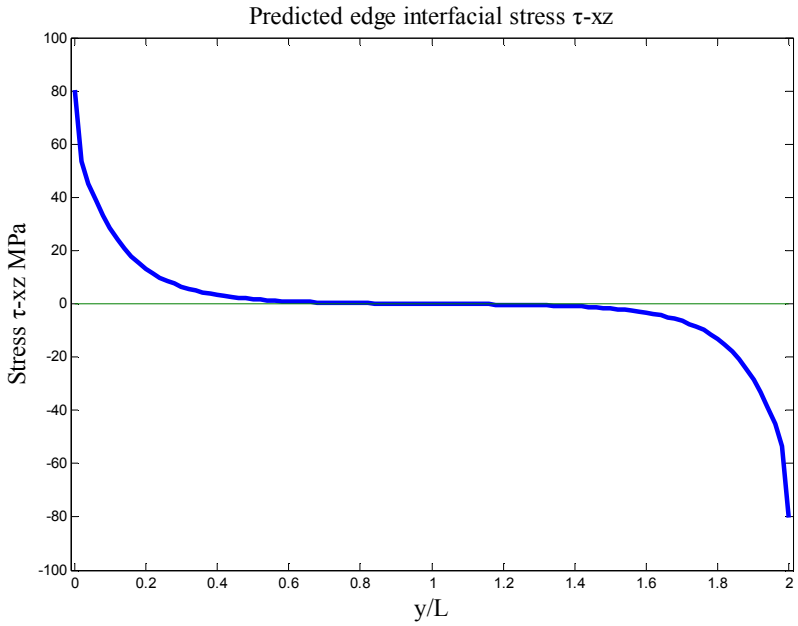

(b)

Figure 4.14. (a) Variation of the interfacial stress τ_{xz} at the 45o/-45o interface without interleaved layers; (b) Variation of the interfacial stress τ_{xz} at the 45º/-45º interface with interleaved layers. Layup of the composite laminate: $[-45º/45º/0º/90º]_s$.

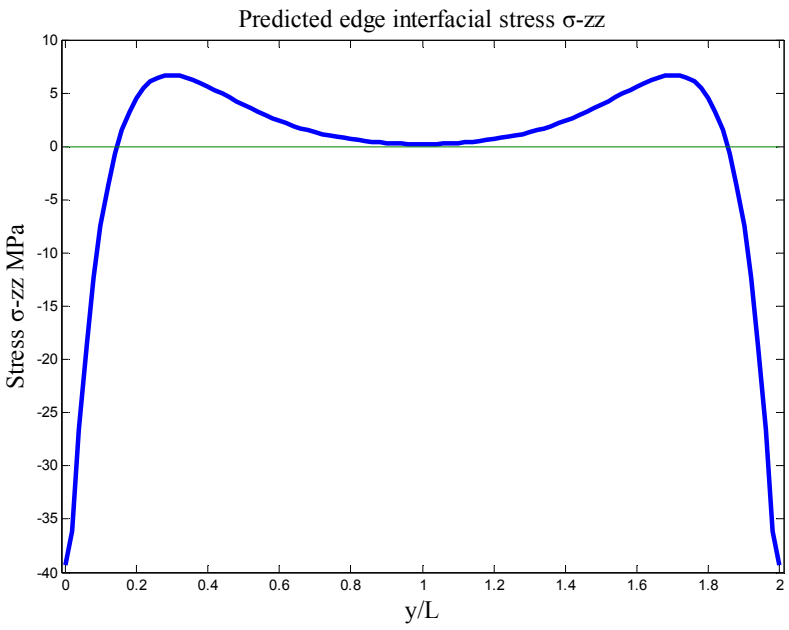

(a)

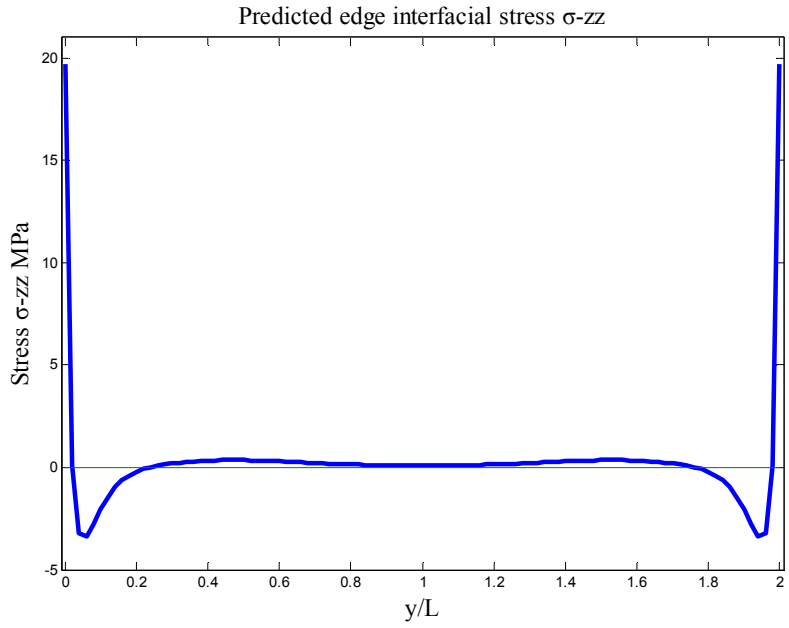

(b)

Figure 4.15. (a) Variation of the interfacial stress σ_{zz} at the 45o/-45o interface without interleaved layers; (b) Variation of the interfacial stress σ_{zz} at the 45°/-45° interface with interleaved layers. Layup of the composite laminate: $[-45^{o}/45^{o}/0^{o}/90^{o}]_{s}$.

In practice, the layup of a composite laminate is commonly designed with multiple oriental angles, so the stress suppression in a composite laminate with multi-angled plies should also be tackled. With the present semi-analytic stress-functional variational method, variations of the peeling and out-of-plane shear stresses of a composite laminate with a layup of $[-45^o/45^o/0^o/90^o]_s$ without interleafing are given in Figs. 4.12 (*a*), 4.13 (*a*), 4.14 (*a*) and 4.15 (*a*). It can be observed from Figs. 4.12 (*a*) and 4.13 (*a*) that the peak value of the out-of-plane shear stress τ_{xz} occurs at the 45^o/-45^o interface, while the peak value of the interfacial peeling stress σ_{zz} appears at the $45^o/0^o$ interface. Thus, the above stress analysis of the composite laminate with the layup $[-45^o/45^o/0^o/90^o]_s$ shows that the interleafing layers should be placed at the 45^o/-45^o and $45^o/0^o$ interfaces. The results of stress variation of the interleaved laminate are shown in Figs. 4.12 (*b*), 4.13 (*b*), 4.14 (*b*), and 4.15 (*b*). The plots show that the out-of-plane shear stress τ_{xz} of the laminate can be efficiently suppressed, of which the peak stress value could be reduced to only one-third that of the virgin laminate. Even though the peak value of the interfacial peeling stress can be significantly reduced, which is only half the one of the virgin laminate, the peak value of the peeling stress at the free edge is only slightly decreased by interleafing layers.

4.2.3. Discussion

As shown in the plots above, interleafing layers have the effect in significantly suppressing both the peeling and out-of-plane shear stresses. After interleafing, the overall fiber volume V_f of the composite laminate is dropped. Based on the Hapin-Tsai model in the mechanics of fiber reinforced composite (Daniel, 2006), the longitudinal and transverse moduli, i.e., E_L and E_T of a

composite laminate can be obtained in the following.In the case of short-fiber reinforced laminates (unidirectionaly distributed):

$$E_L = E_m\left[\frac{1+2(L_f/d_f)\eta_L V_f}{1-\eta_L V_f}\right] \tag{4.1}$$

$$E_T = E_m\left[\frac{1+2\eta_T V_f}{1-\eta_T V_f}\right] \tag{4.2}$$

where $\eta_L = \frac{\frac{E_f}{E_m}-1}{\frac{E_f}{E_m}+2L_f/d_f}$, $\eta_T = \frac{\frac{E_f}{E_m}-1}{\frac{E_f}{E_m}+2}$, and L_f and d_f are referred to the length and diameter of the reinforcing fibers, respectively. In the case of continuous fiber-reinforced composite laminates:

$$E_L = V_f E_{1f} + V_m E_m \tag{4.3}$$

$$E_T = E_m\left[\frac{1+\xi\eta V_f}{1-\eta V_f}\right] \tag{4.4}$$

$$G_{12} = G_m\left[\frac{1+\xi\eta V_f}{1-\eta V_f}\right] \tag{4.5}$$

where $1 < \xi < 2$ in the common case.

As shown in the above equations, when the volume fraction of reinforcing fibers is dropped, the longitudinal, transverse and in-plane shear moduli would be also reduced. Thus, when applying the same uniaxial deformation, the resulting stresses in an interleaved composite laminate would be less than the ones in the virgin one. In addition, the coupling effect in the composite laminate with the layup $[45^o/\text{-}45^o]_s$ is significant, i.e., the out-of-plane shear stress can have an impact on the value of the peeling stress. Such mechanism can be employed to explain the interleafing effect in the composite laminate with the $[45^o/\text{-}45^o]_s$ layup.

4.3. Conclusion

In this chapter, the semi-analytic stress-function variational method has been further utilized for exploring the stress mitigation effect in composite laminates with interleafing layers. Numerical experiments showed that interleafing can mitigate the interfacial stresses in composite laminates and therefore suppress the stress level in these laminates. In addition, since the interleaving layers are typically thermoplastic with the fracture toughness much higher than that of the thermosetting matrix resin (e.g., epoxy) of composite laminates, interleafing can also noticeably enhance the fracture toughness. In addition, interleaving does not change the varying tendency of the interfacial stresses, which means that though the peak value of the stresses has been decreased, the stress variation along interfaces still carries the similar tendency as the one of the virgin laminates. Such an observation is attributed to the fact that stress variation in composite laminates is largely influenced by the geometries of the laminate while the global in-plane mechanical properties (e.g., tensile and shear moduli) of the laminates are not substantially altered after interleafing.

5. STRESS-FUNCTION VARIATION METHOD FOR FREE-EDGE STRESS OF ANALYSIS OF ABCJS

5.1. Introduction

This chapter was targeted to further the stress-function variational method for the interfacial stress analysis of adhesively boned composite joints (ABCJs) made of multi-layered composite laminates. As reviewed in chapter 2, it is common to simultaneously perform stress analysis of adhesively bonded joints and composite laminates. So far, with the expanding utilization of composite laminates in aerospace and ground vehicles, building and bridge repairing, etc., ABCJs have been broadly structured. It is essential to understand the stress state, strength, and failure mechanisms in these structures. In the general case, ABCJs are made of angle-ply composite laminates bonded together with adhesive layers to achieve the load transfer from one composite laminate to the other. Due to the anisotropic properties of angle-ply composite laminates as adherends and multiple boundaries of the ABCJs, ABCJs undergo complicated layer-wise stress states including high stress concentrations at all the free-edges. It is desired to formulate efficient semi-analytic method for determining the stress variation in layer-wise manner. In the recent studies on stress analysis of ABJs made of isotropic adherends, e.g., metals, Wu & Jenson (2011) and Wu & Zhao (2012) have formulated successful stress-function variational methods for accurate, efficient determination of the interfacial stresses in ABJs. Yet, Wu's stress-function variational method could not directly employed for stress analysis of ABCJs. The idea of introducing stress potential functions at interfaces of ABJs as used by Wu and his collaborators (Wu & Jenson, 2011, Wu & Zhao, 2012) have shined the light for

formulating systematic stress-function variational method for stress analysis of ABCJs. In addition, Yin's stress potential functions (Yin 1994a, 1994b) can be further used to approach the layer-wise stress variation in the composite-laminate adherends of the ABCJs.

5.2. Model Formation

Without loss of generality, let us consider an adhesively single-sided strap joint made of a slender cover layer and two identical slender substrate layers, which are bonded with thin adhesive layers. As sketched in Fig. 5.1, the cover and substrate layers are assumed to be made from composite laminates with different layups and material properties, respectively. The coordinate system used for the ABCJ system is shown in Fig.5.1 (*a*) where the *y*-coordinate is set on the symmetric mid-span of the joint directed along the laminate axis; *z* is the vertical coordinate attached to the entroids of cross-section of the joint. The geomeitries of the ABCJ under consideraiton are the follows. The length and thickness of the cover layer are denonted as $2L$ and h_1, respectively. The thickness of the adhesive layer and substrated layer are denoted h_0 and h_2, respectively. In addition, the cover and substrate laminates and the adhesive layer of the joint have an uniform width *b* in *x*-direction. Both of the substrate laminates are assumd to be subjected to tensile tration P_0 along the *y*-direction, which is applied far away from the cover lamainte layer.

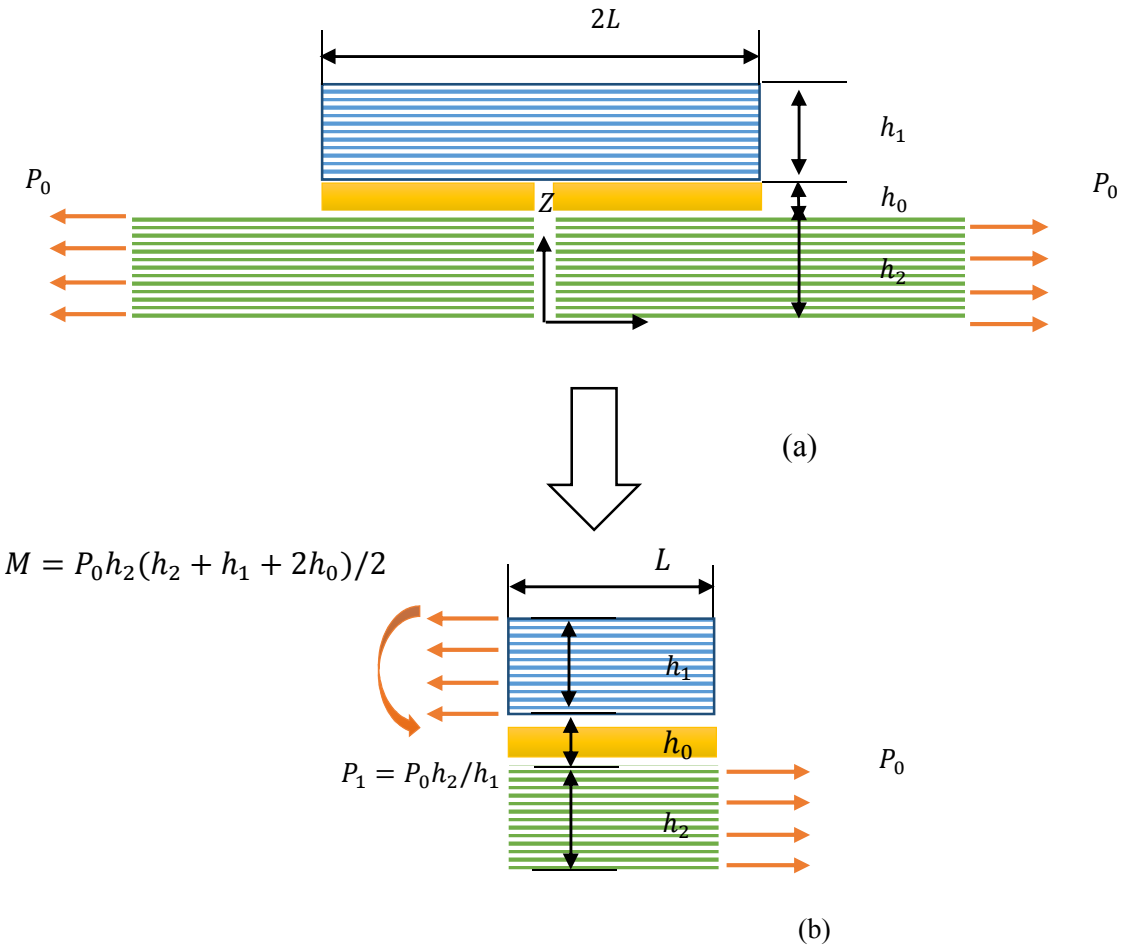

Figure 5.1. Skematical diagram of an adhesively bonded composite joint: (*a*) A slender cover layer bonded with two identical slender substrate layers via a thin adhesive; (*b*) Right-half of the joint based on structural symmetry.

Due to the symmetries of ABCJ and the loading applied at both sides, the stress analysis can be conviently simplified by taking only the right-half portion of the joint. As sketched in Fig 5.1 (*b*), consider the the cover and substrate laminates as well as the adhesive layer to carry the uniform length *L*. The thickness and the width areconstant, respectively. Based on the static equlibrium of the ABCJ, the cover laminate is subjected to the tensile loading P_1 and a bending moment M_0. Since the mismtch of the materical properties across each interfaces of layers of the

ABCJ, the external loads will cause high interfacial shear stresses and normal stresses (in other words, the debonding or peeling stresses) near all the free-edges. No matter mechanical or thermomechanical loads, the interfacial stresses, i.e., σ_{zz}, τ_{xz} and τ_{yz}, are responsible to the debonding failure the ABCJs.

In this problem, the temperature change is treated as uniform throughout the whole joint. In addition, the composite cover and substrate layers are considered as anisotropic, linearly thermoelastic materials, and the thin adhesive layer is dealt with as isotropic, linearly thermoelastic material. Similarly, in order to apply the method introduced in Chapter 3, herein, new boundary conditions are to be formulated at each free edge of the laminate loading state. At the bottom and upper surfaces of the laminate, the coefficients $F^0, G^0, F^0_{,y}, G^0_{,y}, \Psi^0. H^0$ and $F^{i+1}, G^{i+1}, F^{i+1}_{,y}, G^{i+1}_{,y}, \Psi^{i+1}. H^{i+1}$ are considered to be zero due to the stress-free state, respectively. $z_0, z_1, \dots, z_i, z_{i+1}$ are the vertical coordinates of each interfaces from the bottom surface to the upper surface of the laminate, respectively. Yin's formulation is based on the classical laminate plate theory (CLPT). Therein, the coefficients at each boundary can be determined by applying CLPT.

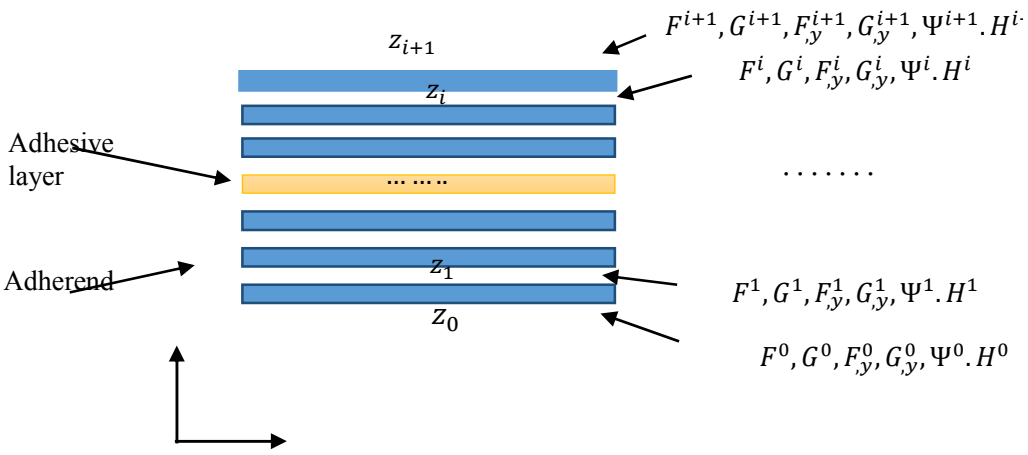

Figure 5.2. Schematic of the vertical coordinates and stree-functions at the interfaces.

5.3. Boundary conditions

Based on the classical laminate theory, assume the deformation at the center of a laminate is strain ε^0 and curvature κ, which can be obtained from the external loading. The load-deformation relationship is determined as (Agarwal, 2006):

$$\begin{bmatrix} N \\ M \end{bmatrix} = \begin{bmatrix} A & B \\ B & D \end{bmatrix} \begin{bmatrix} \varepsilon^0 \\ \kappa \end{bmatrix} \; or \; \begin{bmatrix} \varepsilon^0 \\ \kappa \end{bmatrix} = \begin{bmatrix} a & b \\ c & d \end{bmatrix} \begin{bmatrix} N \\ M \end{bmatrix} \tag{5.1}$$

where $N_y = P_i \,/t$ (i=1,2) and $M_y = M_0$. The in-plane stresses of each ply can be obtained as

$$[\sigma]^k_{x,y} = [Q]^k_{x,y}[\varepsilon^0]_{x,y} + z[Q]^k_{x,y}[\kappa]_{x,y} \tag{5.2}$$

Then, to obtain the stress resultants in x, y, and z-direction as

$$\begin{bmatrix} N_x \\ N_y \\ N_{xy} \end{bmatrix}_k = \int_{z_{k-1}}^{z_k} \begin{bmatrix} \sigma_x \\ \sigma_y \\ \tau_{xy} \end{bmatrix}_k dz \text{ and } \begin{bmatrix} M_x \\ M_y \\ M_{xy} \end{bmatrix}_k = \int_{z_{k-1}}^{z_k} \begin{bmatrix} \sigma_x \\ \sigma_y \\ \tau_{xy} \end{bmatrix}_k z\, dz \tag{5.3}$$

Substitution of Eq. (5.2) into Eq. (5.3) yields

$$N_{x,y}^{k} = [Q]_{xx}^{k}[\varepsilon^{0}]_{x}(z_k - z_{k-1}) + 0.5(z_k^2 - z_{k-1}^2)[Q]_{xx}^{k}[\kappa]_{x} \tag{5.4}$$

As discussed in Chapter. 3, the relationship between each stress component and the corresponding stress potential function is specified as

The in-plane stresses:

$$\sigma_x = F_{,yy}, \sigma_y = F_{,zz}, \tau_{xy} = \Psi_{,z} \tag{5.5}$$

Out-of- plane stresses:

$$\tau_{xz} = -\Psi_{,y}, \tau_{yz} = F_{,yz} \tag{5.6}$$

Since the ratio of width/thickness is larger than 10 in common composite laminates, the out-of-plane shear stresses τ_{xz} and τ_{yz} can be ignored due to the transverse shear deformation is much smaller than others. Hence, $F'^{(i)}_{,y} = G'^{(i)}_{,y} = 0$ are over the entire two edges. In addition, the boundary conditions of the stress functions can be specified in below.

5.3.1. *G(y)*

As mentioned by the Yin (1994a), by integrating σ_{yy} at the boundary edges through the thickness of adherend layers, the stress resultant N_y equates to *G* at the upper interface between the laminate adherend and the adhesive layer, i.e.,

$$N_y = \sum \int \sigma_y^{(i)}\, dz = \sum \int F_{,zz}^{(i)}\, dz = \sum F_{,z}^{(i)}\Big|_{z=z_{i-1}}^{z=z_i} = G^i \tag{5.7}$$

From Eq. (5.7), the stress resultant $N_y^{(1)}$ of the first ply can be obtained by

$$N_y^{(1)} = \int_{z_1}^{z_2} \sigma_{yy}\, dz = G^1 - G^0 \tag{5.8}$$

Since the bottom surface is stress-free condition, substitution of $G_0 = 0$ into Eq. (5.8), it yields

$$N_y^{(1)} = G^1 \tag{5.9}$$

Similarly, the stress resultant $N_y^{(2)}$ through the 2nd ply can be obtained by

$$N_y^{(2)} = \int_{z_2}^{z_3} \sigma_{yy}\, dz = G^2 - G^1 \tag{5.10}$$

Substitution of Eq. (5.9) into Eq. (5.10) results in

$$N_y^{(2)} + N_y^{(1)} = G^2 \tag{5.11}$$

In addition, $N_y^{(3)}$ in the 3rd ply of the laminate adherend is

$$N_y^{(3)} = \int_{z_3}^{z_4} \sigma_{yy}\, dz = G^3 - G^2 \tag{5.12}$$

Hence, G^3 can be obtained as

$$G^3 = N_y^{(1)} + N_y^{(2)} + N_y^{(3)} \tag{5.13}$$

Based on Eq. (5.9), (5.11) and (5.13), it can be concluded that the relationship of G^k at *k*-th interface and $N_y^{(k)}$ through *k*-th ply can be expressed as

$$G^k = \sum_{i=1}^{k} N_y^{(i)} \tag{5.14}$$

From Eq. (5.4), $N_y^{(k)}$ can be determined:

$$N_y^{(k)} = [Q]_y^k [\varepsilon^0]_y (z_k - z_{k-1}) + \frac{1}{2}(z_k^2 - z_{k-1}^2)[Q]_y^k [\kappa]_y \tag{5.15}$$

Combining Eq. (5.14) and (5.15), coefficient G^k at the boundary can be determined by the centroid strain ε^0 and curvature κ as

$$G^k = \sum_{i=1}^{k} \left[[Q]_y^i [\varepsilon^0]_y (z_i - z_{i-1}) + \frac{(z_i^2 - z_{i-1}^2)}{2} [Q]_y^i [\kappa]_y \right] \tag{5.16}$$

5.3.2. *Ψ(y)* and *H(y)*

Similarly, the value of shear stress resultant N_{xy} equats to Ψ of the interface between the adherend and adhesive layer.

$$N_{xy} = \sum \int \tau_{xy}^{(i)} \, dz = \sum \int \Psi_{,z}^{(i)} \, dz = \sum \Psi^{(i)} \Big|_{z=z_{i-1}}^{z=z_i} = \Psi^i \tag{5.17}$$

The stress resultant $N_{xy}^{(1)}$ through the 1st ply can be obtained by

$$N_{xy}^{(1)} = \int_{z_1}^{z_2} \tau_{xy} \, dz = \Psi^1 - \Psi^0 \tag{5.18}$$

Since the bottom surface of the laminate is stress-free, substitution of $\Psi_0 = 0$ into Eq. (5.18) leads to

$$N_{xy}^{(1)} = \Psi^1 \tag{5.19}$$

Similarly, the stress resultant $N_{xy}^{(2)}$ through the 2nd ply can be found as

$$N_{xy}^{(2)} = \int_{z_2}^{z_3} \tau_{xy} \, dz = \Psi^2 - \Psi^1 \tag{5.20}$$

Substitution of Eq. (5.19) into Eq. (5.20), it reads

$$N_{xy}^{(2)} + N_{xy}^{(1)} = \Psi^2 \tag{5.21}$$

Furthermore, the stress resultant $N_{xy}^{(3)}$ through the 3rd ply can be determined as

$$N_y^{(3)} = \int_{z_3}^{z_4} \tau_{xy} \, dz = \Psi^3 - \Psi^2 \tag{5.22}$$

Furthermore, substitution of Eq. (5.21) into Eq. (5.20) yields

$$\Psi^3 = N_{xy}^{(3)} + N_{xy}^{(2)} + N_{xy}^{(1)} \tag{5.23}$$

Hence, at the *k*-th interface, the value of the coefficient Ψ^k can be determined:

$$\Psi^k = \sum_{i=1}^{k} N_{xy}^{(i)} \tag{5.24}$$

From Eq. (5.4), $N_{xy}^{(k)}$ can be derived from ε^0 and κ:

$$N_{xy}^{(k)} = [Q]_{xy}^{k}[\varepsilon^0]_{xy}(z_k - z_{k-1}) + \frac{(z_k^2 - z_{k-1}^2)}{2}[Q]_{xy}^{k}[\kappa]_{xy} \tag{5.25}$$

Substitution of Eq. (5.25) into Eq. (5.24), by applying ε^0 and κ, the value of Ψ^k can be determined:

$$\Psi^k = \sum_{i=1}^{k}[Q]_{xy}^{i}[\varepsilon^0]_{xy}(z_i - z_{i-1}) + \frac{(z_i^2 - z_{i-1}^2)}{2}[Q]_{xy}^{i}[\kappa]_{xy} \tag{5.26}$$

In Yin's (1994a) method, $H(y,\eta)$ is the first order derivative of $\Psi(y,\eta)$ in *z*-direction. Meanwhile, $H^{(i)}$ is the value of $\Psi_{,z}^{(i)}$ at the upper side of the interface, and $H_0(y) = 0$ holds at the bottom surface of the laminate. Therefore, at the *k*-th interface, the following relationship exists

$$H^k = \tau_{xy}(y,0)^{(k+1)} \tag{5.27}$$

where $\tau_{xy}(y,0)^{(k)}$ is the in-plane shear stress at the upper side of the interface. Then, $H(y,\eta)^{(k)}$ can be determined as

$$H^k = [Q]_{x,y}^{k+1}[\varepsilon^0]_{x,y} + + z_k[Q]_{xy}^{k+1}[\kappa]_{xy} \tag{5.28}$$

5.3.3. *F(y)*

Consider that the joint is in the state of static equilibrium, i.e.,

$$\sum M_y = 0 \tag{5.29}$$

Therefore,

$$\sum M_y = M_y + \int \sigma_{yy} dA = M_y + \int \sigma_{yy} t dz = 0 \tag{5.30}$$

where, *t* is selected as the unit width, i.e., $t = 1$. So the stress moment M_y can be expressed as

$$M_y = -\int \sigma_{yy} dz = -\int \frac{\partial}{\partial z}\left(\frac{\partial F}{\partial z}\right) dz \tag{5.31}$$

By integrating by parts of $\int \sigma_{yy} dz$, it leads to

$$M_y = -\int \sigma_{yy} dz = -\left[\left(\frac{\partial F}{\partial z} * z\right) - \int \frac{\partial F}{\partial z} dz\right] = F - z^* G \tag{5.32}$$

where z^* is the vertical coordinate of the top surface of the adherend; F and G are the coefficients at the interface. Based on Eq. (5.32), moment ${M_y}^{(1)}$ through the first ply can be determined as

$${M_y}^{(1)} = -\int_{z_1}^{z_2} \sigma_{yy} dz = (F - zG)|_{z_1}^{z_2} = F^1 - z_2 G^1 - F^0 - z_1 G^0 \tag{5.33}$$

By considering the stress-free condition at the bottom surface, i.e., $F^0 = G^0 = 0$, it leads to

$${M_y}^{(1)} = F^1 - z_2 G^1 \tag{5.34}$$

Similarly, moment ${M_y}^{(2)}$ through the 2nd ply can be determined as

$${M_y}^{(2)} = -\int_{z_2}^{z_3} \sigma_{yy} dz = F^2 - z_3 G^2 - {M_y}^{(1)} \tag{5.35}$$

Substitution of Eq. (5.34) into Eq. (5.35) leads to

$${M_y}^{(2)} + {M_y}^{(1)} = F^2 - z_3 G^2 \tag{5.36}$$

Moment ${M_y}^{(3)}$ through the 2nd ply can be determined as

$$M_y{}^{(3)} + M_y{}^{(2)} + M_y{}^{(1)} = F^3 - z_4 G^3 \tag{5.37}$$

Thus, moment $M_y{}^{(k)}$ through the *k*-th ply can be determined as

$$\sum_{i=1}^{k} M_y{}^{(i)} = F^k - z_{k+1} G^k \tag{5.38}$$

Thus, F^k at the *k*-th interface can be obtained as

$$F^k = \sum_{i=1}^{k} M_y{}^{(i)} + z_{k+1} G^k \tag{5.39}$$

Based on Eq. (5.4), it reads

$$M_{x,y}^k = \int_{z_k}^{z_{k+1}} \left([Q]_{x,y}^k [\varepsilon^0]_{x,y} + z[Q]_{x,y}^k [\kappa]_{x,y} \right) zd = \frac{z^2}{2} [Q]_{x,y}^k [\varepsilon^0]_{x,y} +$$

$$\frac{z^3}{3} [Q]_{x,y}^k [\kappa]_{x,y} \Big|_{z_k}^{z_{k+1}} = \left(\frac{{z_{k+1}}^2}{2} - \frac{{z_k}^2}{2} \right) [Q]_{x,y}^k [\varepsilon^0]_{x,y} + \left(\frac{{z_{k+1}}^3}{2} - \frac{{z_k}^3}{2} \right) [Q]_{x,y}^k [\kappa]_{x,y} \tag{5.40}$$

Substitution of Eq. (5.40) into Eq. (5.39), F^k at the *k*-th interface can be determined as

$$F^k = \sum_{i=1}^{k} \left[\left(\frac{{z_{i+1}}^2}{2} - \frac{{z_i}^2}{2} \right) [Q]_{yy}^i [\varepsilon^0]_{yy} + \left(\frac{{z_{i+1}}^3}{2} - \frac{{z_i}^3}{2} \right) [Q]_{yy}^i [\kappa]_{yy} \right] + z_{k+1} G^k \tag{5.41}$$

5.4. Examples for stress analysis of single strapped adhesively bonded multi-layered composite joints

The importance of estimation of the interfacial stresses of ABCJs for design, strength and failure analysis.. In the following, the above stress-function variational method is used for stress analysis, of an adhesively bonded single-strapped composite joint to demonstrate the numerical accuracy and efficiency of this method. As discussed in Chapter 3 and 4, the normal stress σ_{zz} and shear stress τ_{xz}, τ_{yz} are responsible for the mode I, II and III failure of composite laminates. Thus, the example is employed to determine each stress at the different interfaces of

the joint. The material properties of the unidirectional composite ply in its principal axes are given as:

Adherends (graphite/epoxy composite)

E_1=20 GPa;

E_2= E_3=2.1 GPa;

G_{12}= G_{23}= G_{13}=0.85GPa;

$\upsilon_{12} = \upsilon_{23} = \upsilon_{13} = 0.21$.

where 1,2 and 3 are related to the directions of the fiber, width and thickness of the composite ply, respectively.

Adhesive layer (epoxy)

E_1= E_2= E_3= G_{12}= G_{23}= G_{13}=10 GPa;

$\upsilon_{12} = \upsilon_{23} = \upsilon_{13} = 0.4$

The applied load P_0 is taken as 1 MPa. The layups of both the upper and lower adherends are $[45^o/-45^o]_{2s}$. The geometrical parameters for such an ABCJ are taken as: L=10 mm, h_1= h_2=8 mm and h_0=1 mm.

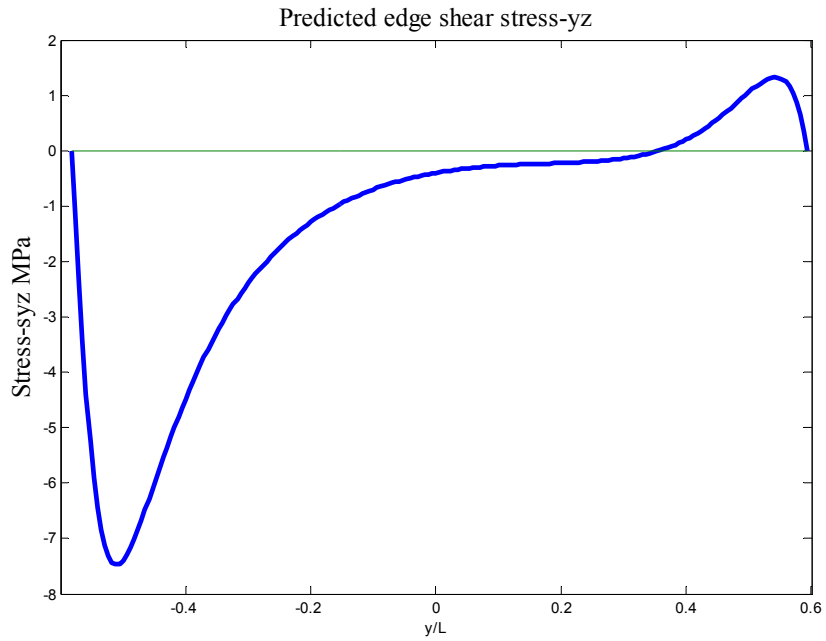

Figure 5.3.τ_{yz} variation at the 45°/-45° interface in the upper adherend.

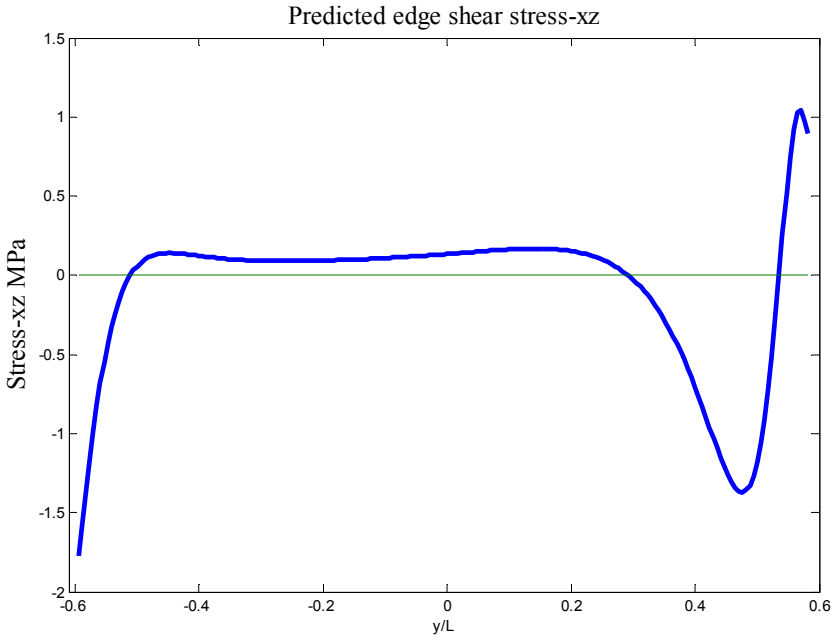

Figure 5.4. τ_{xz} variation at the 45°/-45° interface in the upper adherend.

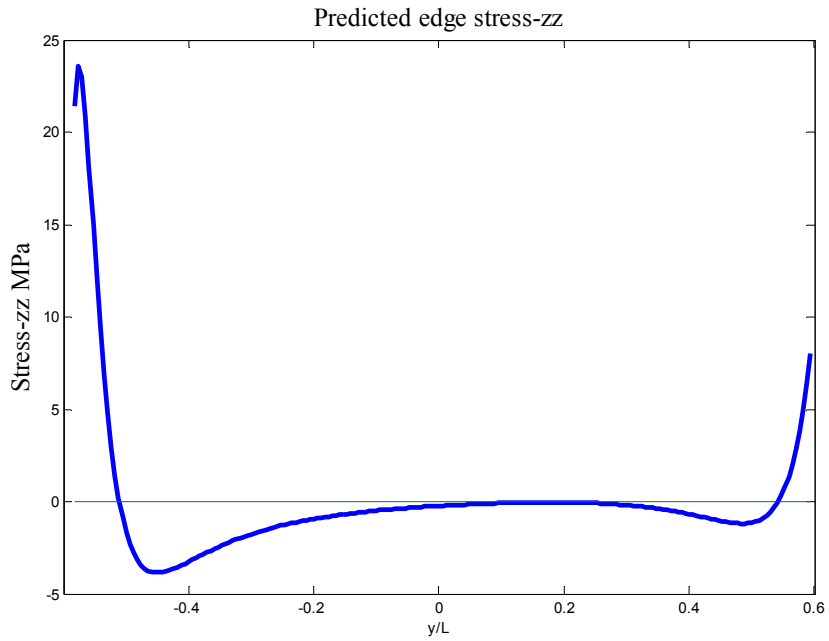

Figure 5.5. σ_{zz} variation at the 45°/-45° interface in the upper adherend.

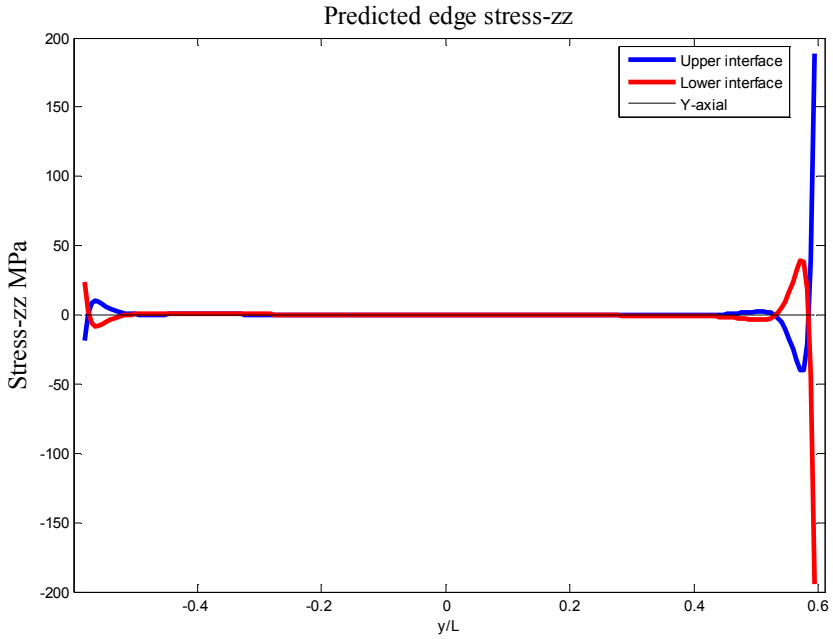

Figure 5.6. σ_{zz} variation along the bonding lines of the upper and bottom interfaces.

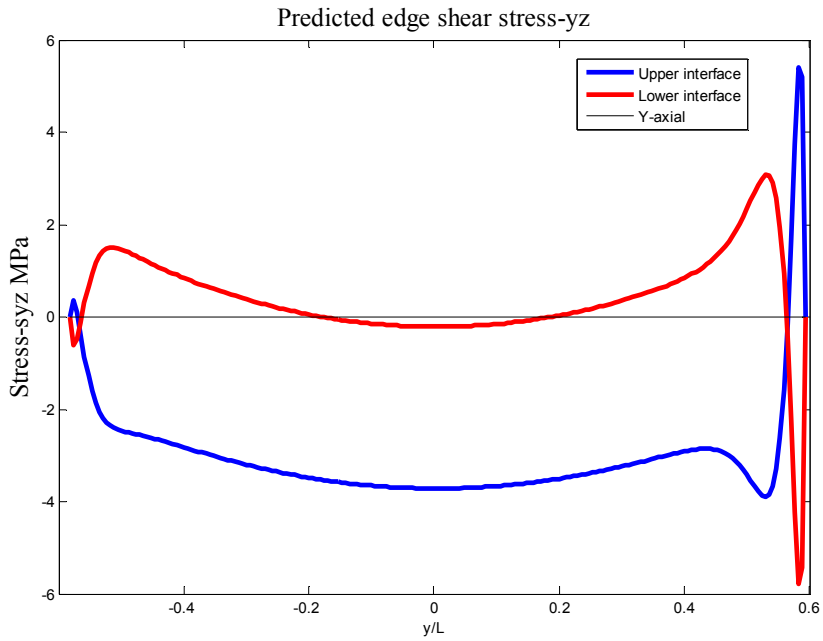

Figure 5.7. τ_{yz} variation along the bonding lines of the upper and bottom interfaces.

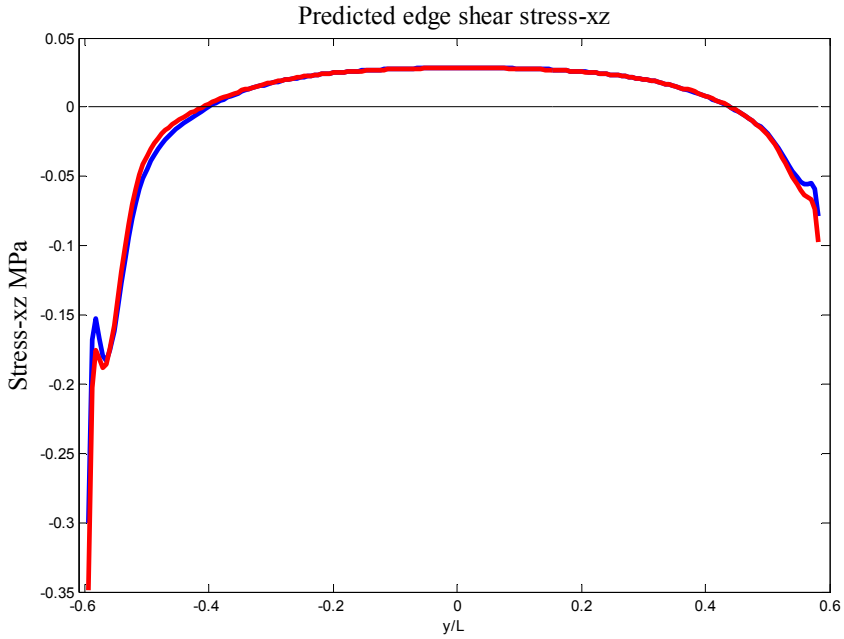

Figure 5.8. τ_{xz} variation along the bonding lines of the upper and bottom interfaces.

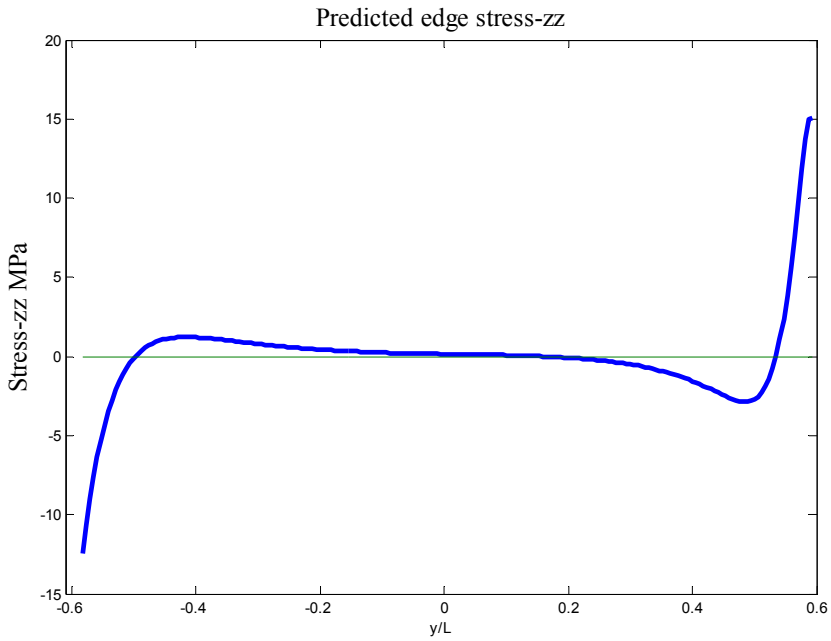

Figure 5.9. σ_{zz} variation along the 45°/-45° interface in the bottom adherend.

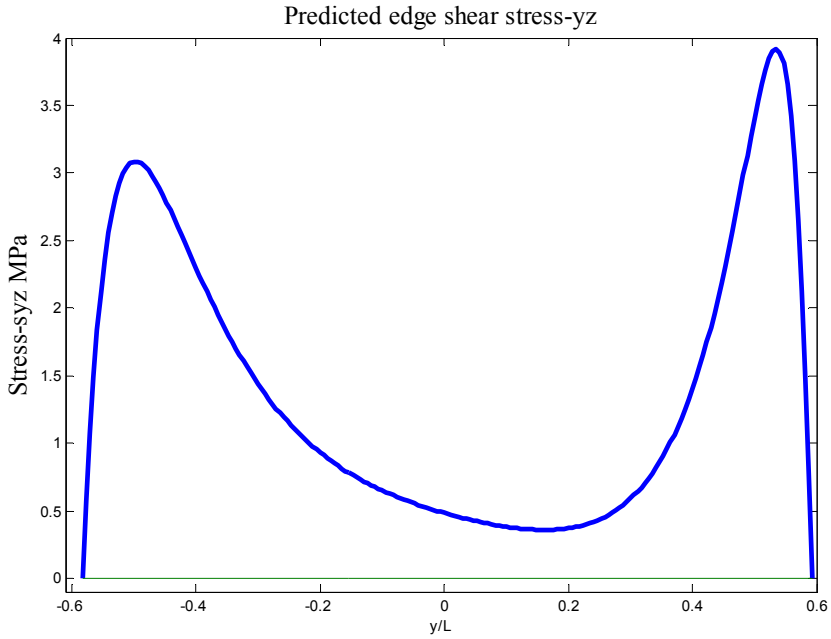

Figure 5.10. τ_{yz} variation along the 45°/-45° interface in the bottom adherend.

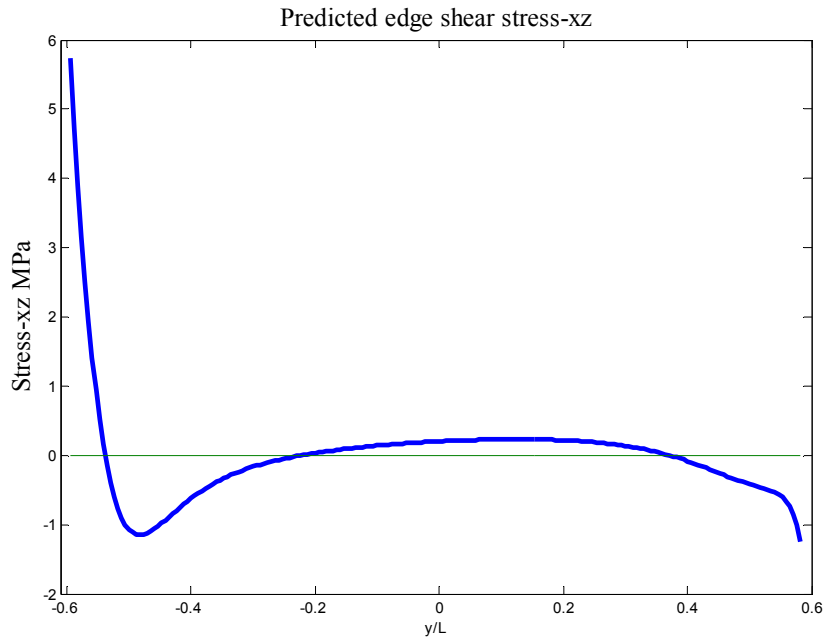

Figure 5.11. τ_{xz} variation along the 45°/-45° interface in the bottom adherend.

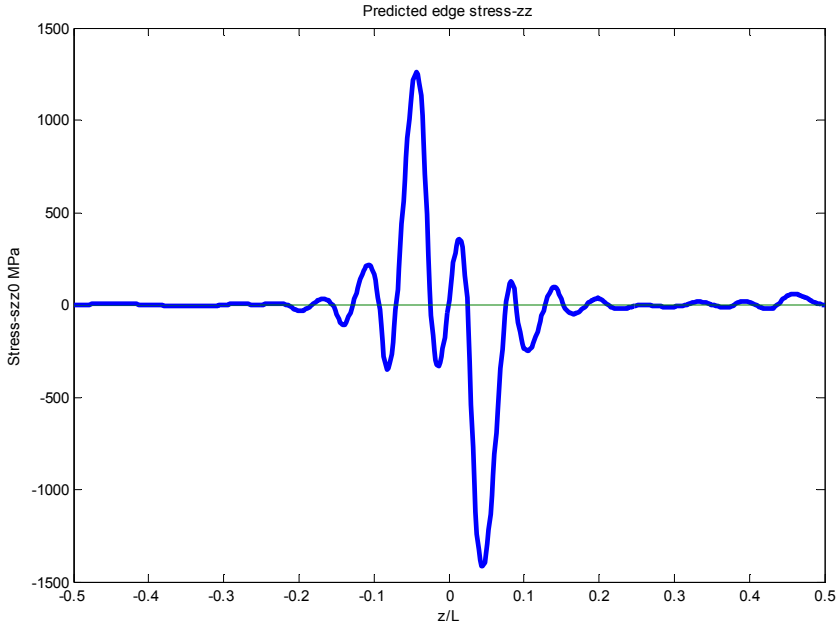

Figure 5.12. σ_{zz} variation at edge through thickness of the joints.

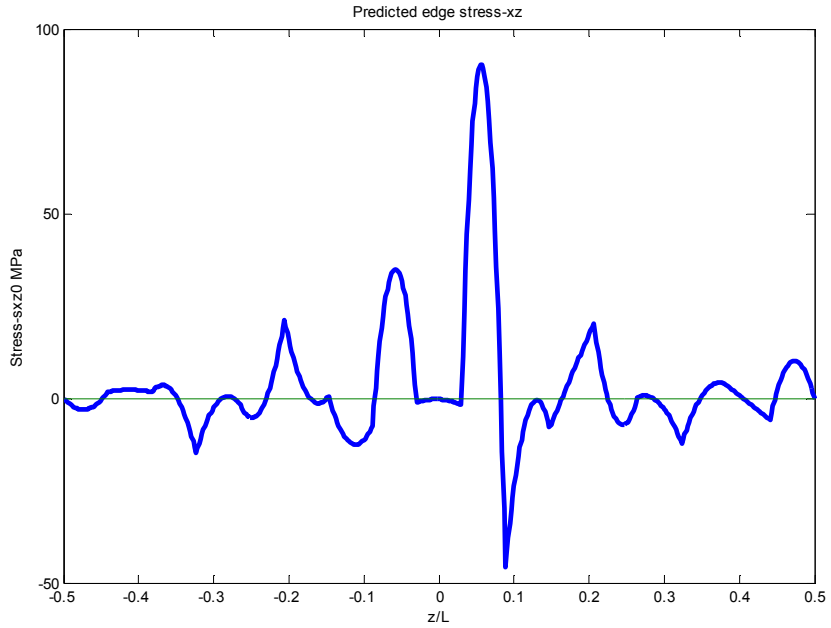

Figure 5.13. τ_{xz} variation at edge through thickness of the joints.

Figs. 5.4-5.6 show variations of the normal stress σ_{zz} and shear stresses τ_{xz} and τ_{yz} at the 45°/-45° interface of the upper adherend. Figs. 5.10-5.12 show variation of the normal stress σ_{zz} and shear stresses τ_{xz} and τ_{yz} at the 45°/-45° interface of the lower adherend. Even though at the 45°/-45° interface, the stresses vary differently due to the loadings at each edge. Figs. 5.7-5.9 show the stress variation at the upper and lower bonding lines. The stresses τ_{yz} and σ_{zz} at the bonding lines shows a similar varying trend but in the opposite direction, and the variation of τ_{xz} at both the upper and lower interfaces are only different at the peak values. Figs. 5.13 and 5.14 show the stress variation of the shear stress τ_{xz} and normal stress σ_{zz} at the edge through thickness. The maximum shear stress τ_{xz} is located at the lower bonding line, while the maximum normal stress σ_{zz} at each of bonding lines. Within the framework of the classic laminate plate theory, an axial tension P_0 applied to the laminate will exert deformation in the

laminate plates in the first place. Then, the deformation will further induce different stress distributions at the edges which may further influence the stress variations at the interfaces.

5.5. Conclusion

In this chapter, an accurate, efficient semi-analytic stress-function variational method has been formulated and utilized for exploring the stress variation in the ABCJs. An adhesively bonded single-strapped joint was taken as an example for demonstrating the capability of the method for stress analysis. The boundary conditions were redefined and accessed within the framework of classic laminate plate theory.

6. CONCLUSION

In summary, adhesively bonded composite joints (ABCJs) and composite laminates have been broadly used in load-carrying aerospace and aircraft structures, ground vehicle, flexible electronic devices, etc. Optimum design and failure prediction of ABCJs and composite multi-layer structures requires accurate and reliable interfacial stress analysis, which plays an essential role for such purpose. In this work, by extending the recent theoretical studies by Wu & Jenson (2011) and Wu & Zhao (2012) on stress-function variation methods for stress analysis of bonded joints and of three layered adhesively bonded joints, and by modifying the seminal method by Yin (1994a, 1994b) and Wu (2003) for stress analysis of composite laminate with semi-finite length, the present stress functional variational methods can be successfully utilized for stress analysis of ABCJs and other multi-layered composite laminate structures with finite length. Several theoretical outcomes had been accomplished in this work as following:

1. By introducing two Lekhnitskii's stress potential functions $F_i(y)$ and $\psi_i(y)$, approached by polynomial functions, the interfacial stress variation in an arbitrary composite laminate can be approximated. By evoking theorem of minimum complementary strain energy, the set of governing ODEs has been obtained for each comply and the adhesive layers. A system of the governing ODEs of the entire joint is assembled from the governing ODEs of each ply and adhesive layer. The resulting set of global governing ODEs of the system was solved by means of eigenfunction method, of which the particular solution is obtained by applying the the traction-free boundary conditions.

2. The solutions given by the present method can be applied for free-edge stress analysis of all types of composite laminates subjected to tension in the present case and can also be

considered for bending twisting and thermomechanical loading with miner modifications. The stress field of the composite laminates and ABCJs predicted by the present semi-analytic stress-function variational method not only satisfies the traction-free boundary conditions, but also is validated by the results available in the literature and by means of FEM. For example, the interfacial stresses in composite laminates with finite length predicated by the present semif-analytic stress-function variational method have been validated FEM results (ANSYS®) gained in this study.

3. By altering the loading conditions and combining the classic laminate plate theory, the stress-function variational method for stress analysis of composite laminates with finite width was successfully modified for the purpose of stress analysis of ABCJs. Thus, all the robust and high-efficiency numerical approaches developed for stress analysis of composite laminates can be utilized for stress analysis of ABCJs. The present method for stress analysis of ABCJs have been successfully validated in the limiting case of adhesively bonded joints of isotropic adherends by using the method developed by Wu & Zhao (2012).

4. The stress-function variational method formulated in this work is capable of predicting the interfacial stress variation along the bonded line and interfaces of laminate adherends simultaneously. The implementation of the present semi-analytic stress-function variational method for stress analysis of ABCJs is straightforward and computationally high efficiency. In contrast, no methods available in the literature can simultaneously predict the ply-wise free-edges stresses of ABCJs.

5. The present semi-analytic stress-function variational method can be conveniently used for scale analysis of the interfacial stress variations of composite laminates with varying length/width ratio, lay-up, and loading conditions (Chapter 3), which is much more efficient and

labor-saving than many other analytic and numerical methods available in the literature including FEM. For example, by employing the present method, it is convenient to determine the variation of the interfacial stress with one parameter of the composite laminate or ABCJs (e.g., number of plies, ply layup, ply thickness, one of material properties, thickness of the adhesive layer, etc.) while the rest of ones are fixed. 6. The present semi-analytic stress-function variational method for ABCJs can be considered as the most general semi-analytic method for accurate, efficient, linear stress analysis of various types of joints, e.g., bonded joints, ABJs, ABCJs, etc. By slight modification of the boundary conditions for a particular joint, the method can be modified for stress analysis of such joint.

In addition, with the success of the present stress-function variational method for stress analysis oflayered structures and ABCJs, the further applications can be initiated as following:

1) Extending the present model on the failure and crack analysis in the layered structures and ABCJs, such as progressive cracking of layered structures, debonding and delamination of ABCJs.

2) Potential applications of the present stress-function variational method for nondestructive evaluation of multilayered structures such as coatings, including static and dynamic methods.

REFERENCE

1. Matthews, F. L., Kilty, P. P. F. and Godwin, E.W. A review of the strength of joints in fiber-reinforced plastics 2: Adhesively bonded joints. Composites, 1982, 13(1), 29–37.
2. Adams, R. D. and Wake,W. C. Structural adhesive joints in engineering, 1984, vol. 15 (Elsevier, New York). Pages 15-26
3. Chamis, C. C. and Murthy, P. L. N. Simplified procedures for designing adhesively bonded composite joints. J. Reinforced. Plastics Composite. 1991, 10 (1), 29–41.
4. Kim, J.-S., Kim C. G., and Hong C. S. Practical design of tapered composite structures using the manufacturing cost concept. Composite Structure, 2001, 51(3), 285–299.
5. Volkersen, O. Die Niektraftverteilung in Zugbeanspruchten mit Konstanten Laschenquerschritten.Luftfahrtforschung, 1938, 15, 41–68.
6. Goland, M. and Reissner, E. The stresses in cemented lap joints. Translation of ASME, Journal of Applied. Mechanics and Materials, 1944, 66(11), A17–A27.
7. Theotokoglou, E. E. and Moan, T. Experimental and numerical study of composite T-joints. Journal of Composite. Materials, 1996, 30(2), 190–209.
8. Renton,W. J. and Vinson, J. R. The efficient design of adhesive bonded joints. Journal of Adhesively Composites, 1975, 175–193.
9. Srinivas, S. Analysis of bonded joints. NASATN D-7855, 1975.
10. Dattaguru, B., Everett, R. A., Whitcomb, J. D., and Johnson, W. S. Geometrically nonlinear-analysis of adhesively bonded joints. Translation of ASME, Journal of Engineering Materials and Technology, 1984, 106(1), 59–65.

11. Pickett, A. K. and Hollaway, L. The analysis of elastic–plastic adhesive stress in bonded lap joints in FRP structures. Composite Structure, 1985, 4, 135–160.
12. Allman,D. J. A theory for the elastic stresses in adhesive bonded lap joints. The Quatarly Journal of Mechanics and Applied Mathematics, 1977, 30,415–436.
13. Yang, C. and Pang, S. S. Stress–strain analysis of single-lap composite joints under cylindrical bending. Composite Engineering, 1993, 3, 1051–1063.
14. Yang, C. and Pang, S. S. Stress–strain analysis of single lap composite joints under tension. Translation of ASME, Journal of Engineering Materials and Technology, 1996, 118, 247–255.
15. Wu, Z. J., Romeijn, A., and Wardenier, J. Stress expressions of single-lap adhesive joints of dissimilar adherends. Composite Structure, 1997, 38(1–4), 273–280.
16. Tong, L. An assessment of failure criteria to predict the strength of adhesively bonded composite double lap joints. Journal of Reinforced. Plastic Composite, 1997, 16(8), 698–713.
17. Frostig, Y., Thomsen, O. T., and Mortensen, F. Analysis of adhesive-bonded joints, square-end, and spew-fillet – high-order theory approach. Journal of Engineering Mechanics, 1999, 125(11), 1298–1307.
18. Zou, G. P., Shahin, K., and Taheri, F. An analytical solution for the analysis of symmetric composite adhesively bonded joints. Composite Structure, 2004, 65(3–4), 499–510.
19. Zhang, J., Bednarcyk, B. A., Collier, C., Yarrington, P., Bansal, Y., and Pindera, M. J. Analysis tools for adhesively bonded composite joints, part 2: unified analytical theory. AIAA Journal, 2006, 44(8), 1709–1719.
20. Adams, R. D. and Harris, J. A. The influence of local geometry on the strength of adhesive joints. International Journal of Adhesion and Adhesives, 1987, 7(2), 69–80.

21. Groth, H. L. Stress singularities and fracture at interface corners in bonded joints. International Journal of Adhesion and Adhesives, 1988,8(2), 107–113.
22. Gleich, D. M.,Van Tooren, M. J. L. and Beukers, A. Analysis and evaluation of bondline thickness effects on failure load in adhesively bonded structures. Journal of Adhesion Science and Technology, 2001, 15(9), 1091–1101.
23. Magniez K, De Lavigne C, Fox BL. The effects of molecular weight and polymorphism on the fracture and thermo-mechanical properties of a carbon fibre composite modified by electrospun poly (vinylidene fluoride) membranes. Polymer 2010; 51(12):2585–96.
24. Li G, Li P, Zhang C, Yu Y, Liu H, Zhang S, et al. Inhomogeneous toughening of carbon fiber/epoxy composite using electrospun polysulfone nanofibrous membranes by in situ phase separation. Composites Science and Technology. 2008; 68(3–4): 987–94.
25. Akangah P, Lingaiah S, Shivakumar K. Effect of Nylon-66 nanofiber interleaving on impact damage resistance of epoxy/carbon fiber composite laminates. Composite Structure, 2010; 92(6): 1432–9.
26. Zhang J, Yang T, Lin T, Wang CH. Phase morphology of nanofibre interlayers: Critical factor for toughening carbon/epoxy composites. Composites Science and Technology, 2012; 72(2): 256–62.
27. Zhang J, Lin T, Wang X. Electrospun nanofibre toughened carbon/epoxy composites: effects of polyetherketone cardo (PEK-C) nanofibre diameter and interlayer thickness. Composites Science and Technology, 2010; 70(11): 1660–6.
28. Liu L, Liang YM, Xu GY, Zhang HS, Huang ZM. Mode I interlaminar fracture of composite laminates incorporating with ultrathin fibrous sheets. Journal of Reinforced Plastics and Composites, 2008; 27(11): 1147–62.

29. Liu L, Huang ZM, He CL, Han XJ. Mechanical performance of laminated composites incorporated with nanofibrous membranes. Material Science Engineering, A2006; 435–436: 309–17.
30. Magniez K, Chaffraix T, Fox B. Toughening of a carbon-fibre composite using electrospun poly (Hydroxyether of Bisphenol A) nanofibrous membranes through inverse phase separation and inter-domain etherification. Materials, 2011; 4(11): 1967–84.
31. Delale, F., Erdogan, F., and Aydinoglu, M. N. Stresses in adhesively bonded joints – a closed-form solution. Journal of Composite Materials, 1981, 15, 249 – 271.
32. Wu, X.F., Jenson, R.A., 2011. Stress-function variational method for stress analysis of bonded joints under mechanical and thermal loads. International Journal of Engineering. Science, 49, 279-294.
33. Wu, X.F., Jenson, R.A., Zhao, Y., 2014 Stress-function variational method approach to the interfacial stresses and progressive cracking in surface coatings. Mechanical Materials, 69, 195-203.
34. Wu, X.F., Zhao, Y., 2013. Stress-function variational method for interfacial stress analysis of adhesively bonded joints. International Journal of Solids Structure, 50, 4305-4319.
35. Wei Xu, Li G. Q, 2010, Finite difference three-dimensional solution of stresses in adhesively bonded composite tubular joint subjected to torsion. International Journal of Adhesion and Adhesives, 30 (2010) 191–199.
36. Yousefsani, S.A., Tahani, M., 2013a. Accurate determination of stress distribution in adhesively bonded homogenous and heterogeneous double-lap joints. European Journal of Mechanics, A 39, 197-208.

37. Yousefsani, S.A., Tahani, M., 2013b. Analytic solution for adhesively bonded composite single-lap joints under mechanical loadings using full layerwise theory. International Journal of Adhesion and Adhesives, 43, 32-41.
38. Sun, J.Y., Lu, N.S., Oh, K.H., Suo, Z.G., Vlassak, J.J., 2013. Islands stretch test for measuring the interfacial fracture energy between a hard film and a soft substrate. Journal of Applied Physics, 113, 223702.
39. Suo, Z.G., 2012. Mechanics of stretchable electronics and soft machines. MRS Bull, 37, 218-225.
40. Suo, Z.G., 2003. Reliability of interconnect structures in: Gerbeich, W., Yang, W., Interfacial and Nanoscale Failure. Elsevier, Amsterdam, Netherland, 265-324.
41. Goncalves, J.P.M., de Moura, M.F.S.F., de Castro, P.M.S.T., 2002. A three-dimensional finite element model for stress analysis of adhesive joints. International Journal of Adhesions and. Adhesives, 22, 357-65.
42. Her, S.C., 1999. Stress analysis of adhesively-bonded lap joints. Composite Structure, 47, 673-8.
43. Heslehurst, R.B., Hart-Smith, L., 2002. The science and art of structural adhesive bonding. SAMPLE Journal, 60-71.
44. Higgins, A., 2000. Adhesive bonding of aircraft structures. International Journal of Adhesions and Adhesives, 20, 367-76.
45. Jiang, H.Q., Khang, D.Y., Fei, H.Y., Kim, H., Huang, Y.G., Xiao, J.L., Rogers, J.A., 2008. Finite width effect of thin-films buckling on compliant substrate: experimental and theoretical studies. Journal of Mechanics and Physics Solids, 56, 2585-2598.

46. Wu, X.F., Dzenis, Y.A., 2002. Closed-form solution for a mode-III interfacial edge crack between two bonded dissimilar elastic strips. Mechanics Research Communications, 29, 407 – 412.

47. Wu, X.F., Dzenis, Y.A., Fan, T.Y., 2003. Two semi-infinite interfacial cracks between two bonded dissimilar elastic strips. International Journal of Engineering Science, 41, 1699 – 1710.

48. Wu, X.F., Jenson, R.A., 2011. Stress-function variational method for stress analysis of bonded joints under mechanical and thermal loads. International Journal of Engineering Science, 49, 279 – 294.

49. Wu, X.F., Lilla, E., Zou, W.S., 2002. A semi-infinite crack between two bonded dissimilar elastic strips. Archive of Applied Mechanics, 72, 630 – 636.

50. Tomblin, J., Davies, C., 2004. Bonded structures industry survey in: 2004 FAA Workshop on Bonded Structures, Seattle, WA, 2004, June.